ABSTRACT

Title of Dissertation: LARGE-SCALE NEURAL NETWORK MODELING: FROM NEURONAL MICROCIRCUITS TO WHOLE-BRAIN COMPLEX NETWORK DYNAMICS

Qin Liu, Doctor of Philosophy, 2018

Dissertation directed by: Professor, Steven M. Anlage, Department of Physics, University of Maryland-College Park
Senior Investigator and Chief, Barry Horwitz, Brain Imaging and Modeling Section, National Institutes of Health

Neural networks mediate human cognitive functions, such as sensory processing, memory, attention, etc. Computational modeling has been proved as a powerful tool to test hypothesis of network mechanisms underlying cognitive functions, and to understand better human neuroimaging data. The dissertation presents a large-scale neural network modeling study of human brain visual/auditory processing and how this process interacts with memory and attention.

We first modeled visual and auditory objects processing and short-term memory with local microcircuits and a large-scale recurrent network. We proposed a biologically realistic network implementation of storing multiple items in short-term memory. We then realized the effect that people involuntarily switch attention to salient distractors and are difficult to distract when attending to salient stimuli, by

incorporating exogenous and endogenous attention modules. The integrated model could perform a number of cognitive tasks utilizing different cognitive functions by only changing a task-specification parameter. Based on the performance and simulated imaging results of these tasks, we proposed hypothesis for the neural mechanism beneath several important phenomena, which may be tested experimentally in the future.

Theory of complex network has been applied in the analysis of neuroimaging data, as it provides a topological abstraction of the human brain. We constructed functional connectivity networks for various simulated experimental conditions. A number of important network properties were studied, including the scale-free property, the global efficiency, modular structure, and explored their relations with task complexity. We showed that these network properties and their dynamics of our simulated networks matched empirical studies, which verifies the validity and importance of our modeling work in testing neural network hypothesis.

LARGE-SCALE NEURAL NETWORK MODELING: FROM NEURONAL MICROCIRCUITS TO WHOLE-BRAIN COMPLEX NETWORK DYNAMICS

by

Qin Liu

Dissertation submitted to the Faculty of the Graduate School of the
University of Maryland, College Park, in partial fulfillment
of the requirements for the degree of
Doctor of Philosophy
2018

Advisory Committee:
Professor Steven Anlage, Chair
Dr. Barry Horwitz (advisor)
Professor Edward Ott
Professor Wolfgang Losert
Professor Daniel Butts

Acknowledgements

I would like to thank all people supported, helped and companied me for the last six years. In particular:

Dr. Barry Horwitz, for his help throughout my Ph.D. research, for introducing me into a completely new field and for those inspiring conversations on science, culture, books and everything else.

Prof. Anlage, for taking the responsibility as my co-advisor in University of Maryland although he had many reasons for not doing so.

Antonio Ulloa, Paul Corbitt, Ian DeWitt, for great time working together and helpful discussions.

Peisen Ma and Yinglun Wang, for being there all the time no matter that you are in Australia or Florida. And all my friends – sorry I can't name all of you – for the happiness we shared.

Jun Ma, for her patience and encouragement, and for believing in me.

My family in China, for their encouragement and support through my whole education.

Table of Contents

List of Tables

List of Figures

List of Abbreviations

DMS	delay matched-to-sample
EC	entorhinal cortex
EEG	electroencephalography
FC	functional connectivity
fMRI	functional magnetic resonance imaging
IT	inferior temporal
LSNM	large-scale neural modeling
MEG	magnetoencephalography
MTL	medial temporal lobe
PFC	prefrontal cortex
PET	positron emission tomography
ST	superior temporal
TVB	the Virtual Brain (software package)
WM	working memory

Chapter 1: Introduction

1. 1 Techniques for studying brain functions and thesis motivation

The past few decades have witnessed an explosion of studies on brain neural networks of human and other primates. Due to the complexity and importance of the human brain, these studies came from a number of different fields, such as neuroscience, psychology, mathematics and physics, and the area of brain research has become a testing ground for interdisciplinary techniques.

Several types of data can be collected from studies of human/non-human primates cognitive functions using different techniques. Behavioral studies usually concern the performance of subjects doing cognitive tasks: accuracy and response time. Psychological studies have designed a number of cognitive tasks that tried to isolate and test certain brain function, such as recognition, categorization, short-term memory encoding, etc. Some general but important features and patterns can be summarized out of behavioral data, e.g., the capacity of human working memory is 7±2 items (G. A. Miller, 1956). The limitation of behavioral data is obvious: the detailed mechanisms of the human brain mediating these functions and behaviors cannot be observed.

Anatomical studies (including lesion studies) can help on determining the connectivity between human brain regions and understanding how one region contributes to brain cognitive functions. Lesions (abnormalities or damages) occurred in human/nonhuman primates have been widely used and have provided a lot of fundamental knowledge. For example, lesions of prefrontal cortex severely impair the

performance of subjects on short-term memory related tasks (Levy & Goldman-Rakic, 1999), which proves that the prefrontal cortex plays a prominent role in short-term memory storage and processing. Studies using anatomical/lesions techniques assume that brain regions affect different cognitive functions independently and a lesion locally does not affect other undamaged brain regions. However, the complex network structure of primate cortical network determines that a small change of one region (i.e., a node in the complex network), can cause significant changes in other regions. Furthermore, to understand how human neural networks mediate cognitive functions one needs to know the temporal dynamics of neurons/regions, which anatomical studies obviously cannot capture.

Electrophysiological and imaging techniques make it possible to record the neural activity while performing cognitive tasks. Electrophysiological techniques are usually invasive thus can only be used in monkey studies and occasionally in patients, while imaging techniques are mostly used in human studies. There are many techniques available now to record brain activity. Fig. 1.1 shows the spatial and temporal resolutions of these techniques.

Electroencephalography (EEG) and magnetoencephalography (MEG) are two popular neuroimaging techniques. EEG measures voltage fluctuations due to ionic current within neurons during synaptic transmission using electrodes placed on the scalp, while MEG measures the magnetic fields induced by the ionic currents. The most common magnetometer used in MEG is SQUIDs (superconducting quantum interference devices). EEG/MEG can detect changes over milliseconds but the spatial

resolution is poorer than functional magnetic resonance imaging, which arose in the 1990s.

Functional magnetic resonance imaging (fMRI) is the most popular neuroimaging technique in the study of cognitive functions. It measures brain activity by detecting changes associated with blood flow, because blood flow to one region increases if the region is in use. The blood-oxygen-level dependent (BOLD) signal is primarily used. In 1990, Seiji Ogawa and colleagues showed that hemoglobin has different magnetic properties in its oxygenated and deoxygenated forms (deoxygenated hemoglobin is paramagnetic and oxygenated hemoglobin is diamagnetic) (Ogawa, Lee, Kay, & Tank, 1990). The BOLD signals reflect mainly the inputs to brain regions and the integrative processing within, rather than the output firing of neurons (Logothetis, Pauls, Augath, Trinath, & Oeltermann, 2001).

The spatial resolution of fMRI is its main advantages over EEG/MEG. Voxels, three-dimensional cuboids, are the smallest units that fMRI can measure. The sizes of voxels are set by the slice thickness and the grid imposed on the slice by the scanning process. Smaller voxels contain fewer neurons and less blood flow, hence are more difficult for scanning. The temporal resolution of fMRI is poorer than EEG/MEG. The sampling time is typically 1 or 2 seconds. In principle, the sampling time can be smaller but it cannot add additional information, because of the blurred intrinsic hemodynamic response (the change in the MR signal from neural activity is called the hemodynamic response) and finite signal-to-noise ratio (S. G. Kim, Richter, & Ugurbil, 1997).

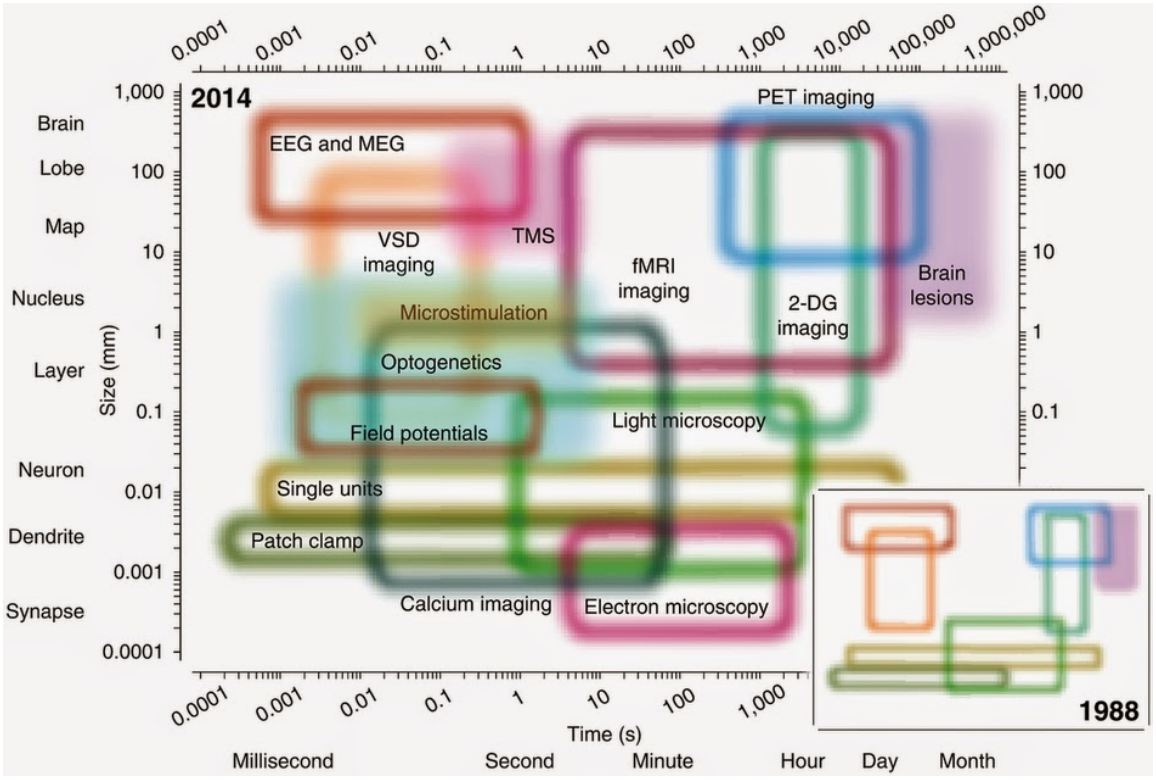

Figure 1.1 The spatial and temporal resolutions of different neuroimaging techniques. The figure is adopted from Sejnowski, Churchland and Movshon, 2014, Nature Neuroscience (Sejnowski, Churchland, & Movshon, 2014).

Another important technique is single-unit recording. Currently, single-unit recording can provide single-neuron resolution while the aforementioned imaging techniques cannot. However, single-unit recording is invasive thus can only be applied a limit brain region, and to nonhumans or else to human patients undergoing neurosurgery.

The data collected from the aforementioned methods, however, often appear to be unrelated or even contradictory. One cannot easily explain a set of behavioral data with functional magnetic resonance imaging (fMRI) data, or vice versa. This is due to the fact that the purposes, experimental conditions, and temporal and spatial resolutions of different techniques are usually different. Therefore, modeling techniques can be powerful tools for addressing such issues. Computational modeling of human brain relates the data from anatomical, behavioral, electrophysiological and imaging studies, and can be used to test theoretical hypothesis of brain cognitive functions. In this thesis, the author will show how we achieved these goals with a large-scale neural network model of cortical processing of visual/auditory objects.

In the rest of this chapter we will review the related literature of neuroscience (including anatomical, electrophysiological and imaging studies), computational efforts and complex network theory of the human brain.

1. 2 Background review of brain functions of interest

In this section, I provide a brief review of some important background knowledge for our modeling work. Since the thesis is a biologically realistic modeling study of a human neural network, it is necessary to start with the anatomical

correspondence of the model. Memory and visual/auditory objects processing are the two main components in our model, which will be reviewed in the following.

1. 2. 1 Anatomy of human brains

In human and other primates, the cerebrum (the cerebellum is not of interest in this thesis) is covered by cerebral cortex, a highly folded sheet of neurons with an average thickness of approximately 3 mm. The cerebral cortex controls our sensory processing, memory, attention, language and many other functions, which is also what we are trying to model (part of the cortex though). The cerebral cortex can be divided and labeled into different regions, across its surface, based on their functions; on the other hand, the cerebral cortex can be divided into several layers, 6 in most regions, and each layer contains a unique distribution of cell types and connection paradigm.

The cerebral cortex conventionally can be divided into 4 lobes (5 or 6 by some authors): frontal lobe, parietal lobe, occipital lobe, temporal lobe(Squire et al., 2012). See Fig. 1.2 for the locations of each lobe.

The parietal lobe is more focused on spatial sensory information processing which is not dealt with in this thesis (object processing). The frontal lobe is responsible for high order processing and contains many dopamine-responsive neurons, thus playing an important role in reward, motivation, decision-making, attention and short-term memory maintenance. The occipital lobe contains the early-stage visual processing areas: primary visual cortex (V1), secondary visual cortex (V2) and extrastriate cortex (V3, V4, V5/MT). The temporal lobe is the major region for a

number of functions including auditory information processing, visual features integration (information received from early stage areas in occipital lobe), multisensory information integration, etc., and is also associated with short-term memory encoding and maintenance, long-term memory encoding, storage and retrieval. Limbic lobe and insular cortex sometimes are considered as lobes in 6-lobe classification. The limbic lobe is related to long-term memory consolidation and emotional processing, which contains the hippocampus, amygdala, etc. The insular cortex is widely believed to be involved consciousness related processing like emotion, self-awareness and interpersonal experience.

1. 2. 2 Memory

Understanding memory is a key to understanding other higher cognitive functions. The past three decades have witnessed an explosion of studies on memory in both humans and other primates. Memory can be classified by different standards for various purposes, such as declarative memory, procedural memory, etc. For our interest, memory is categorized into short-term memory and long-term memory. Short-term memory was originally defined as a storage place before the information is consolidated into long-term memory (Atkinson & Shiffrin, 1968). Now this notion has been updated to the concept of "working memory", which was proposed by Baddeley and Hitch (Alan D. Baddeley & Hitch, 1974). Working memory is defined as a cognitive process that includes not only the transient holding but also the manipulation of information. The information processed in working memory is involved in decision making, language, selective attention and guiding future

planning (A. Baddeley, 1986).

Anatomically, two brain regions are thought to be essential for object working memory maintenance: the prefrontal cortex (PFC) and the inferior temporal cortex (IT). PFC has been considered to play the central role. A large number of nonhuman primate studies using single-neuron recordings (Funahashi, Bruce, & Goldman-Rakic, 1989; J. Fuster, Bauer, & Jervey, 1982; E. K. Miller, Erickson, & Desimone, 1996) and lesions (Levy & Goldman-Rakic, 1999) have supported the involvement of the PFC in working memory-related processes. Human brain-imaging studies (Courtney, Petit, Maisog, Ungerleider, & Haxby, 1998; D'Esposito et al., 1995; Haxby, Ungerleider, Horwitz, Rapoport, & Grady, 1995; Husain, Tagamets, Fromm, Braun, & Horwitz, 2004; Riley & Constantinidis, 2015), using positron emission tomography (PET) and functional magnetic resonance imaging (fMRI), have also revealed the crucial role that PFC plays in both object and spatial working memory.

The inferior temporal area is also believed to play some complementary role in working memory maintenance. Fuster and Jervey (J. M. Fuster & Jervey, 1982) first revealed in primate single-unit recording studies that inferior temporal neurons exhibit sustained, increased activity during the short delay of a delay match-to-sample task (detailed in next paragraph). A number of later studies have also supported the notion that inferior temporal cortex is important for the maintenance of visual object information (Horel, Pytko-Joiner, Voytko, & Salsbury, 1987; Petrides, 2000; Ranganath & D'Esposito, 2005).

A series of cognitive tasks using working memory, such as the delayed match-to-sample (DMS) task and Sternberg's recognition task (Sternberg, 1966, 1969), have

been designed to test different aspects of human/monkey working memory. The DMS task, sometimes a specific type of delayed response task, consists of two stimuli with a short delay period between them. The subjects are required to decide whether the second stimulus is the same as the first stimulus. The delay period makes the task a test of working memory. One can increase the difficulty by adding distractors during the delay period, or use mixed visual auditory stimuli. The Sternberg's task is more difficult as it requires the subjects to remember a list of items and decide, after a short delay period, whether a probe is a match of one the list of items.

These tasks have been extensively used in the study of the behavior of neurons and microcircuits related to working memory maintenance in the PFC (Funahashi, Inoue, & Kubota, 1993; J. M. Fuster & Alexander, 1971, 1973; Kubota & Niki, 1971; Schon, Ross, Hasselmo, & Stern, 2013). However, the underlying neurobiological mechanisms for the brain activations seen in these studies and the interactions between PFC and other brain regions, such as inferior temporal cortex, to support working memory operations are not well understood.

1. 2. 3 "What" and "where" pathways

This section provides a brief answer to the following question: how is visual/auditory information transported to the working memory system from eyes/ears? In 1982, Mishkin and Ungerleider (Ungerleider & Mishkin, 1982) first found from monkey lesion studies that visual features and spatial information are processed separately. After the first-stage processing in early visual cortex (V1, V2), visual information follows two main pathways ("streams" by some authors). The

ventral “what” pathway, proceeds ventrally in the brain (through visual area V4, the inferior temporal cortex, see Fig. 1.2 and Fig. 2.1C for more details), and is responsible for object feature identification and recognition, such as shape, color, texture, etc. The dorsal “where” pathway begins from V1/V2, goes dorsally through V5, V6 and into the posterior parietal cortex. The “where” pathway is related to the processing of spatial information, such as the object relative location, motion and the control of eye movements.

The visual ventral pathway processes an object by decomposing the object’s visual information by its natural features (lines, colors, shape, etc.) and then integrating them into a distributed representation of the object. Some factors, other than those natural stimuli features that have been decomposed in visual cortex, can significantly influence the ventral visual processing. Attention, working memory, and the saliency level of incoming stimulus are some of these factors.

The processed information of the visual ventral pathway can be further forwarded into working memory (given a certain attention condition and stimulus salience fit for working memory encoding). The visual ventral pathway is also strongly associated with long-term memory through the connection between the inferior temporal cortex in the pathway and the medial temporal lobe which is involved with storing long-term memories.

Recently, there is increasing evidence showing that humans possess two, ventral and dorsal, auditory pathways as well. Similar to visual processing, the auditory ventral pathway is responsible for auditory objects (words, phonemes,

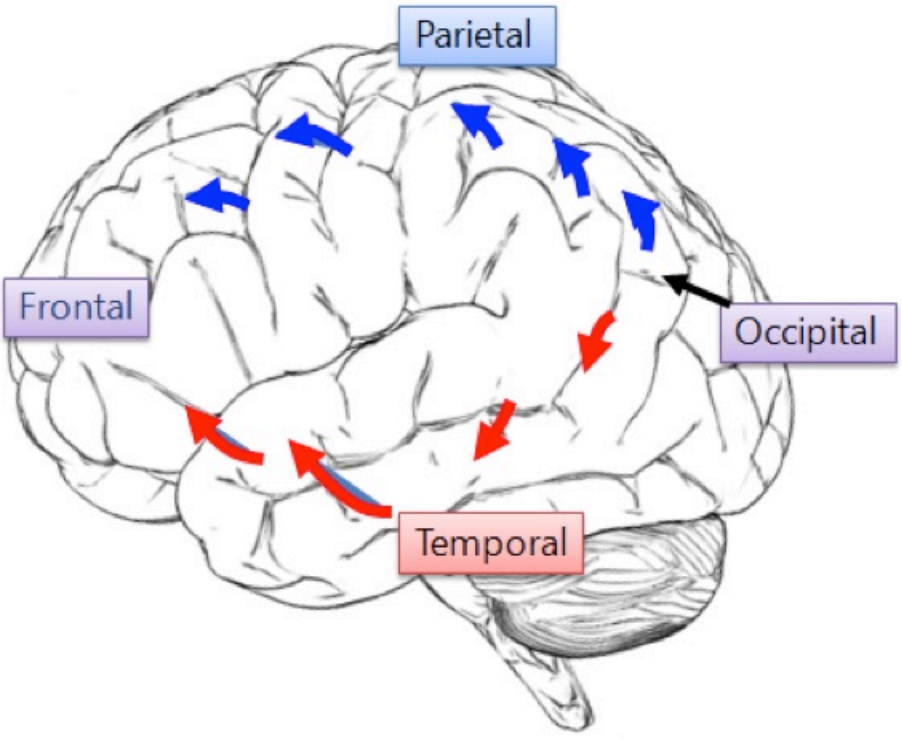

Figure 1.2 The ventral (red arrows) and dorsal (blue arrows) pathways of human visual processing. The ventral pathway is involved in the processing of visual features, which is of interest in our modeling. The figure is adopted from http://mikeclaffey.com/psyc170/notes/notes-vision.html.

natural sounds) recognition (DeWitt & Rauschecker, 2012). The auditory dorsal pathway was originally studied for its role in spatial information processing as the visual dorsal pathway, but later has been shown to play a more general role in sensorimotor integration and control, i.e., mapping auditory sensory representations onto articulatory motor representations.

In the present work, we only model the ventral "what" pathways for both visual and auditory processing, their interactions with short-term memory, and how attention and stimulus saliency can affect the processes.

1. 3 Computational Efforts

1. 3. 1 Notable large-scale neural network models

Because vision, audition and memory are such important processes, many research groups have developed conceptual or computational models for these processes. We and others have argued that large-scale neural network models can be powerful tools for addressing such issues (Chaudhuri, Knoblauch, Gariel, Kennedy, & Wang, 2015; Corchs & Deco, 2002; Garagnani, Wennekers, & Pulvermuller, 2008; Gisiger & Kerszberg, 2006; Tagamets & Horwitz, 1998). The word "large-scale" indicates that the model is not confined within a local brain region.

One of the most well-known large-scale brain models is the Human Brain Project with the Blue Brain Project as its centerpiece, funded by the European Union. With the ultimate goal stated as "tracking the emergence of intelligence" and simulating the entire human brain (Markram, 2006), the project so far has modeled the whole brain of rodents. The whole model to date has included about a million

neurons and each neuron is modeled with complex details, such as spatial morphology and ion channel composition.

Spaun is a large-scale model developed by Eliasmith and his collegues (Eliasmith et al., 2012). The number of neurons in the model is approximately 2.5 million. The single neuron model it uses is a version of a spiking model, which is simpler than the Blue Brain Project's neuronal model. The model includes the ventral visual processing pathway, motor control regions and decision-making regions so that it could perceive visual inputs and generate output by moving its mechanical arm. Spaun is a task-based model that can perform eight different cognitive tasks, whereas the HBP cannot.

Izhikevich and Edelman (Izhikevich & Edelman, 2008) developed one large-scale thalamo-cortical model that consists of 100 million neurons. The model was used to study spontaneous activity and rhythms of spiking activity. Compass is another large-scale model, as part of the DARPA Synapse project. Recently they reported a simulator with 500 billion neurons, which is 5 times of the number in human brains (Preissl et al., 2012).

Except for these whole-brain scale models with millions of simulated neurons, there are many other large-scale models focusing on specific brain functions, such as working memory (J. D. Murray, Jaramillo, & Wang, 2017; Tagamets & Horwitz, 1998), long-term memory (Gisiger & Kerszberg, 2006), spontaneous decision-making (Garagnani et al., 2008), etc. These models aim to test large-scale hypothesis for the networks mediating specific cognitive tasks.

1. 3. 2 The large-scale neural model (LSNM) in the Horwitz lab

Horwitz has pioneered applying neural network modeling to functional neuroimaging (e.g., PET, fMRI, MEG) data (Horwitz, Duara, & Rapoport, 1984; Horwitz et al., 1992). The large-scale neural model (LSNM) proposed by Tagamets and Horwitz in 1998 was based on the visual ventral pathway and hypothetical working memory circuits that simulated a DMS task for visual objects (Horwitz & Tagamets, 1999; Tagamets & Horwitz, 1998). The model aimed to understand better the neural substrate of different cognitive tasks and human imaging studies using PET and fMRI.

LSNM was later updated for transcranial magnetic stimulation (TMS), structural equation modeling, function magnetic resonance imaging (fMRI) and magnetoencephalography (MEG) simulations (Horwitz & Banerjee, 2012; Husain et al., 2002; J. Kim & Horwitz, 2009). A similar model was also developed to perform auditory tasks for fMRI simulations (Husain et al., 2004) based on the hypothesis that the sensory cortices involved in visual and auditory object processing perform similar operations but act on different features.

Ulloa and Horwitz (Antonio Ulloa & Barry Horwitz, 2016) embedded the visual LSNM model into a whole brain framework using The Virtual Brain (TVB) software package (Sanz Leon et al., 2013). TVB is a simulator that combines: (i) white matter structural connections among brain regions to simulate long-range connections, (ii) a neuronal population model to simulate local brain activity, and forward models that convert simulated neural activity into simulated functional neuroimaging data.

Table 1.1 A comparison between our model and some other notable large-scale models

	Neurons	Tasks/behaviors	Neuron complexity
LSNM	1×10^4	~20 tasks	Low/high
HBP	1×10^6	Neural behaviors	High
Spaun	2.5×10^6	6 tasks	Low
Izhikevich	5×10^{11}	Neural behaviors	Low

TVB whole brain framework makes possible the observations of how task execution networks (our models) can affect the intrinsic network (non-task nodes in TVB connectome). Ulloa and Horwitz (Ulloa & Horwitz, 2018) quantified the changes between passive states and task-evoked intrinsic activity using graph theoretical metrics.

Recently, we extended the model with: (i) a gating mechanism so that the model can handle distractors or store multiple items in short-term memory (Liu, Ulloa, & Horwitz, 2017); (ii) integrate the visual and auditory models so that visual-auditory bimodal objects can be processed; (iii) incorporate an exogenous attention module in order to simulate saliency capture and crossmodal attention switch.

A brief comparison between LSNM and some other notable large-scale models is shown in Table 1. For our purposes, the number of neurons included does not need to be very large as we only process simplified information (2D geometric shapes and tonal contours). The reason or the benefit of such simplification is that we do not need complicated inputs to test the mechanism beneath object processing, so the saved computational resources can be used to extend the model to implement

more complicated cognitive functions such as attention and memory. Our modeling framework, unlike many of the others, is capable of simulating neural data, behavioral performance data, and functional neuroimaging data, and is embedded in an anatomical human brain model.

1. 4 Complex network measures

A network is a set of items, which are called as vertices or sometimes nodes, with connections between them, called edges or simply connections. In the mathematical literature this is often defined as a "graph" (in the following text, "graph" and "complex network" are used interchangeably). In recent years, the analysis of networks has been massively applied in the study of social networks, the Internet, biology and many social sciences fields (Newman, 2003).

Horwitz et al. (Horwitz et al., 1984) studied the functional connectivity between different brain regions using glucose metabolic rates. The inception of fMRI in early 1990s brought more researchers to the field of brain functional connectivity studies. Friston (K. Friston, 1994) distinguished functional connectivity, effective connectivity and structural connectivity: the structural connectivity refers to physical attachment or anatomical tracts that link two nodes (neurons, brain regions); the functional connectivity (FC) is defined as the temporal correlation among the activity of different neurons/regions, and was measured by cross-relating the time-series of their activity; effective connectivity represents direct or indirect causal influences of one region on another. Later, McIntosh and colleagues (McIntosh et al., 1994; McIntosh, Nyberg, Bookstein, & Tulving, 1997) demonstrated that transition between cognitive states not only changes pattern of brain activation, but also changes co-

activation and connectivity, which suggested that the functionality of brain region has to be interpreted in the network context (Sporns, 2012). These experimental findings and theoretical constructions led naturally to the possibility of applying graph (complex network) theory in the field of brain connectivity analysis (Bassett et al., 2010).

In constructing a network for human brains, nodes/vertices can be neurons, cortical columns or brain regions/subregions, and edges/connections can be any type of connectivity between structural, functional and effective connectivity. In chapter 4, we will go back to this issue with more details.

The application of network theories has some unique advantages over traditional analytic techniques in cognitive neuroscience. First, complex network theory provides a reductionistic perspective to the study of human brains. Graphs give a topological abstraction of neural networks that can reduce the complexity in a number of ways. By parceling the brain into nodes/vertices, network analysis hides many features and details that are not required in the study of whole brain organizations and dynamics. Second, by using the network abstraction we ignore most of the variability between subjects, which helps on identifying the stable properties among human brains. Furthermore, the parceling scheme can be of different scales, from neurons to brain regions, which facilitates the comparison of structural connectivity and functional connectivity.

Many famous and interesting properties of human brain networks have been reported using network analysis, such as small-worldness, the scale-free property, etc (Watts & Strogatz, 1998). In Chapter 4, with more knowledge about our model, we

will see how network metrics, based on our simulation, can reflect and predict human cognitive behavior which in turn verifies the validity of the model.

1. 5 Contributions of the author

1. 5. 1 Modeling the neural mechanism of managing multiple items in working memory

The original models (Husain et al., 2004; Tagamets & Horwitz, 1998) successfully simulated auditory and visual ventral processing and the maintenance of working memory, yet some limitations existed and one of them was that only one item could be held in the working memory at a time. The author extended the visual model by incorporating a "gating" mechanism to solve the problem of storing multiple items in working memory (Qin et al., 2017), which will be detailed in Chapter 2.

We successfully implemented multiple working memory tasks using the same model and produced neuronal patterns in visual cortex, IT and PFC that match experimental findings. These working memory tasks can include distractor stimuli, or can require that multiple items be retained in mind during a delay period (Sternberg's task). Besides electrophysiology data and behavioral data, we also generated fMRI BOLD time-series from our simulation. Our results support the involvement of inferior temporal cortex for the working memory maintenance and suggest the cortical architecture that reflects the neural mechanism by which the brain performs particular working memory tasks. Furthermore, we noticed during simulations of memorizing a list of objects, the first and the last item in the sequence

were recalled best, which may implicate the neural mechanism behind this important psychological effect (i.e., the primacy and recency effects).

1. 5. 2 Modeling visual-auditory bimodal processing and crossmodal attention capture of salient stimuli

The neural mechanisms underlying endogenous (top-down) and exogenous (bottom-up) attention, and how attention is controlled or allocated in crossmodal perception are poorly understood. The word "top" refers to higher order brain regions, such as prefrontal cortex, and "bottom" refers to early-stage processing areas. The author investigated these issues by integrating the visual and auditory large-scale neural network models. We then modeled and incorporated into our visual-auditory object-processing model the neuronal mechanisms for the control of endogenous and exogenous attention (Liu et al., in preparation).

The model successfully performed various bimodal working memory tasks, and produced behavioral, electrophysiological and fMRI results that matched experimental findings. Furthermore, in our visual-auditory bimodality simulations, we found that working memory load in one modality would reduce the distraction from the other modality, and a possible network mediating this effect is proposed based on our model. This part is shown in Chapter 3.

1. 5. 3 Analyzing the network changes with experimental conditions using complex network measures

We ran simulations using our model embedded in a high-resolution connectome which parcels the brain into 998 nodes, and constructed functional connectivity networks for different cognitive tasks with various complexity. These tasks include passive viewing/listening, delayed match-to-sample task with one item stored in working memory (visual or auditory), Sternberg's task which requires a list of items to be remembered and visual-auditory attention switching task which requires both visual and auditory regions to be involved.

We used simulated synaptic activity to calculate functional connectivity (FC) matrices and generated FC networks. We power scaled the connection strength distribution and showed the scale-free property of FC networks for different task-evoked intrinsic activity. Some important network theoretical metrics were computed using FC matrices and how these metrics change with task complexity was shown with different thresholds. We studied temporal dynamics of these metrics and found that: working memory load reduces the global efficiency of functional connectivity networks, while salient stimuli perception increases the global efficiency. In Chapter 4, we will discuss in detail these issues.

Currently, the model includes 26 modules representing different brain regions and 10752 simulated neurons. The model can successfully perform 16 different (although conceptually related) cognitive tasks (see Chapter 5 for a complete list). When constructing the model, a module is not designed specifically for certain tasks per se. We first make hypotheses based on the experimental literature about how

cognitive tasks of interest are performed and what brain regions are involved. Then we build new modules to represent new brain regions. In training the model to perform tasks, we do not use supervised or reinforcement learning methods, which are typically used in deep learning fields but are not biologically realistic. Parts of the connection weights in our model are determined using an unsupervised learning algorithm, and the rest of the connections are hand-wired based on experimental results.

In Chapter 5, we will present a summary of all the author's works and ongoing projects.

Chapter 2: Visual ventral processing and managing multiple objects in working memory

In this chapter, I will present a large-scale neural network model that can perform multiple short-term memory tasks for novel objects, with the simulated neuronal behaviors and simulated fMRI patterns matching experimental data. The model successfully implemented three versions of delayed matched-to-sample (DMS) tasks with or without distractors, and a variation of Sternberg's recognition task that required the model to hold multiple items in working memory. A primacy/recency effect emerged during the simulations of memorizing a list of objects, i.e., the first and the last item in the sequence were recalled best, which may implicate the neural mechanisms behind this important psychological effect. Finally, we have placed our model in a whole-brain connectome framework (Antonio Ulloa & Barry Horwitz, 2016). In this chapter, we will restrict our attention to the visual processing model.

2. 1 The neuronal microcircuit

A flavor of the Wilson-Cowan model is used as the neuronal microcircuit, namely the basic units of our model. As shown in Fig. 2.1A, the employed modified Wilson-Cowan unit consisting of an interacting excitatory and inhibitory pair of elements (Tagamets & Horwitz, 1998; Wilson & Cowan, 1972), which can be considered as a simplified representation of a cortical column. The excitatory elements correspond to the pyramidal neuronal populations and the inhibitory elements correspond to the inhibitory interneurons. The model involves only simulated neurons, modified Wilson-Cowan units, which are coupled with each other,

and there is no other outside decision-making or computation process.

The input synaptic activity to each microcircuit can also be evaluated and combinations of this activity were related to the fMRI or MEG/EEG signals via a forward model. The simulated electrical activity of the *i*th excitatory unit and the *i*th inhibitory unit at time *t* are given by the following equations (2.1) and (2.2) respectively:

$$\frac{dE_i(t)}{dt} = \Delta S_e(E_i(t), I_i(t), in_{iE}(t)) - \delta E_i(t) \quad (2.1)$$

$$\frac{dI_i(t)}{dt} = \Delta S_i\big(E_i(t), I_i(t), in_{iI}(t)\big) - \delta I_i(t) \quad (2.2)$$

where Δ is the rate of change, δ is the decay rate, and $in_{iE}(t)$, $in_{iI}(t)$ are the incoming inputs from other nodes.. Thus, the activity variables $E_i(t)$ and $I_i(t)$ follow first-order kinetics with the inverse of δ. S_e and S_i are functions of the activity variables $E_i(t)$ and $I_i(t)$, and also incoming inputs from other nodes. These two functions control the nonlinearities, which are usually chosen to be sigmoidal in order to reflect neuronal behaviors realistically. Now, Eqs. (2.1) and (2.2) become:

$$\frac{dE_i(t)}{dt} = \Delta\left(\frac{1}{1 + e^{-K_E[w_{EE}E_i(t) + w_{IE}I_i(t) + in_{iE}(t) - \phi_E + N(t)]}}\right) - \delta E_i(t) \quad (2.3)$$

and

$$\frac{dI_i(t)}{dt} = \Delta\left(\frac{1}{1 + e^{-K_I[w_{EI}E_i(t) + in_{iI}(t) - \phi_I + N(t)]}}\right) - \delta I_i(t) \quad (2.4)$$

where K_E, K_I are gain constants, w_{EE}, w_{IE}, w_{EI} are the connectivity weights within one neuronal unit, ϕ_E, ϕ_I are the input threshold, $N(t)$ is the noise. $in_{iE}(t)$ is given by:

A

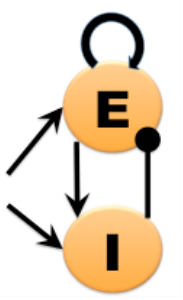

B

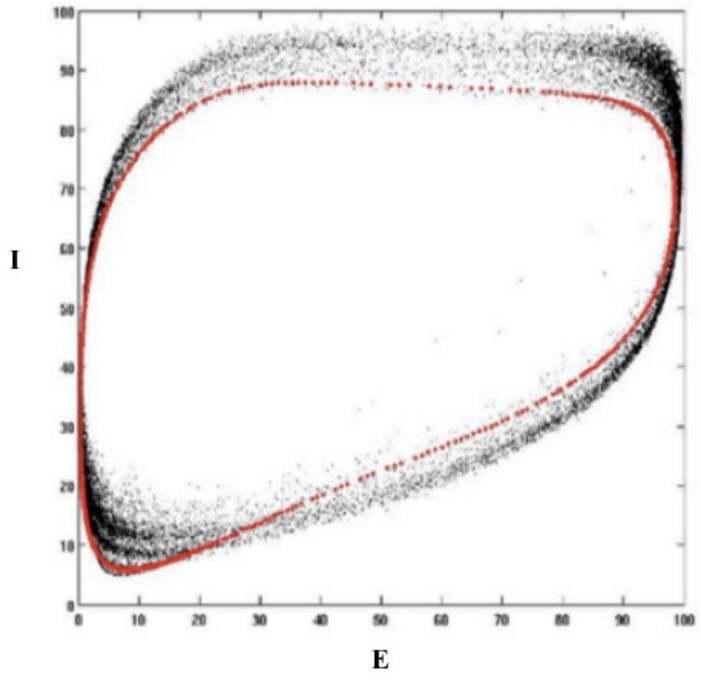

C

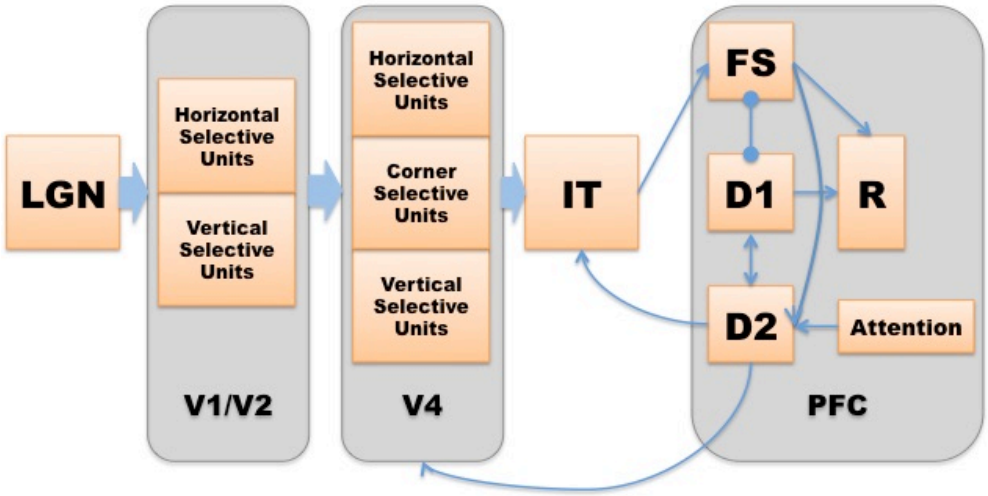

Fig. 2.1 Neuronal microcircuit and structural model. **A.** Structure of a Wilson-Cowan microcircuit, which can be considered as a simplified representation of a cortical column. Each microcircuit consists of an excitatory and an inhibitory element with the excitatory element corresponding to the pyramidal neuronal population in a column and the inhibitory element corresponding to the inhibitory interneurons. **B.** The phase trajectories of a Wilson-Cowan unit. The red dots are solutions without noise. The black dots are solutions with noise. **C.** Network diagram of the original visual model of Tagamets and Horwitz (1998). Arrows denote excitatory connections; lines ending in circles denote inhibitory connections. See text for details.

$$in_{iE}(t) = \sum_j w_{ji}^E E_j(t) + \sum_j w_{ji}^I I_j(t) + \sum_j c_{ji} z_{ji}^C C_j(t) \quad (2.5)$$

where w_{ji}^E and w_{ji}^I are the weights for connections from the excitatory (E) and inhibitory (I) elements of jth LSNM unit to the excitatory element of ith LSNM unit, C_j is the electrical activity of the connectome excitatory unit j connected to LSNM unit i, and z_{ji}^C is the connection weight. c_{ji} is a coupling term obtained by the Gaussian pseudo-random number generator of Python. $in_{iI}(t)$ is given by:

$$in_{iI}(t) = \sum_k w_{ki}^E E_k(t) + \sum_k w_{ki}^I I_k(t) \quad (2.6)$$

where w_{ki}^E and w_{ki}^I are the weights for connections from the excitatory (E) and inhibitory (I) elements of kth LSNM unit to the excitatory element of ith LSNM unit. In Fig. 2.1A, excitatory (E) connections are marked as arrows and inhibitory (I) connections are marked as circles.

The differential equations (2.3) and (2.4) are solved for each neuronal unit on each time step of simulation. The time step is typically set to be 5 milliseconds. The simulated Wilson-Cowan units are coupled with each other through E-E, E-I or I-E connections. Figure 2.1B shows the phase portrait (the activity of one excitatory unit versus its corresponding inhibitory unit) of one simulated neuronal unit. The red trajectory is simulated without noise while the black trajectories are simulated with noise. The value selections of parameters in equations (3) and (4) aim to reflect the mean features of neuronal populations in the real world. Please refer to Wilson and Cowan (1972) and Tagamets and Horwitz (1998) for more details.

2. 2 The structural model

The structural network of the visual model is shown in Fig. 2.1C. Each neuronal population in our model consisted of 81 microcircuits, which will be explained in detail in the following. Shape is the feature used in the model to characterize a visual object. Model neurons in modules representing early visual cortex were assumed to be orientation selective (for simplicity, horizontal and vertical orientations were used). Beginning in striate visual cortex, the ventral processing pathway extends into the inferior temporal lobe and projects into ventrolateral prefrontal cortex. The modules that comprise the visual model include ones representing primary and secondary visual cortex (V1/V2), area V4, anterior inferotemporal cortex (IT), and prefrontal cortex (PFC). Each of these regions contains one or more neural populations with different functional attributes (discussed below). The response properties of the simulated neuronal populations employed were based on known monkey neural electrophysiological data (e.g., (Funahashi, Bruce, & Goldman-Rakic, 1990). An important assumption for the visual model, inferred from such experimental data, was that the spatial receptive field of neurons increased along the ventral processing pathway.

In the model, the early visual areas V1 and V2 are combined and are designed to consist of orientation selective units (for simplicity we have only employed horizontal selective units and vertical selective units). Single-neuron recording experiments in primates have confirmed that neurons exist in both V1 and V2 areas that respond preferentially to visual features such as line orientation, edges and colors

(Hubel, Wiesel, & Stryker, 1977; Peterhans & von der Heydt, 1993; Roe & Ts'o, 1995). This formulation is unchanged from the original Tagamets & Horwitz (Tagamets & Horwitz, 1998) model.

The V4 area is designed as a continuation of the shape processing pathway and consists of three populations of units: horizontal selective units, vertical selective units and corner selective units. They are constructed to have an increased spatial receptive field relative to V1/V2, i.e., they respond to longer horizontal and vertical line segments, and also corners formed by adjacent pairs of horizontal and vertical lines. Experimental studies provide the basis for this design; neurons in area V4 share similar properties with earlier areas but appear to encode more complex properties of shape (Desimone & Schein, 1987; Gallant, Braun, & Van Essen, 1993). As with V1/V2, this module is the same as in the original model. We did add one new item, however; there is now feedback connectivity from V4 to V1/V2.

The next processing module of the model corresponds to inferior temporal cortex and is denoted by IT. The IT module functions as a feature integrator and generates the initial rough representation of a percept. In single-neuron recordings, as we mentioned in the introduction, IT areas exhibit various active behaviors during the short delay periods that might be relevant to visual feature selective activity and visual information maintenance (Fuster et al., 1982; Horel et al., 1987; Miyashita, 1988; Petrides, 2000; Ranganath & D'Esposito, 2005). IT was also a module in the original model.

In our new model, we have added a new module - the entorhinal cortex - to serve as a gate between IT and PFC in order to prevent new information overwriting

A

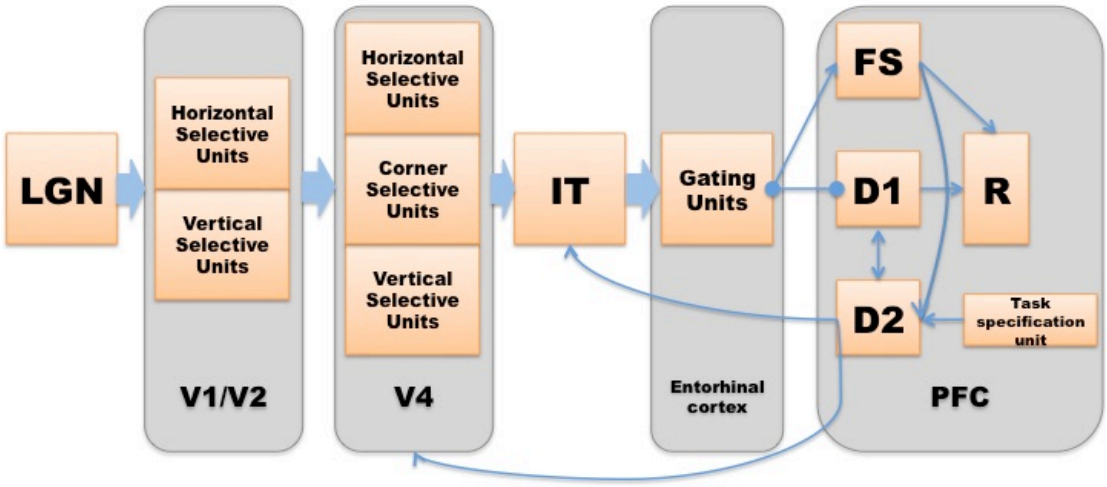

B

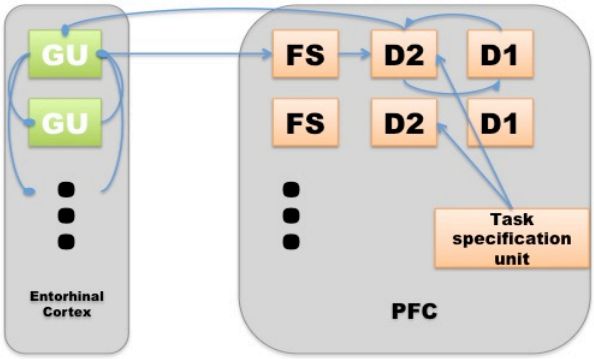

Fig. 2.2 The structural design of extended vLSNM. **A.** The network structure of the modified vLSNM. Compared to the original vLSNM structure (Tagamets & Horwitz, 1998; Ulloa & Horwitz, 2016), (1) a gating module (GA) has been added, which is tentatively located in the entorhinal cortex; (2) multiple sets of working memory modules (D1 and D2 in PFC) are used, instead of one set of D1 and D2 units in the original model. **B.** The entorhinal cortex and additional working memory modules are designed to act as a gate between IT and PFC. Multiple groups of entorhinal neurons and prefrontal cortex neurons are incorporated to hold multiple items in short-term memory. The entorhinal neurons competitively inhibit each other so that a group of gating neurons will be activated when a stimulus comes in and inhibits other groups of gating neurons. Once the item is stored, an inhibitory feedback from PFC to entorhinal cortex will suppress the active gating neurons and release other gating neurons so that the remaining gating neurons are ready for new stimuli.

previous PFC storage. We designed the gating mechanism by incorporating several groups of neurons in entorhinal cortex that competitively inhibit one another (see Fig. 2.1B). The purpose of such a mechanism is to avoid the working memory of one stimulus being overwritten by later incoming stimuli. The involvement of entorhinal cortex in working memory encoding has been supported by multiple experimental studies (for a review, see (Lech & Suchan, 2014), although the actual neural mechanisms remain unclear. In our design, a group of gating neurons will be activated when a stimulus comes in and inhibits other groups of gating neurons. Once the item is stored in this working memory buffer, an inhibitory feedback from PFC to entorhinal cortex will suppress the active gating neurons and release other gating neurons so that the remaining gating neurons are ready for new stimuli. By such a design, we are assuming that each group of entorhinal gating neurons could be used only once during a task trial.

Model neurons in the PFC module, in a short-term memory task condition, can be delineated into four types based on experimental data acquired by Funahashi et al. (Funahashi et al., 1990). In our model (see Fig. 2.2A), the submodule FS contains cue-sensitive units that in general reflect the activities in the IT module. D1 and D2 submodules form the short-term memory units by exciting one another during the delay period. In our modified model, we now have multiple sets of D1 and D2 submodules built into the model such that holding more than one item in short-term memory is possible (see Fig. 2.2B). R serves as a response module (output). It responds when a displayed stimulus (probe) matches the cue stimulus that is being held in short-term memory. Note that we assume that there are a limited number of

gating units and a similar limited number of D1-D2 units, since empirical studies indicate that only a limited number of items can be simultaneously kept in short-term memory (e.g., the so-called 7±2 (G. A. Miller, 1956)). For computational simplicity, in this paper we will employ no more than three items.

Although arbitrary, a task specification module is located in the superior frontal gyrus of the Virtual Brain model. The module provides a low-level, diffuse incoming activity to the D2 module in the prefrontal area which can be interpreted as an attention level. The attention level/task parameter can be modulated and is specified before each trial in a simulation. When the attention level is low, the working memory modules are not able to hold a stimulus throughout the delay period.

Ulloa and Horwitz (Antonio Ulloa & Barry Horwitz, 2016) embedded the vLSNM into a whole brain framework using The Virtual Brain (TVB) software package (Sanz Leon et al., 2013). TVB is a simulator that combines: (i) white matter structural connections among brain regions to simulate long-range connections, (ii) a neuronal population model to simulate local brain activity, and forward models that convert simulated neural activity into simulated functional neuroimaging data. In the current paper, TVB neurons provide neural noise to the embedded vLSNM. The structural connectome we employ is that due to Hagmann et al. (Hagmann et al., 2008), which comprises 998 regions of interest (ROIs), and the simulated neuronal microcircuits at each TVB node are Wilson-Cowan units.

We first found the hypothetical regions of interest (ROIs) corresponding to each module in our LSNM and the connected nodes in Hagmann's connectome. Then we embedded our revised model of microcircuits and network structure into the

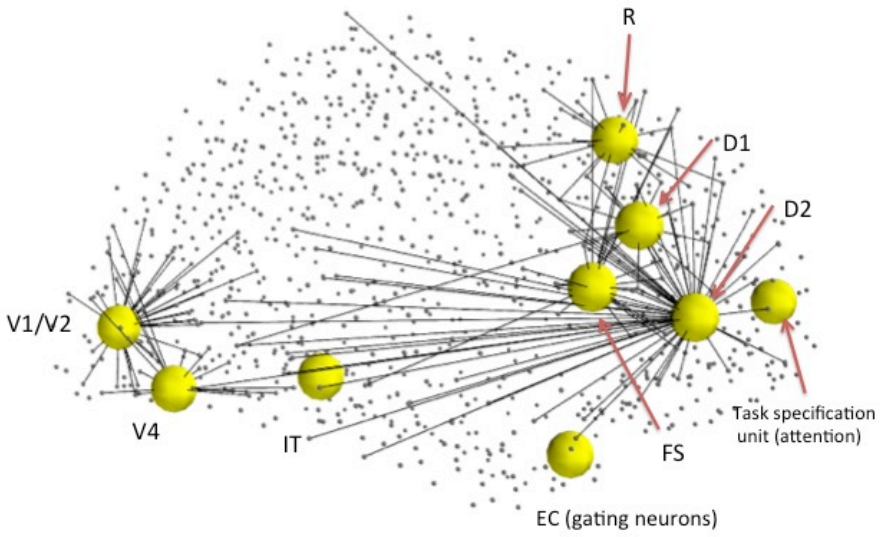

Fig. 2.3 Embedded model in Hagmann's connectome (Hagmann et al., 2008). We first found hypothetical locations for our model's regions of interest (ROIs) and the connected nodes in the connectome (small dots connected to ROIs). We embedded our model of microcircuits and network structure into the structural connectome model of Hagmann et al. (2008). See Ulloa and Horwitz (2016) for details.

connectome. We ran the simulations using our in-house simulator in parallel with Hagmann's connectome using the Virtual Brain software (Sanz Leon et al., 2013). Fig. 2.3 shows the embedded model in the Hagmann's connectome. Overall, the vLSNM embedded in TVB was able to perform the DMS task, generated simulated neural activities in the various brain regions that match empirical data from non-human preparations, and produced simulated functional neuroimaging data that generally agree with human experimental findings (see Ulloa and Horwitz, 2016, for details).

Table 2.1 The Talairach coordinates (Talairach, 1988) and the closest node in the Hagmann's connectome (Hagmann et al., 2008) corresponding to visual LSNM modules. Note that the locations of FS, D1, D2 and FR are not explicitly known (see text) and were chosen only to demonstrate validity of the method.

Modules	Talairach location	Source	Host connectome node
V1/V2	(18, -88, 8)	Haxby et al., 1995	(14, -86, 7)
V4	(30, -72, -12)	Haxby et al., 1995	(33, -70, -7)
IT	(28, -36, -8)	Haxby et al., 1995	(31, -39, -6)
EC	(25, -12, -25)	Hagmann et al., 2008	(25, -12, -25)
FS	Location selected for illustrative purposes		(47, 19, 9)
D1	(42, 26, 20)	Haxby et al., 1995	(43, 29, 21)
D2	Location selected for illustrative purposes		(42, 39, 2)
FR	Location selected for illustrative purposes		(29, 25, 40)

The Talairach coordinates (Talairach, 1988) and the closest node in Hagmann's connectome for each of the vLSNM modules discussed above were identified (see Table 1), based on visual experimental findings (Haxby et al., 1991). As to the prefrontal module, which contains four submodules (FS, D1, D2, R), we used the Talairach coordinates of the prefrontal cortex in Haxby et al. (1995) for the D1 submodule and assigned the locations of adjacent nodes for the rest of the

submodules (FS, D2, R) (see Table 2.1). This arrangement is due to the fact, as mentioned above, that the four types of neuronal populations were based on the experimental findings in monkey PFC during a delayed response task (Funahashi, Bruce, & Goldman-Rakic, 1990). It is not known if these four neuronal types were found in separate anatomical locations in PFC or were found in the same brain region.

2. 3 Simulated experiments

We use the extended model to perform a number of simulated experiments that can include not only one stimulus, but others as well, some of which can be considered to be distractors. The complete set of simulated experiments is the following:

Experiment 1: Single stimulus

We first displayed a single stimulus to the model as a test to observe the responses of different modules of the model to a transient visual input. No response is required. The attention/task parameter is set to a high value (0.3).

Experiment 2: Delayed match-to-sample task

This experiment implemented the original delayed match-to-sample (DMS) task to demonstrate that the new model (with an added node – the entorhinal cortex) continues to perform the DMS task and gives the same results as the original model (Antonio Ulloa & Barry Horwitz, 2016). One typical DMS trial consists of the presentation of a stimulus, an ensuing delay period, a presentation of a probe (the same or a new stimulus) and at the end of it, the simulated subjects need to decide

whether the probe is the same as the first stimulus presented (see Fig. 2.4A). The attention/task parameter is set to high (0.3) during a trial.

Experiment 3: Delayed match-to-sample task with distractors

We implemented a version of DMS task with intervening distractors. The simulated subjects were shown two distractors before the probe was displayed (see Fig. 2.4B). The attention/task parameter is set to high (0.3) for the first stimulus and decreased to low (0.05) following the presentation of the distractors.

Experiment 4: "ABBA" task

A special version of the distractor task (the "ABBA" task) is used. The "ABBA" task was employed by Miller et al. (E. K. Miller, Gochin, & Gross, 1993) in monkey electrophysiology experiments. The model is supposed to hold its response when repeated distractors ("B") are shown and to respond only to the matched stimulus ("A") (see Fig. 2.4C).

Experiment 5: Sternberg's recognition task

A variant of Sternberg's recognition task (Sternberg, 1966, 1969) was used. On each trial of the simulation, three stimuli were presented sequentially, followed by a delay period and then a probe. The subjects' task was to decide whether the probe was a match to any of the three stimuli presented earlier (see Fig. 2.4D). The Sternberg paradigm with visual objects has been used in many studies, and thus allows us to compare our simulated results with experimental results.

A top-down task control is also used before each trial. The top-down task control informs the model that the trial is a DMS task, DMS task with distractors, an "ABBA" task, in which only the first stimulus is the target to be remembered, or a

A

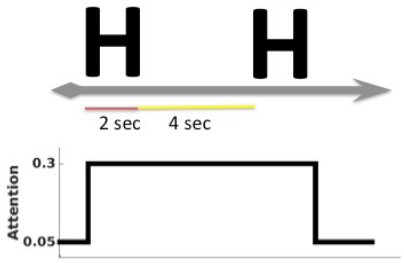
2 sec
4 sec
Attention
0.3
0.05

B

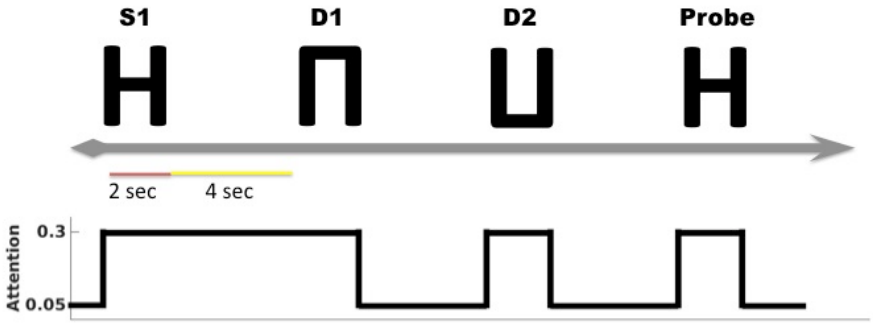
S1
D1
D2
Probe
2 sec
4 sec
Attention
0.3
0.05

C

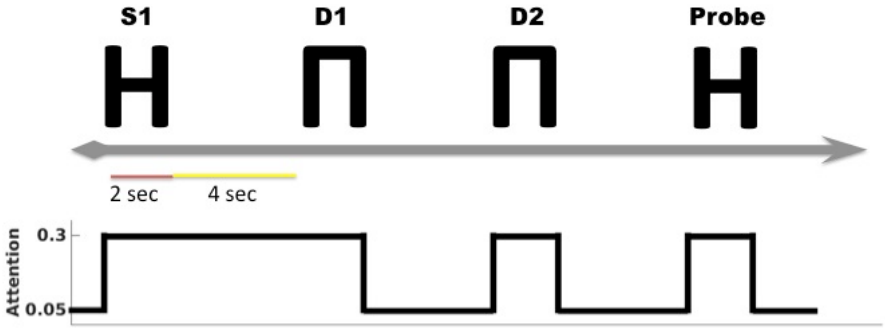
S1
D1
D2
Probe
2 sec
4 sec
Attention
0.3
0.05

D

Fig. 2.4 Timeline designs of implemented tasks. **A**. The timeline and task-parameter/attention level of a single delayed match-to-sample trial. The simulated subjects' task is to identify whether the probe is a match with the first stimulus. **B**. The timeline for a single trial of a DMS task with distractors. The simulated subjects need to ignore the two intervening distractors and only respond to the probe. **C**. The timeline for a single trial of an "ABBA" task, i.e., a DMS task with two repeated distractors. **D**. The timeline for a single trial of Sternberg's recognition task. The simulated subjects are shown a list of stimuli and their task is to decide, after a delay, whether the probe is a match with any stimulus in the list.

Sternberg's recognition task, in which there are multiple targets to remember. The top-down control doesn't change the network structure; it only controls the attention module so as to apply high attention to targets and low attention to distractors.

2. 4 Simulating fMRI

The integrated synaptic activity is computed prior to computing fMRI BOLD activity, by spatially integrating over each LSNM module and temporally integrating over 50 ms (Horwitz & Tagamets, 1999):

$$rSYN = \sum IN_i(t) \tag{2.7}$$

where $IN_i(t)$ is the sum of absolute values of inputs to the excitatory and inhibitory elements of unit i, at time t:

$$IN_i(t) = w_{EE}E_i(t) + w_{EI}E_i(t) + |w_{IE}I_i(t)| + \sum_{k,i} w_{ki}E_k(t) \tag{2.8}$$

The last term is the sum of synaptic connections from all other LSNM units and connectome nodes to the ith unit in LSNM. There are 81 such units in each module (except attention modules which will be discussed later).

In simulating an fMRI study, the model alternately implements a block of DMS task trials (three trials) and a block of control task trials (three trials). The control task used degraded shapes and each trial of the control task followed the design of the DMS task in Experiment 2, except that the attention/task parameter is set to a low value. We first computed the integrated synaptic activity for select regions of interests (ROIs) (Ulloa & Horwitz, 2016). Using the integrated synaptic activity of ROIs as the input to the fMRI BOLD balloon model of hemodynamic

response (Stephan, Weiskopf, Drysdale, Robinson, & Friston, 2007; Antonio Ulloa & Barry Horwitz, 2016), we calculated the simulated fMRI signal time-series for all our ROIs and then down sampled the time-series to correspond to a TR value of 2 seconds.

In each of the tasks, the simulated stimulus was on for 2 seconds (one time step in the model is considered to have a duration of 5 ms) followed by a 4 seconds delay period. After each trial, the model was reset in the intertrial interval. When performing the tasks, we varied the connectivity weights between brain regions by slight amounts to create multiple "subjects" (see (Antonio Ulloa & Barry Horwitz, 2016)). In both the DMS task and the Sternberg's recognition task, the short delay periods between the presentations of stimuli and the probe are the main elements that make the two tasks tests of short-term memory.

2. 5 Results

2. 5. 1 Response to a single stimulus

Fig. 2.5 shows the responses of the different modules of the model when a single visual input (a shape composed of horizontal and vertical line segments) was displayed. The attention level was set to high. Each module of the model exhibited proper behaviors in the simulation. Early visual cortex (V1/V2) responded quickly to the stimulus and displayed a sharp decrease in activity when the stimulus disappeared. As the visual input propagated deeper into the network, the average activity displayed slower and smoother responses. For instance, the average activity

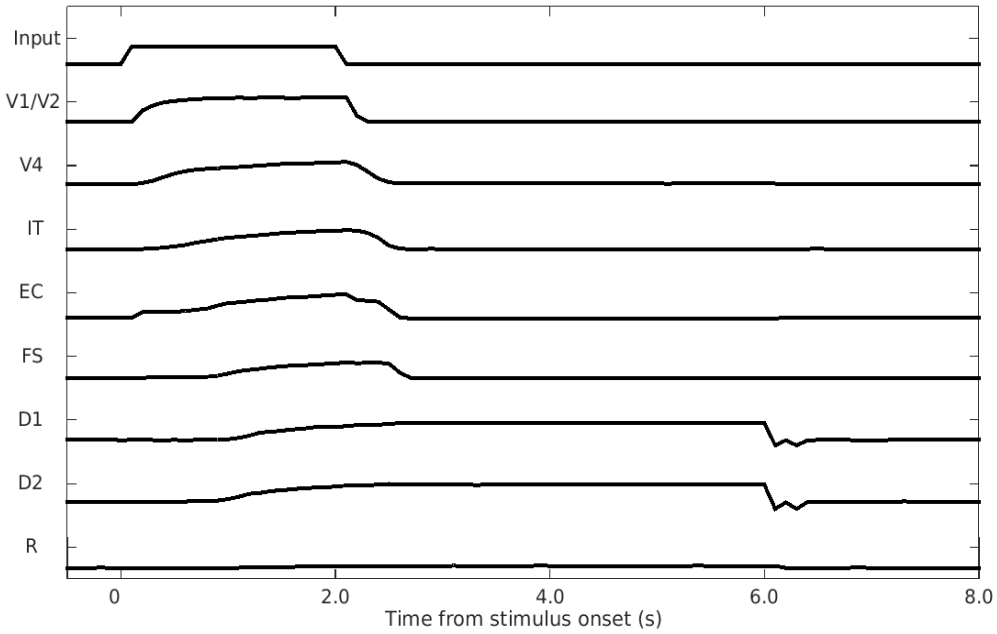

Fig. 2.5 Response of the model to a single stimulus. One stimulus is shown to the model for 2 seconds, followed by a 4-second delayed period before resetting. The vertical axis is the normalized mean neuronal activity (i.e., normalized firing rate) in the different modules.

of working memory modules (D1, D2) slowly climbed during the presentation of the stimulus and displayed persistent activity in the delay period when the stimulus disappeared. The response module (R) showed only noise since only one stimulus was presented.

2. 5. 2 Delayed match-to-sample task

We ran simulations of the delayed match-to-sample condition using both our extended vLSNM and the original vLSNM (Tagamets & Horwitz, 1998; Ulloa & Horwitz, 2016). The simulated neuronal activities of the extended vLSNM and the original vLSNM are shown in Fig. 2.6A. As shown in Table 2.2, the accuracy of simulations run using the extended model is as high as the simulations run using the original model.

The new model also improved the performance of the inferotemporal and prefrontal areas compared with the original model (see Fig. 2.6B). The module representing the inferotemporal area showed higher-than-baseline mean activation level during the delay periods in the delayed match-to-sample task, which eliminated the discrepancy between previous simulation and experimental results. As pointed out in the Introduction, the neurons of the IT module of the original LSNM of Tagamets and Horwitz (Tagamets & Horwitz, 1998) did not show increased activity during the delay period of a DMS trial, in contradiction with nonhuman electrophysiological findings (J. Fuster et al., 1982). To address this small yet important disagreement, we added a feedback connection from the D2 module in PFC to IT. Fig. 2.6A shows the

A

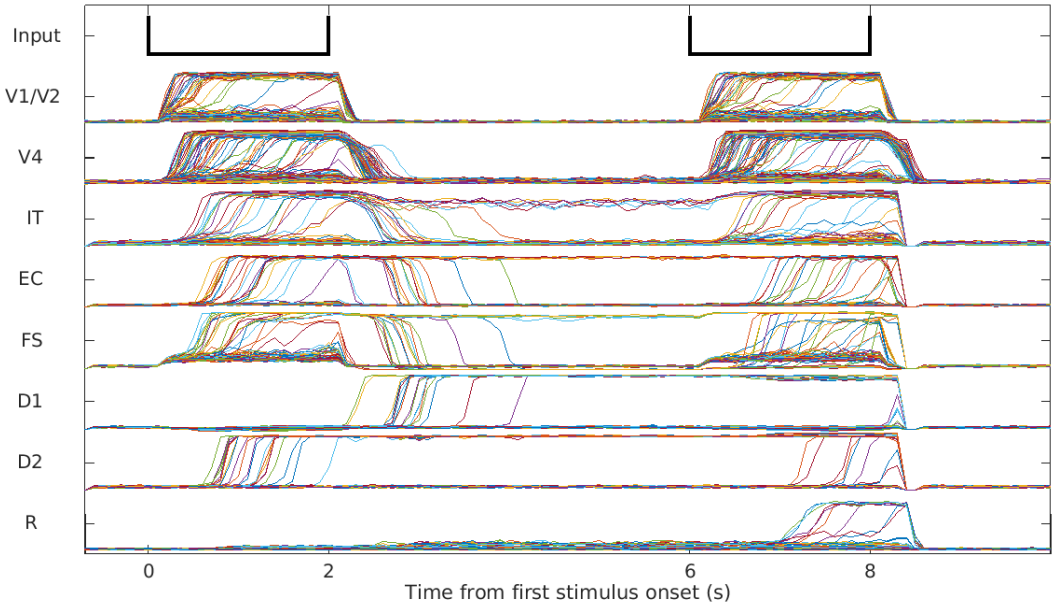

B

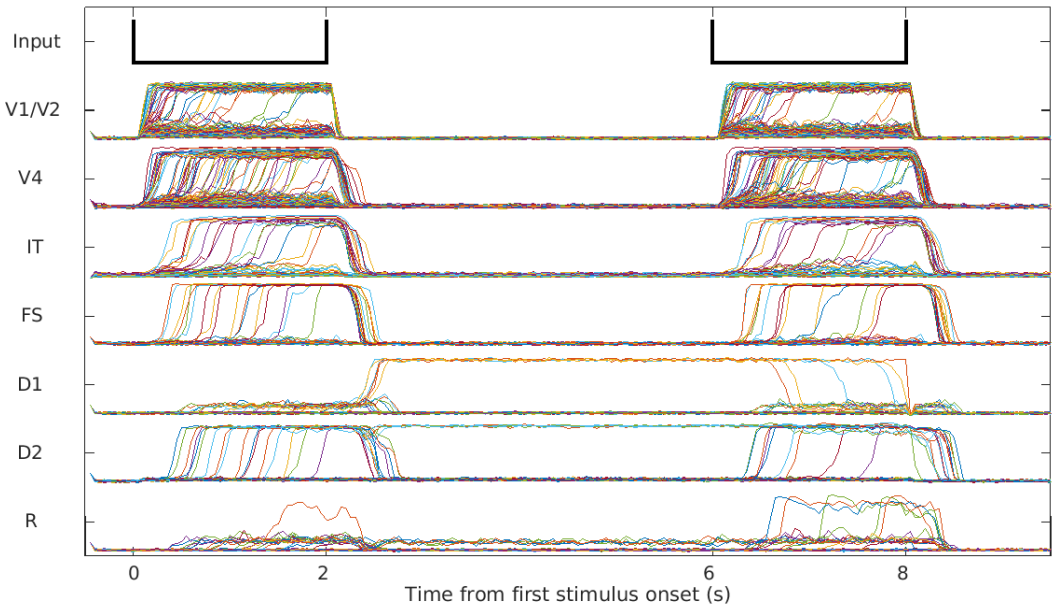

Fig. 2.6 A. Neuronal activities of the excitatory neurons in the different modules during one trial of the DMS task simulated using the extended model. **B**. The excitatory neuronal activities of the different modules during one trial of DMS task simulated using the original model. In the simulations with the new model, the IT module showed activity during the delay period, which does not occur for the original model. Each line corresponding to one simulated neuronal unit.

Table 2.2 Performances of 10 simulated subjects during 4 tasks (DMS task, DMS task with distractors, ABBA task, Sternberg's recognition task). Performances are measured by counting the number of neuronal units in the decision-making module (R) firing above a certain threshold during the response period.

Subject	DMS	DMS w/ distractors	ABBA	Sternberg
S1	92.3%	90.5%	88.7%	90.3%
S2	81.0%	80.5%	80.7%	78.7%
S3	92.0%	92.0%	89.7%	87.0%
S4	86.5%	84.0%	82.3%	82.0%
S5	88.5%	89.0%	87.0%	87.7%
S6	77.5%	75.5%	75.7%	73.0%
S7	81.0%	79.5%	79.0%	78.7%
S8	73.0%	69.5%	68.0%	69.3%
S9	79.0%	79.5%	79.0%	78.0%
S10	84.0%	81.0%	81.7%	79.7%
Mean	84.5%	82.1%	81.2%	80.4%
Standard deviation	6.02%	6.63%	6.15%	6.22%

mean activities of selected modules in a simple delayed match-to-sample task from which the delay activation of the inferotemporal area can be seen.

When looking into individual behaviors of inferotemporal neurons of the extended model, we noticed that these neurons exhibited selectivity to different stimuli (Fig. 2.7). Among activated inferotemporal neurons, most responded to all stimuli with or without delay activity, but neurons with selective activity can be observed in each trial. The data for the multiple-item holding Sternberg's task also displayed similar behaviors of stimulus-selectivity. We did not observe similar behaviors in PFC. This difference between the model's IT and PFC is consistent with experimental results (E. K. Miller et al., 1996) and shows that PFC is mostly involved in working memory and decision-making and thus supporting the idea that PFC neurons have little or no contribution in coding complex visual features.

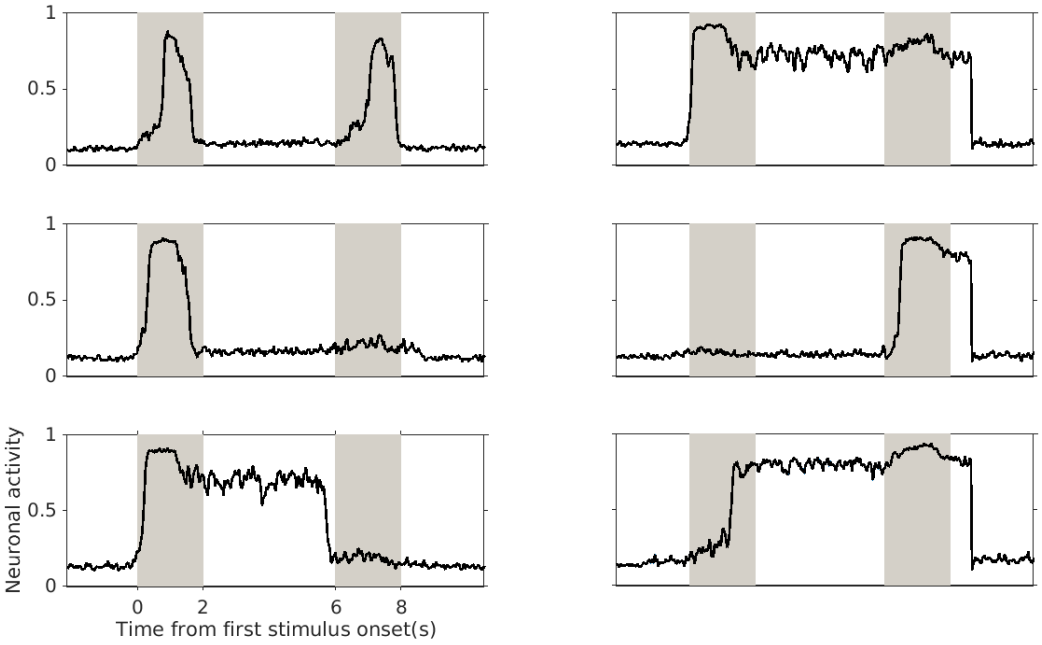

Fig. 2.7 Different types of excitatory neuronal activity and selectivity behaviors of simulated inferotemporal neurons during one DMS trial. Each of the gray stripes represents the presentation of one stimulus and the white stripes between them represent the delay periods. We observed that the simulated neurons in the IT module exhibited several different activity patterns and selectivity to different stimuli. Most of activated inferotemporal neurons responded to both stimuli with or without delay activity (top panel), but in each trial we observed neurons that responded only to the first or the second stimulus (middle and bottom panels); neurons with delay activity are shown in the bottom panel).

A

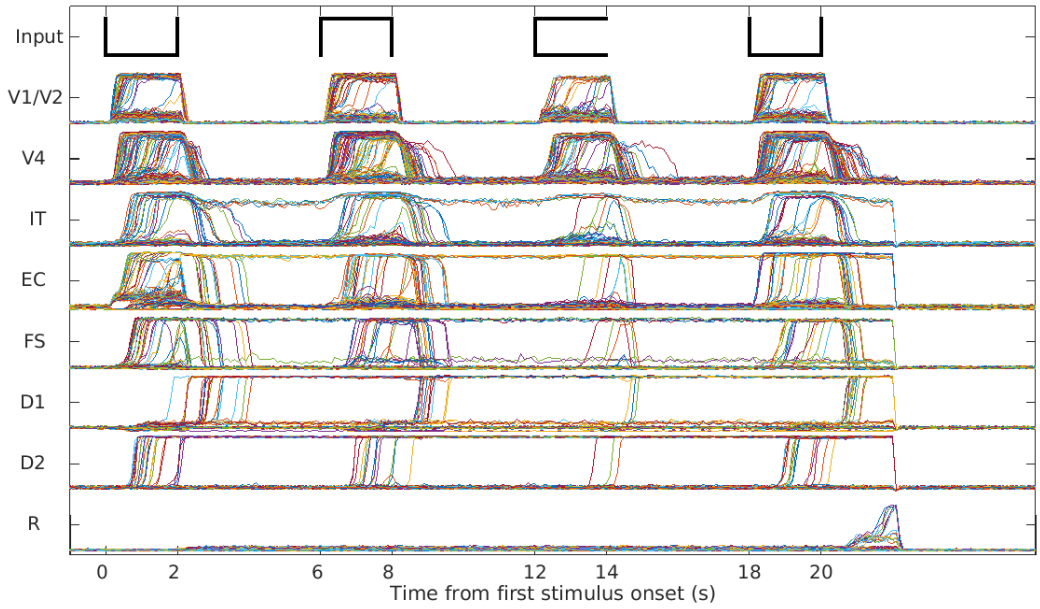

B

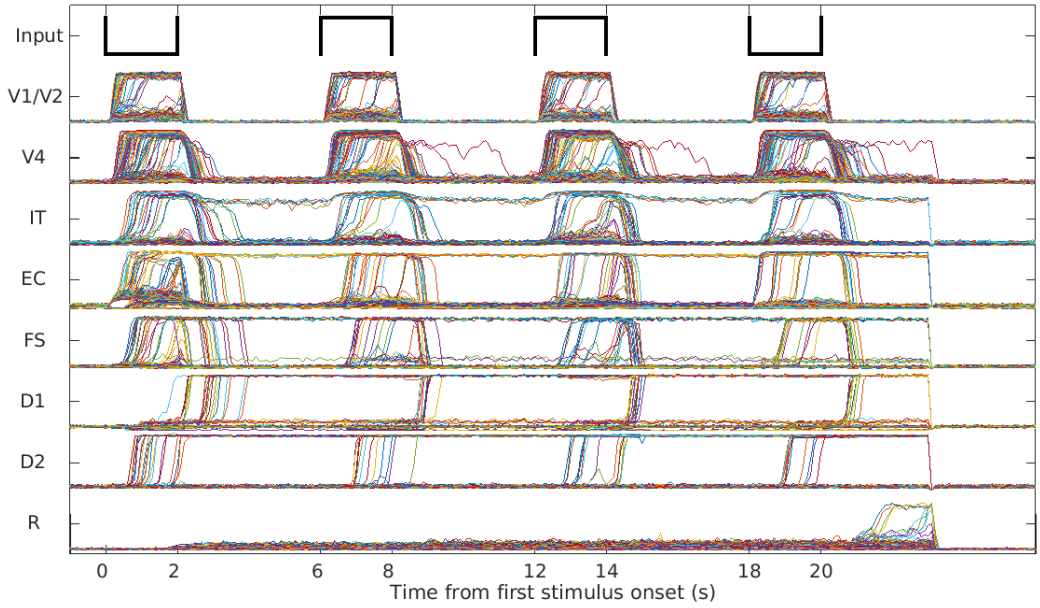

Fig. 2.8 A. Neuronal activities for DMS task with two intervening distractors. **B**. The neuronal activities for the "ABBA" task. The two distractors were held in PFC with low attention (the persistent activities in D1 and D2 modules). The response module in both tasks properly avoided the distractors and responded when the probe was a match of the first stimulus.

2. 5. 3 DMS task with distractors and the "ABBA" task

The model performed the DMS task with distractors and the "ABBA" task at a slightly lower accuracy rate than the simple DMS task (see Table 2.2). Fig. 2.8 shows the simulated neuronal activities of the different modules. Note that the response units display activity greater than background noise only to the stimulus that matches the target.

During the simulation shown in Figs. 2.8A and 2.8B, four separate groups of entorhinal neuronal units responded respectively to the four items and passed the information to prefrontal cortex for storage and comparison. The target (first stimulus) and intervening distractors are all stored in working memory modules (D1 and D2), but in separate groups of neuronal units during the simulation. The target is stored with high attention while the intervening distractors are stored with lower attention. Consequently, the storage of distractors is weaker than the storage of targets, i.e., fewer simulated neuronal units in their D1 and D2 modules showed persistent activity throughout the trial.

2. 5. 4 Sternberg's recognition task

Fig. 2.9 shows the simulated neuronal activity of each module in three trials of Sternberg's recognition task, in which the model successfully responded to two matched cases and rejected 1 non-matched case. The average accuracy rates of 10 simulated subjects can be found in Table 2.3.

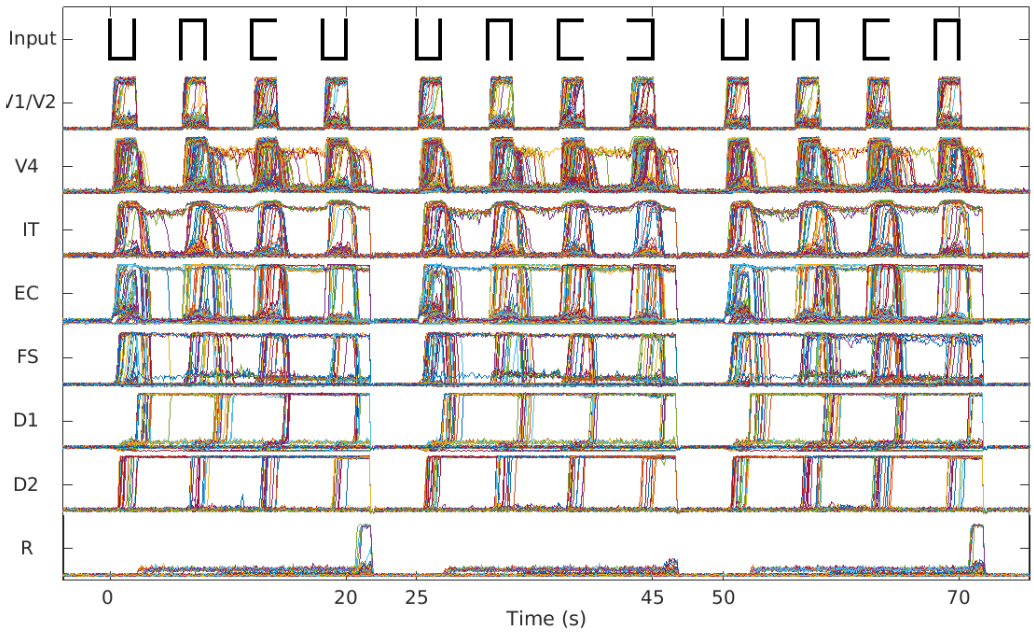

Fig. 2.9 Neuronal activities for Sternberg's task. Three trials of Sternberg's recognition task are shown. In each trial, the first three stimuli are the targets that the model needs to hold in working memory. In the first and last trial, the probe (last stimulus) was a match of one of the targets (the first and the second, respectively) and the response module R made proper responses. In the second trial shown, the probe was not a match of any of the targets and R didn't respond to it.

In the simulated results of the Sternberg's recognition task, we noticed a significant primacy/recency effect. When the test stimulus is a match with the first or the last item of the three items remembered, the model has a greater chance to make a correct response than when the test stimulus is a match with the second item (see Table 2.3). The recency effect is stronger than the primacy effect. We will discuss our tentative explanation of this finding in the Discussion.

Table 2.3. Performances of 10 simulated subjects during Sternberg's task when the probe is a match of the first, the second and the third target, respectively.

	Target 1	**Target 2**	**Target 3**
S1	91%	87%	93%
S2	81%	76%	79%
S3	86%	85%	90%
S4	81%	80%	85%
S5	88%	87%	88%
S6	72%	70%	77%
S7	78%	79%	79%
S8	70%	66%	72%
S9	78%	77%	79%
S10	79%	78%	82%
Mean	80%	79%	82%
Standard deviation	6.28%	6.53%	6.17%

In simulating the holding of multiple items in short-term memory, one interesting finding related to the feedback from PFC to IT is that many simulated neurons in both PFC and IT displayed a progressive increase in activity level across the DMS trial with multiple distractors and the Sternberg task (Fig. 2.10). This type of behavior could not be observed once we removed the feedback from PFC to IT.

A

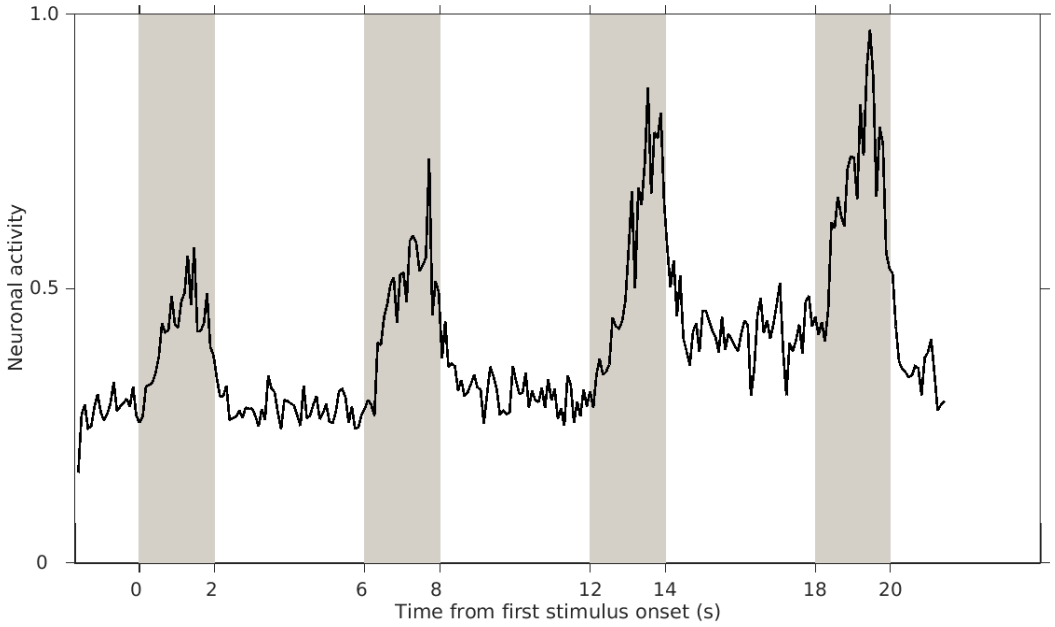

B

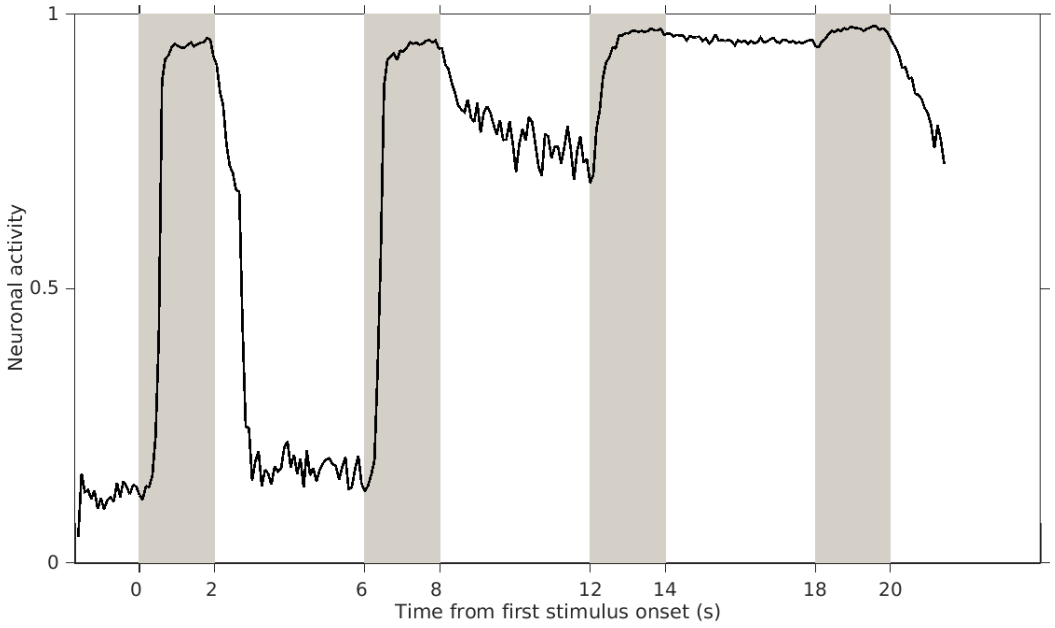

Fig. 2.10 Simulated neurons with climbing activities during one trial of Sternberg's task. **A**. Activity of one neuron found in the PFC module. **B**. Activity of one neuron found in the IT module. Each of the grey stripes indicates the presentation of one stimulus and the white stripes between the grey are delay periods.

We found neurons with climbing activity in both PFC and IT while monkey physiological studies have reported such activity only in PFC (Miller et al., 1996).

2. 5. 5 Simulated fMRI BOLD signal

As discussed in the Methods section, we implemented an experiment that consisted of alternative blocks of DMS trials and control trials (passive viewing of degraded shapes), and then calculated the integrated synaptic activity and fMRI BOLD time series for select regions of interest (ROIs). Fig. 2.11A and Fig. 2.11B show the integrated synaptic activity and fMRI BOLD signal, respectively, for ROIs during three blocks of DMS task (grey) and three blocks of the control task (white). Each block consists of three trials. We can conclude from the figures that the modules of higher order show more signal change between the DMS and control tasks. Early visual cortex V1/V2 did not show much change between DMS trials and control trials, but higher order modules such as PFC module and entorhinal cortex module displayed much larger changes.

Fig. 2.11C shows a comparison, using signals from V4 module as an example, between the integrated synaptic activity and fMRI BOLD signal. From the figure we see that using such a block design, the simulated BOLD signal cannot isolate the detailed response profile for each stimulus, as is well known to the experimental research community.

We also performed a simulated event-related experiment by extending the delay period to 20 seconds in order to show a more complete response curve in BOLD signal for each incoming stimulus. Fig. 2.12 shows the simulated fMRI BOLD

A

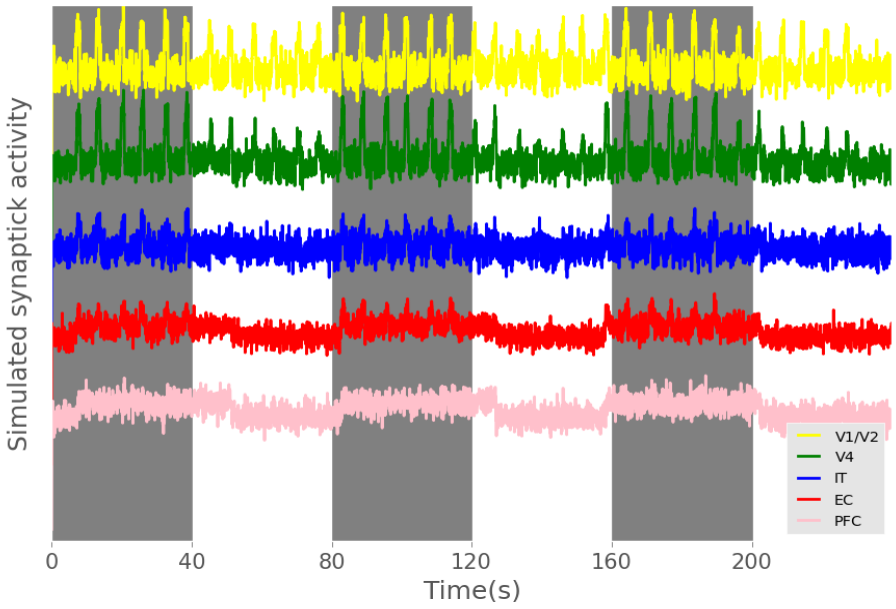
Simulated synaptick activity
0
40
80
120
160
200
Time(s)
V1/V2
V4
IT
EC
PFC

B

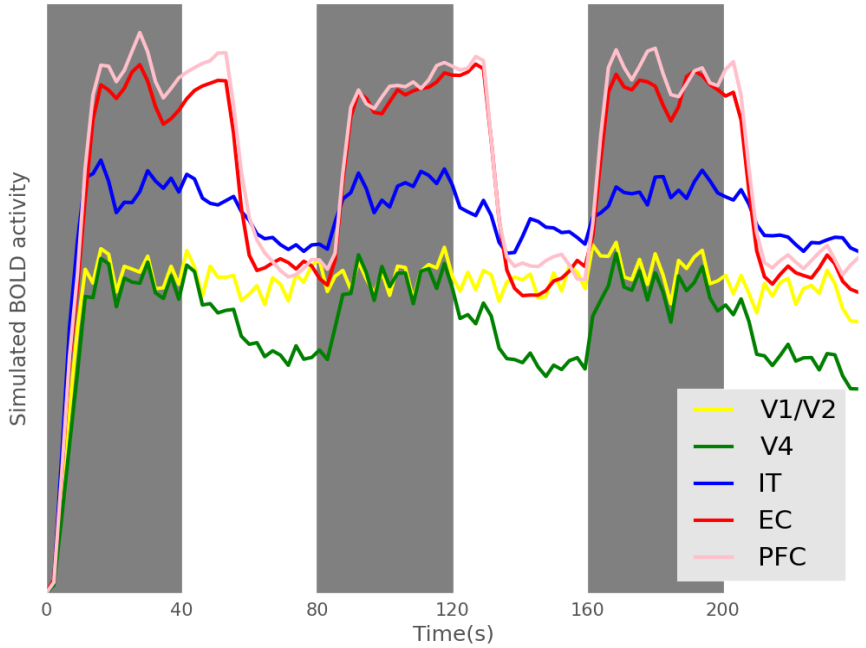
Simulated BOLD activity
0
40
80
120
160
200
Time(s)
V1/V2
V4
IT
EC
PFC

C

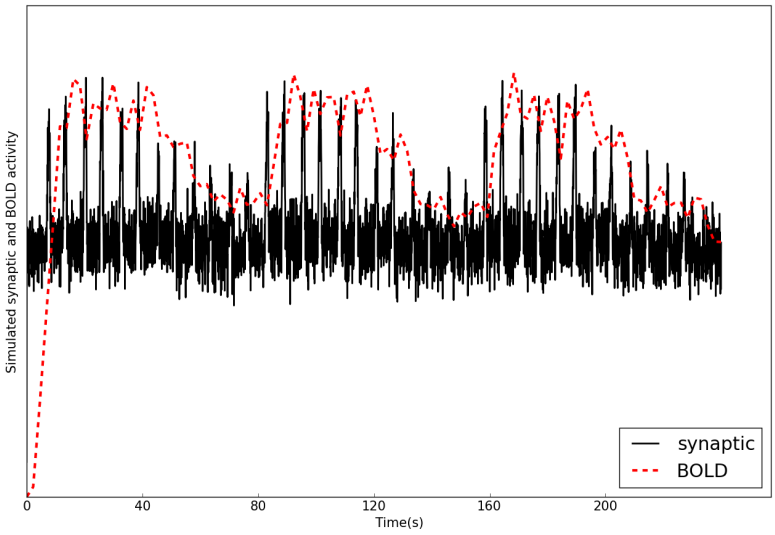

Fig. 2.11 A simulated experiment with three blocks of alternative DMS trials (gray stripes) and control trials (white stripes) was implemented. Each block consisted of three trials. **A**. The integrated synaptic activity of different modules. **B**. The simulated fMRI BOLD signal of the different modules. Modules of higher order have larger difference in activity between the DMS and control tasks. **C**. A comparison of the simulated synaptic activity and the fMRI BOLD signal of the V4 module during the simulated experiment for one task and one control block.

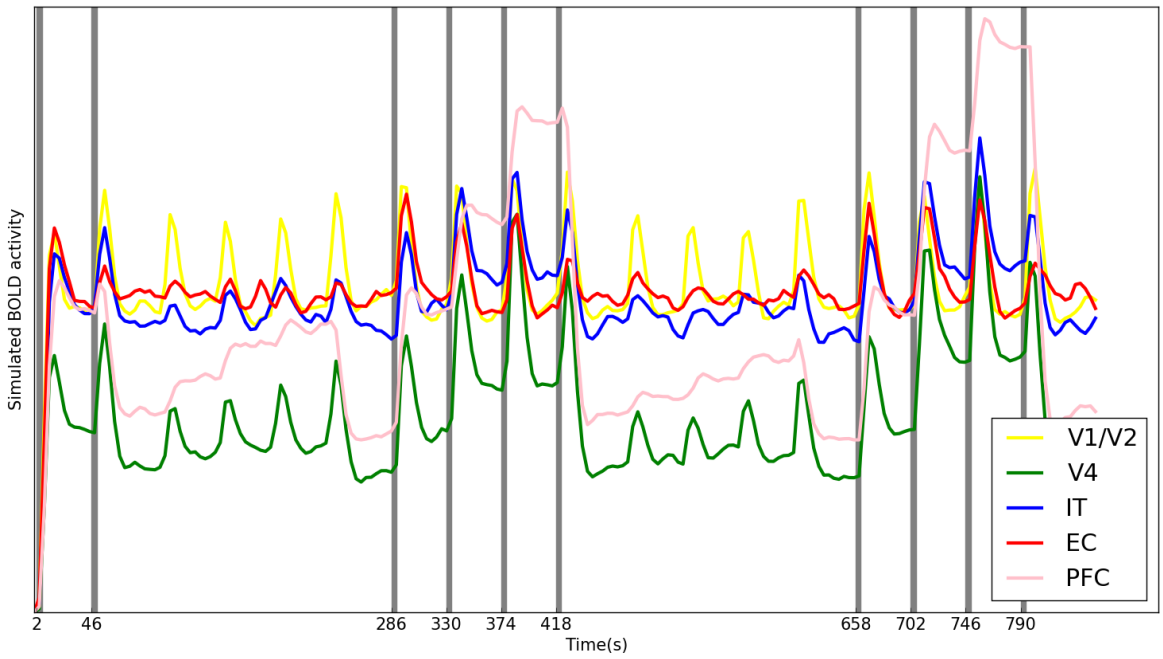

Fig. 2.12 The simulated fMRI BOLD signals of different modules of an event-related experiment. Each gray bar represents the presentation of a stimulus. The experiment consists of one DMS trial (first two gray bars), one DMS trial with two distractors (the middle four gray bars) and one trial of Sternberg's task (the last four gray bars). Passive viewing of 4 stimuli separates each of these task trials. The V4 (orange), IT (blue), EC (black) and PFC (red) modules showed higher fMRI BOLD signals when the working memory load increased (DMS vs. Sternberg's task).

signal for an event-related design that consists of a DMS trial, a DMS trial with two intervening distractors and a Sternberg's task trial. The signal differences between these tasks and the control task (passive viewing) were calculated and are shown in Table 2.4.

Table 2.4. The mean signal change (in percentage) of specific task from control task (passive viewing). Both integrated synaptic activity and fMRI data of different brain regions are shown. Paired t-test was used for the signal difference and * = $p<0.05$.

	Integrated synaptic activity			**fMRI**		
	DMS	DMS w/distractors	Sternberg's task	DMS	DMS w/distractors	Sternberg's task
V1	6.533*	5.318*	8.702*	2.739	1.841	3.028
V4	25.786*	27.861*	29.250*	23.034*	25.548*	26.947*
IT	13.318*	16.470*	18.852*	11.750*	14.824*	15.773*
EC	8.161*	8.803*	10.182*	5.709*	8.871*	9.098*
PFC	25.083*	28.915*	32.594*	20. 623*	23.647*	26.992*

By employing such a design, we could examine the effect of working memory load (by comparing the DMS task with the Sternberg task) and the effect of attention (by comparing the Sternberg's task with the DMS task with distractors). The V1/V2 module did not show statistically significant differences in terms of mean fMRI BOLD signals between the DMS tasks and the control tasks. We observed that the entorhinal cortex displayed greater activity, compared with the control task, during encoding (stimuli presentations) and retrieval (probe presentations) but not during maintenance (delay periods), which was consistent with experimental findings (Schon, Quiroz, Hasselmo, & Stern, 2009). V4, IT and PFC showed increased activity during the delay periods, which indicated their roles in working memory maintenance. The activity of PFC increases when multiple items are stored, which agrees with the

experimental evidence for both visual working memory (Cairo, Liddle, Woodward, & Ngan, 2004; Druzgal & D'Esposito, 2003; Rypma, Berger, & D'Esposito, 2002; Rypma & D'Esposito, 1999) and verbal working memory (Veltman, Rombouts, & Dolan, 2003). We also noticed the effect of working memory load for V4 and IT during encoding and maintenance (stimuli presentations and delay periods), but not during the retrieval phase (probe presentation).

2. 6 Discussion

We have presented a simulation study of several short-term memory tasks using an extended version of a previously constructed large-scale neural model. We successfully implemented multiple short-term memory tasks using this extended model and produced neuronal patterns in visual cortex, IT, EC and PFC that match experimental findings. These short-term memory tasks can include distractor stimuli, or can require that multiple items be retained in mind during a delay period.

Fuster and Jervey (J. M. Fuster & Jervey, 1982) first revealed in primate single-unit recording studies that inferior temporal neurons exhibit sustained, increased activity during the short delay of a delay match-to-sample task. A number of later studies have also supported the notion that inferior temporal cortex is important for the maintenance of visual object information (Horel et al., 1987; Petrides, 2000; Ranganath & D'Esposito, 2005). The neuronal behaviors in IT across short delays in DMS trials were indicated to be relevant to object-selective activity and associative learning (Erickson & Desimone, 1999; E. K. Miller et al., 1993; Miyashita, 1988). The extended version of our large-scale neural model, compared to

the original version, explicitly implements this critical role for IT, which is important for extending our model to incorporate a long-term memory component.

Fuster and colleagues first reported the presence of PFC neurons with climbing activity across delay periods in DMS trials without distractors (Quintana & Fuster, 1992). Similar behavior was also observed in DMS trials with distractors (E. K. Miller et al., 1996). Fuster and colleagues interpreted the climbing activity as expectation. Our model doesn't have expectation built-in; rather, our simulations suggest that the climbing activity is related to feedback from PFC to IT, i.e., a recurrent loop is formed with feedback from PFC to IT so that the information stored in PFC can strengthened itself through the loop, and it represents the working memory distributed in the network. These two notions of the neural mechanism for the observed climbing behavior may in fact complement one another.

We modeled working memory using the D1-D2 microcircuit as a fixed state. Meanwhile, the recurrent connectivity between PFC and IT in our model enables a network dependent mechanism of working memory represented by the "climbing neurons" we observed. There is experimental evidence for both views of working memory. Persistent activity of neurons in PFC was observed during the delay period by Funahashi et al. (Funahashi et al., 1990), while some neuronal activity in PFC declined and was reactivated during delay period (Barak, Tsodyks, & Romo, 2010; Rainer & Miller, 2002), indicating the existence of a dynamic mechanism for working memory.

In the simulations of DMS with distractors and the "ABBA" task, we assumed that the intervening distractors are also stored in the prefrontal cortex. Due to the low

attention level applied, the storage of distractors is weaker than the storage of targets. Experimental studies in visual search and incidental learning supports our assumption that the distractors are stored in working memory (Goolsby, Shapiro, & Raymond, 2009; Williams, Henderson, & Zacks, 2005). We used separate working memory modules to handle distractors in the DMS task based on the fact that the attention paid to the distractors is lower than the target and the target has a special status in working memory that is not shared by the distractors (Peters, Goebel, & Roelfsema, 2009). The structural network of multiple working memory modules was inspired by a similar scheme proposed by Ulloa et al. in an auditory model that dealt with long-duration tonal patterns (Ulloa et al., 2008). The capacity limit of working memory is implemented by limiting the number of memory pools (we used three, but the number is arbitrary). Once the memory pools are all filled, further items will not be stored and the corresponding BOLD signal will reach a plateau. This was instantiated in our model for simplicity, but future research could aim toward determining whether or not this assumption is warranted.

Whereas the classic view is that working memory has a limited number of slots (Cowan, 2001), some recent experimental and modeling studies propose working memory as a continuous resource that is distributed among all remembered items (Bays & Husain, 2008; Fougnie, Suchow, & Alvarez, 2012; Keshvari, van den Berg, & Ma, 2013; Ma, Husain, & Bays, 2014). According to this view, the precision of memory, which decreases as more items are remembered, is the key metric of working memory limits instead of the quantity of memory items. In our model, the

working memory representations of different items are stored in non-overlapping PFC modules, which, in the future, could be integrated into one continuous module.

Even though we did not explicitly set out to incorporate a primacy and recency effect in our model, nonetheless, we observed such effects in our simulation results. In our model, the observed primacy effect in the Sternberg task was a result of decayed attention. In our simulated experimental design, the attention applied to the prefrontal area decays with time and higher attention helps the working memory network encoding for new items. The neural basis underlying the experimentally observed recency effect has been debated (A. D. Baddeley & Hitch, 1993). Based on our simulation, we suggest that the gating mechanism, specifically competitive inhibition and the inhibitory feedback from PFC to entorhinal cortex, may contribute to the recency effect. The inhibitory feedback from PFC to entorhinal area reduces the competition level among gating neurons; thus, later incoming stimuli have less inhibition and stronger representations in working memory. Previous experiments have shown that these effects are sensitive to the duration of the delay periods (Wright, 1999), which we have not observed in our simulation study, possibly due to a lack of a "forgetting" mechanism in the current version of the model.

Because working memory is such an important cognitive process, many research groups have developed models of this process. They range from purely cognitive models (A. Baddeley, 1992) to computational models of varying levels of complexity (e.g., (D. J. Amit, Fusi, & Yakovlev, 1997; Ashby, Ell, Valentin, & Casale, 2005; Dehaene & Changeux, 1989; Rolls, Dempere-Marco, & Deco, 2013); for reviews, see (Barak & Tsodyks, 2014; Durstewitz, Seamans, & Sejnowski, 2000;

Maex & Steuber, 2009). Many computational models aimed to account for both behavioral and neural activity observed in monkey electrophysiological studies during the delay portion of a delayed response task. For instance, one approach, exemplified by Amit and colleagues (e.g., (D. J. Amit et al., 1997) employed recurrent excitatory connections in a cell assembly to maintain stable activity patterns (i.e., attractors). In initial studies, Hebb-like learning methods were employed to generate synaptic weights that reinforced the connections between specific neurons. These attractor models initially dealt with maintaining in short-term memory one or more previously learned images. More recent work has extended these models so that novel images can also be handled (e.g., (Y. Amit, Yakovlev, & Hochstein, 2013). Although a number of modeling efforts addressing working memory have focused on the prefrontal cortex, a substantial number have also argued that the basal ganglia play an important role as well (e.g., (Ashby et al., 2005; Monchi & Taylor, 1999). The modeling framework proposed by Ashby et al. (Ashby et al., 2005) is of particular interest because, like the model we presented in this paper, it also provides a distributed neurocomputational model that incorporates multiple, interacting brain regions, and aims to account for both neurophysiological data and behavioral data. Furthermore, the authors argue that this approach, like ours, also can account for human neuroimaging data (Ashby & Valentin, 2007).

The basal ganglia and the thalamus have been implicated in working memory function. Lesions of caudate and medial dorsal nuclei of the thalamus can severely impair working memory capacity (Kubat-Silman, Dagenbach, & Absher, 2002). However, as pointed out by Ashby et al. (2005), lesions of the caudate and medial

dorsal nuclei of the thalamus can impair but will not abolish working memory, and this has been found experimentally (e.g., Gabrieli et al, 1996; Janahashi et al., 2002). It is worth noting that the examples used in this paper deal with a rather limited working memory capacity (i.e., no more than three objects).

The interactions between the PFC and the basal ganglia and the thalamus have also been interpreted as a gating mechanism (Braver & Cohen, 2000; J. D. Cohen, Braver, & O'Reilly, 1996; O'Reilly & Frank, 2006). For example, the O'Reilly-Frank working memory model incorporates a prefrontal cortex that controls both itself and other brain areas in a task-dependent manner. It does this by employing learning mechanisms that involve a number of subcortical structures including the basal ganglia that act as a gating mechanism for updating working memory. However, the EC is considered to be directly involved in the visual ventral (object) processing pathway and declarative memory encoding (Preston & Eichenbaum, 2013).

In the current paper, we chose parameters for the added components of the model so as to provide a reasonable match to the electrophysiological data, although we did not employ explicit model-fitting to any particular data set. As pointed out by Ashby et al. (2005), there is much variability between cells in monkey electrophysiological data, which may preclude quantitative data fitting. Moreover, another reason that explicit data-fitting was not employed was that there are numerous data sets (behavioral performance, electrophysiological data in multiple brain regions, fMRI activation and connectivity data, MEG/EEG data) that we want our model to account for. These data have different featural and temporal characteristics. It is not clear to us how in principle one should go about fitting all

these data simultaneously. In fact, as far as the neuroimaging data is concerned, other researchers (e.g., Friston, Preller et al., in press) have just begun to develop a systematic approach to this problem.

Some caveats of our work include: the attention level and the top-down task control we used in the model are not realistically modeled; we hypothesized that the entorhinal cortex was responsible for a gating process, which needs to be confirmed by experiments; the locations we chose for prefrontal nodes (D1, D2, FS, R) in the Virtual Brain are somewhat arbitrary.

In summary, we have performed several short-term memory tasks using one large-scale neural network model, and studied various neuronal behaviors in the inferotemporal cortex and prefrontal cortex. We modeled working memory with local microcircuits (D1, D2) and a large-scale recurrent network (PFC, IT), which produced neuronal behaviors that matched experimental findings. For generating a brain-like environment, we embedded the model into The Virtual Brain framework. The model in the future can be extended to incorporate more brain regions and functions, such as long-term memory. Our results indicate that computational modeling can be a powerful tool for interpreting human and nonhuman primate neuroimaging data.

Chapter 3: Modeling visual-auditory bimodal processing and crossmodal attention capture of salient stimuli

3. 1 Attention

Attention is a crucial cognitive function for humans to select goal-relevant information among vast sensory stimuli in the environment. On the other hand, attention can be captured by salient goal-irrelevant distractors. This mechanism allows us to focus on behavioral goals while staying vigilant to environmental changes, which is usually described as two separate types of attention: endogenous (voluntary/goal-driven) attention and exogenous (involuntary/stimulus-driven) attention (Posner & Cohen, 1984). Endogenous attention is thought to be controlled by a top-down process, starting from frontal lobe and connecting back to early sensory areas. In contrast, exogenous attention behaves primarily in a bottom-up manner, triggered by distractions which are task irrelevant but salient in a given context (Hopfinger & West, 2006; Yantis & Jonides, 1990).

Working memory, where selected information is temporarily stored, relies on endogenous attention for protection from distractions. However, working memory is not completely protected and is capable of handling unexpected and salient distractions mediated by exogenous attention. Early studies on the relationship between working memory and attention focused mostly on the role of endogenous attention in working memory encoding and maintenance (A. Baddeley, 1986, 1996). Later, some EEG and behavioral studies have shown that working memory can also

control exogenous attention and reduce distractions (Berti & Schroger, 2003; SanMiguel, Corral, & Escera, 2008), yet little is known about the brain network mediating such effect. The present study aimed to investigate and propose a possible neural mechanisms of how endogenous and exogenous attention interact with each other, and how working memory controls exogenous attention switching.

As we have shown in Chapter 1, the large-scale neural model of visual object processing is a powerful tool for testing the neural mechanisms mediating cognitive functions. Later an auditory object processing model was built in parallel with the visual model (Husain et al., 2004). The two large-scale neural models were designed to perform a short-term recognition memory delayed match-to-sample (DMS) task. During each trial of the task, a stimulus S1 is presented for a certain amount of time, followed by a delay period in which S1 has to be kept in short-term memory. When a second stimulus (S2) is presented, the model has to respond as to whether S2 matches S1. Recently, the visual model was extended to be able to manage distractors and multiple objects in short-term memory (Liu et al., 2017). The extended visual model successfully performed the DMS task with distractors and Sternberg's recognition task (where subjects are asked to remember a list of items and indicate whether a probe is on the list).

In this chapter, we present a simulation study of crossmodal attention capture, and how working memory load can affect this process. We first extend the aforementioned large-scale neural model with "endogenous attention" and "exogenous attention". Attention is the neuronal activity in attention modules that are connected to working memory. We add a pair of modules representing the

"exogenous attention" for auditory and visual processing. These two modules compete with each other based on the salience of auditory and visual stimuli, and assign the value of attention together with endogenous attention. The endogenous attention is set according to task specification before each simulation. Then we simulate crossmodal attention allocation and various bimodal (i.e., auditory and visual) short-term memory tasks. Simulations show the "working memory load effect", i.e., higher working memory load in one modality reduces the distraction from another modality, which has been reported in a number of experimental studies (Berti & Schroger, 2003; SanMiguel et al., 2008). In the present study, we interpret saliency as the amplitude of an input signal.

Furthermore, we also note that higher working memory load can increase distraction from the same modality. We propose the neural mechanisms that underlie crossmodal attention switch and how working memory load modulates attention allocation between different modalities.

3. 2 The structural network of auditory processing and attention

The structural network of the combined auditory and visual model is shown in Fig. 3.1. We use a flavor of Wilson-Cowan units as the basic units of our model, which consists of one excitatory unit and one inhibitory unit (see Fig. 2.1A). One basic unit can be considered as a simplified representation of a cortical column. Each module of the auditory network is explained in detail in the following. Submodules of A1 and A2 are organized as 1×81 arrays of basic units, and all the other modules are

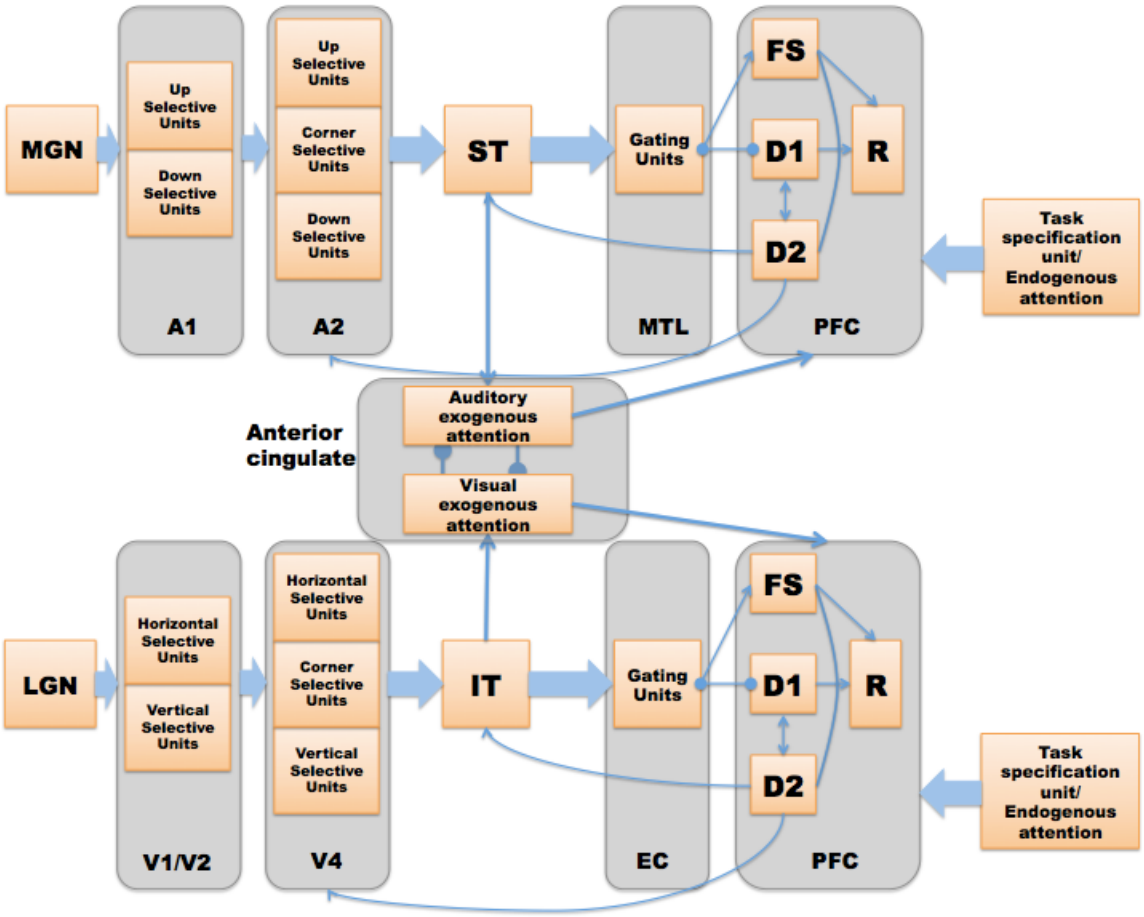

Figure 3.1 The network diagram of the large-scale auditory-visual neural model. Arrows denote excitatory connections; lines ending in circles denote inhibitory connections. The anterior cingulate (the red dot) (A. Ulloa & B. Horwitz, 2016) (A. Ulloa & B. Horwitz, 2016) performs as the exogenous attention module and where the visual-auditory attention competition occurs. See text for details.

9×9 arrays of basic units. For the details of the visual model, please see (Liu et al., 2017; Tagamets & Horwitz, 1998).

A1

In the auditory model, the early cortical auditory areas are combined as A1, which is analogous to the V1/V2 module in the visual model. A1 corresponds to the core/belt area in monkeys (Kaas & Hackett, 1999; Rauschecker, 1998) and the primary auditory area in the transverse temporal gyrus in human or Brodmann Area 41 (Talairach, 1988). Based on experimental evidence that the neurons in primary auditory area are responsive to the direction of frequency modulated sweeps (Bieser, 1998; Mendelson & Cynader, 1985; S. A. Shamma, Fleshman, Wiser, & Versnel, 1993), module A1 is designed to consist of two types of neuronal units: upward-sweep selective and downward-sweep selective units. The two submodules are organized as 1×81 arrays of basic units due to the fact that in auditory cortex sounds are represented on a frequency-based, one-dimensional (tonotopic) axis (Schreiner, Read, & Sutter, 2000; S. Shamma, 2001).

A2

The A2 module is designed to be a continuation of A1 and consists of three populations of units: upward sweep selective units, downward sweep selective units and contour selective units. The upward sweep selective units and downward sweep selective units have a longer spectro-temporal window of integration than those in A1 so that they are selective for longer frequency sweeps. The contour selective units are selective to changes in sweep directions, which are analogous with the corner selective units in the visual model. The A2 module represents the lateral belt/parabelt

areas of primate auditory cortex. In experiments, parabelt neurons are found to be selective to band-pass noise stimuli and FM sounds of a certain rate and direction (Rauschecker, 1997).

ST

The third processing module of the auditory model is ST which stands for superior temporal cortex, including superior temporal gyrus and/or sulcus and the rostral supratemporal plane. Functionally, ST is equivalent to the IT (inferior temporal) module in the visual model, and acts as a feature integrator, containing a distributed representation of the presenting stimulus (Hackett, 2011; Tagamets & Horwitz, 1998). This functional equivalency is supported by experimental studies that neurons in ST respond to complex features of stimuli (Kikuchi, Horwitz, & Mishkin, 2010) and a lesion of ST impairs auditory delayed match-to-sample performance (Colombo, Rodman, & Gross, 1996; Fritz, Mishkin, & Saunders, 2005).

MTL

The module MTL represents the medial temporal lobe which serves as a gate between ST and PFC. The gating mechanism is incorporated to avoid the working memory of one stimulus being overwritten by later-arriving stimuli. Anatomical studies on monkeys (Munoz, et al. 2009) have revealed that medial temporal lobe ablation disconnects the rostral superior temporal gyrus from its downstream targets in thalamus and frontal lobe.

Several groups of neurons in MTL are designed to competitively inhibit one another so that only one group of gating neurons will be activated when a stimulus

comes in. Once the item is stored in this working memory buffer, an inhibitory feedback from PFC to MTL cortex will suppress the active gating neurons and release other gating neurons so that the remaining gating neurons are ready for new stimuli. We are assuming that each group of entorhinal gating neurons could be used only once during a task trial.

PFC

The module PFC represents the prefrontal cortex in both visual and auditory models. In the visual model, neurons in the PFC module can be delineated into four types based on experimental data acquired by Funahashi et al. (Funahashi et al., 1990). In our auditory model, the same four types of neuronal populations were employed analogously (Husain et al., 2004). Submodule FS contains cue-sensitive units that in general reflect the activities in the IT (ST) module. D1 and D2 submodules form the short-term memory units by exciting one another during the delay period. Recently, we have built in multiple sets of D1 and D2 submodules into the visual model (Liu et al., 2017) and successfully implemented tasks that held more than one item in short-term memory, and in the present study we employ the same extension in the auditory model. R serves as a response module (output). It responds when a displayed stimulus (probe) matches the cue stimulus that is being held in short-term memory. Note that we assume that there are a limited number of gating units and a similar limited number of D1-D2 units, since empirical studies indicate that only a limited number of items can be simultaneously kept in short-tem memory (e.g., the so-called 7±2 (G. A. Miller, 1956); others have proposed a more limited capacity such as 3 or 4 (Cowan, 2001)). For computational simplicity, in this paper we will employ no more than

three items.

Anterior cingulate cortex (ACC)

The newly added ACC is represented by a pair of modules where the outputs of visual and auditory processing stream are taken as inputs and used to generate exogenous attention. The anterior cingulate is known for its possible role in integrating sensory information from different brain regions for salience computation (Etkin, Egner, & Kalisch, 2011; Menon & Uddin, 2010). In our model, ACC receives its inputs from IT in the visual model and ST in the auditory model, and assigns values to the visual and auditory attention/task-specific unit. In the current study, ACC processes the visual-auditory bimodality competition that leads to involuntary attention switch. ACC is also potentially crucial in modeling the processing of visual-auditory association (Wang, Tse, & Morris, 2012).

Fig. 3.2 shows the embedded visual and auditory models in the Hagmann's connectome. We first found the hypothetical regions of interest (ROIs) corresponding to each module in our model and the connected nodes in Hagmann's connectome. Then we embedded our revised model of microcircuits and network structure into the connectome (see Ulloa and Horwitz, 2016, for details). We ran the simulations using our in-house simulator in parallel with Hagmann's connectome using the Virtual Brain software (Sanz Leon et al., 2013).

In both the visual and auditory models, a task specification module is used to provide low-level, diffuse incoming activity to the D2 module in the prefrontal area which can be interpreted as an attention level. The module is located arbitrarily in the

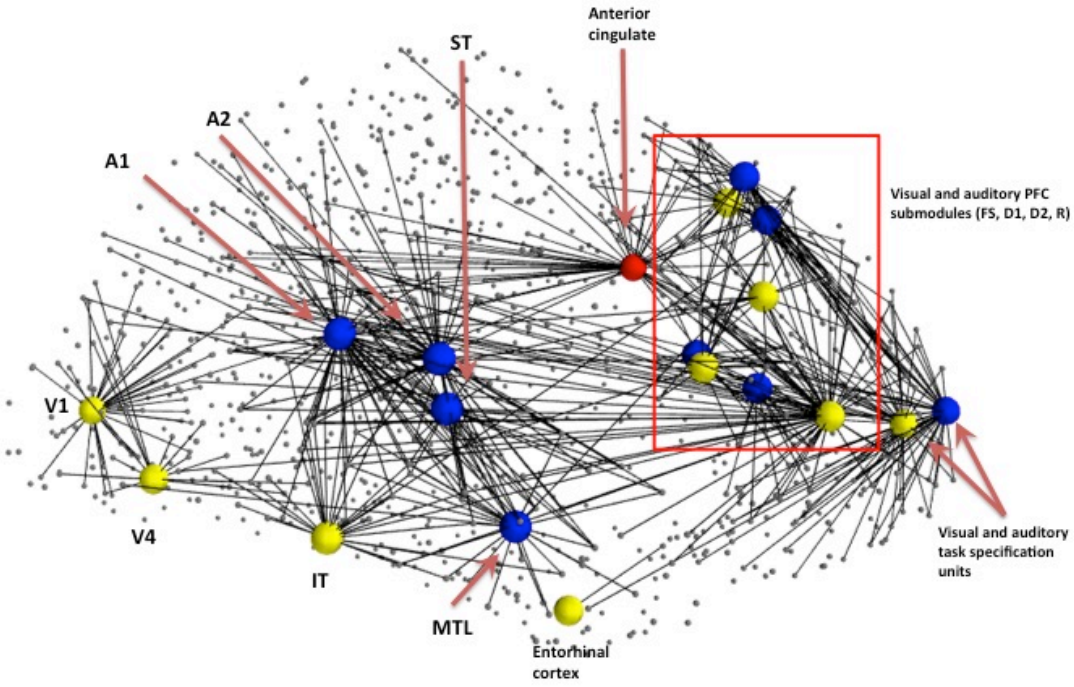

Figure 3.2 Embedded model in Hagmann's connectome (Hagmann et al., 2008). We first found hypothetical locations for our model's regions of interest (ROIs) and the connected nodes in the connectome (small dots connected to ROIs). We embedded our model of microcircuits and network structure into the structural connectome model of Hagmann et al. (2008). See Ulloa and Horwitz (2016) for details.

superior frontal gyrus of the Virtual Brain model. The attention level/task parameter can be modulated by the outputs of the ACC module. When the attention level is low, the working memory modules are not able to hold a stimulus throughout the delay period.

3. 3 Simulated experiments

We use the extended auditory model and the combined auditory-visual model to perform a number of simulated experiments that can include not only one stimulus, but others as well, some of which can be considered to be distractors. The complete set of simulated experiments is the following:

3. 3. 1 Auditory short-term memory simulation experiments

a. Auditory delayed match-to-sample task. This experiment implemented the original delayed match-to-sample (DMS) task to demonstrate that the new auditory model (with an added module – the entorhinal cortex, and the linkage between visual and auditory models) continues to perform the DMS task and gives the same results as the original model (Antonio Ulloa & Barry Horwitz, 2016). One typical DMS trial consists of the presentation of a stimulus, an ensuing delay period, a presentation of a probe (the same or a new stimulus) and at the end of it, the simulated subjects need to decide whether the probe is the same as the first stimulus presented (see Fig. 3.3B). The attention/task parameter is set to high (0.3) during a trial.

b. Auditory delayed match-to-sample task with distractors. The simulated subjects were shown two distractors (visual or auditory) before the probe was

A

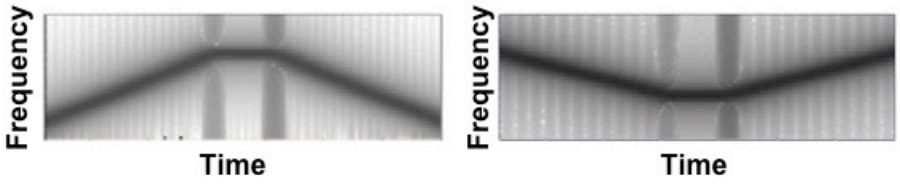
Frequency
Time
Frequency
Time

B

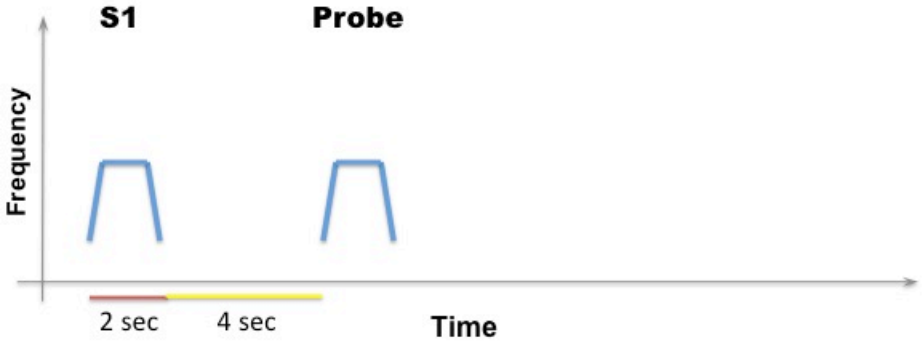
S1
Probe
Frequency
2 sec
4 sec
Time

C

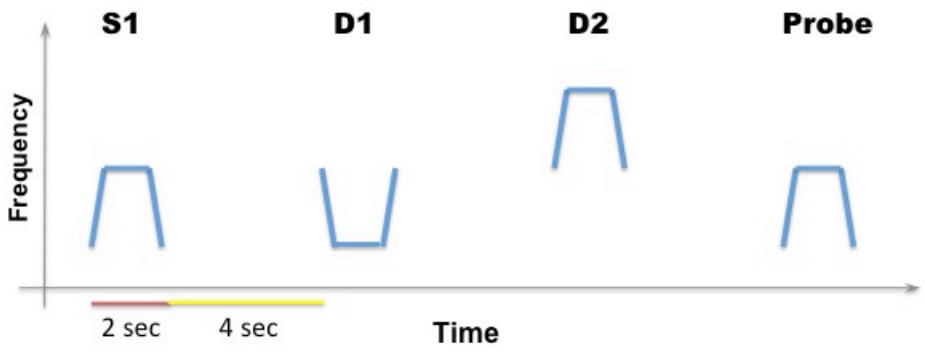

D

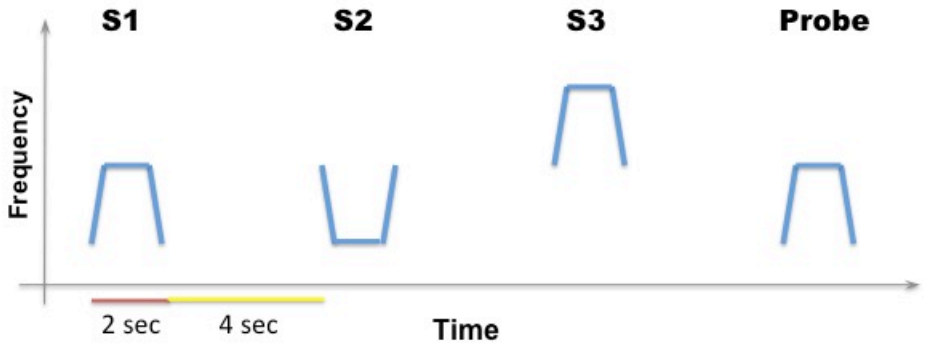

Figure 3.3 Timeline designs of implemented tasks. **A.** Two examples of the auditory objects (tonal contours) we used as stimuli of cognitive tasks. **B**. The timeline for a single trial of auditory delayed match-to-sample (DMS) task. The simulated subjects' task is to identify whether the probe is a match with the first stimulus. **C.** The timeline for a single DMS trial with distractors. The simulated subjects need to ignore the intervening distractors and only respond to the probe. **D.** The timeline for a single trial of the auditory Sternberg's recognition task. The simulated subjects need to remember a list of tonal contours and their task is to decide whether the probe is a match with any stimulus in the list.

displayed (see Fig. 3.3C). The attention/task parameter is set to high (0.3) for the first stimulus and decreased to low (0.05) following the presentation of the distractors.

c. Auditory version of Sternberg's recognition task. An auditory variant of Sternberg's recognition task (Sternberg, 1966, 1969) was used. On each trial of the simulation, three auditory stimuli were presented sequentially, followed by a delay period and then a probe. The subjects' task was to decide whether the probe was a match to any of the three stimuli presented earlier (see Fig. 3.3D). The Sternberg paradigm with visual/auditory objects has been used in many studies, and thus allows us to compare our simulated results with experimental results.

3. 3. 2 Visual-auditory bimodality experiments

a. Bimodality DMS task with various attention settings: endogenous attention only, exogenous attention only, both endogenous and exogenous attention, see Fig. 3.4A. A block of visual DMS trials and a block of auditory DMS trials were implemented simultaneously. The saliency of visual stimuli and auditory stimuli varied from trial to trial. The attention/task parameter assigned to each modality was determined based on the real-time output of the anterior cingulate module. In general, higher saliency of one stimulus will result in higher attention in the corresponding modality.

b. Bimodality distraction task with different working memory load, see Fig. 3.4B. The simulated subjects were asked to remember 1~3 visual stimuli before an

A

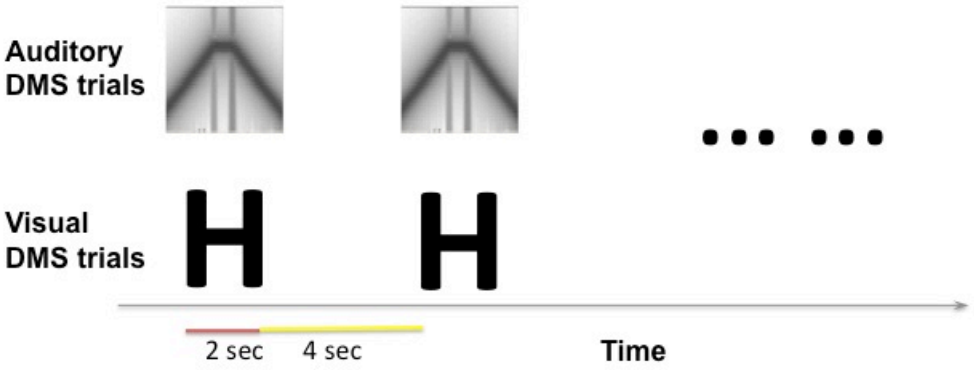

B

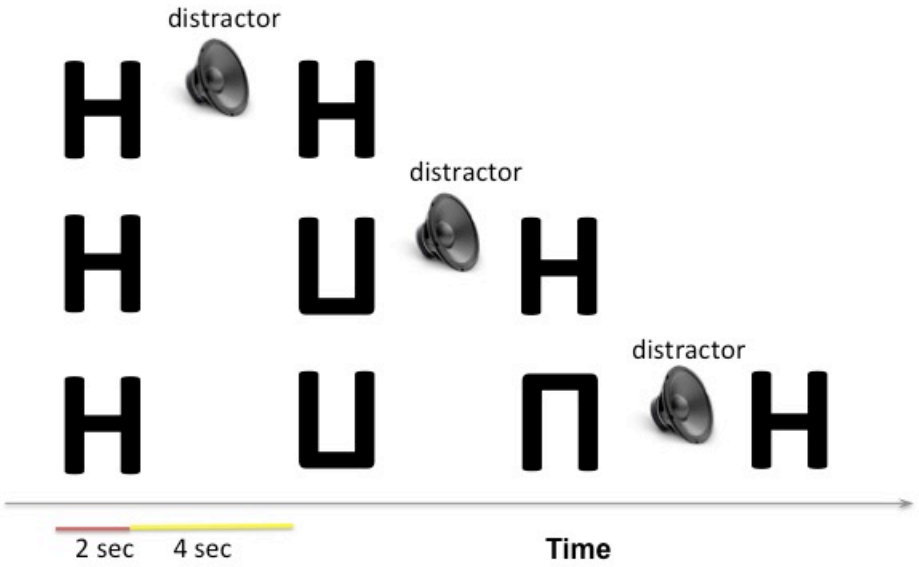

Figure 3.4 Designs of bimodality tasks. **A.** Bimodality Delayed Match-to-sample task: Auditory and visual stimuli of different saliency levels are presented simultaneously. Case 1 (endogenous + exogenous attention). The simulated subjects are required to attend auditory stimuli only and need to decide whether the second stimulus is the same as the first. Visual stimuli are distractors. Case 2 (exogenous attention only). The simulated subjects can choose to attend to auditory or visual stimuli based on the saliency. **B.** Bimodality distraction task with different working memory load. The model is asked to remember one to three visual items and decide if the final probe is a match of any stimulus in its working memory. An auditory distractor is presented before the probe.

auditory distractor occurred. The endogenous attention is set to attend to visual stimuli.

3. 3. 3 fMRI experiments

Simulated fMRI signals can be calculated for each of the tasks discussed above. The direct outputs are the electrical activity of simulated neuronal units. Prior to generating fMRI BOLD time series, we first calculate the integrated synaptic activity by spatially integrating over each module and temporally over 50 ms (Tagamets & Horwitz, 1998). Using the integrated synaptic activity of select regions of interests (ROIs) as the input to the fMRI BOLD balloon model of hemodynamic response (Stephan et al., 2007; A. Ulloa & B. Horwitz, 2016), we calculated the simulated fMRI signal time-series for all our ROIs and then down-sampled the time-series to correspond to a TR value of 2 seconds. For more mathematical and other technical details, see Appendix and Ulloa and Horwitz, 2016 (A. Ulloa & B. Horwitz, 2016).

In simulating an fMRI experiment for the aforementioned cognitive tasks we implement two types of design schemes: block design and event-related design. In an experiment with block design, one stimulus is followed by a 2-second delay period, and the model alternately performs a block of task trials (3 trials) and a block of control trials (3 trials). The control trials use degraded shapes and random noises. While with event-related design, the delay period that follows each stimulus is extended to 20 seconds in order to show a more complete response curve in the BOLD signal.

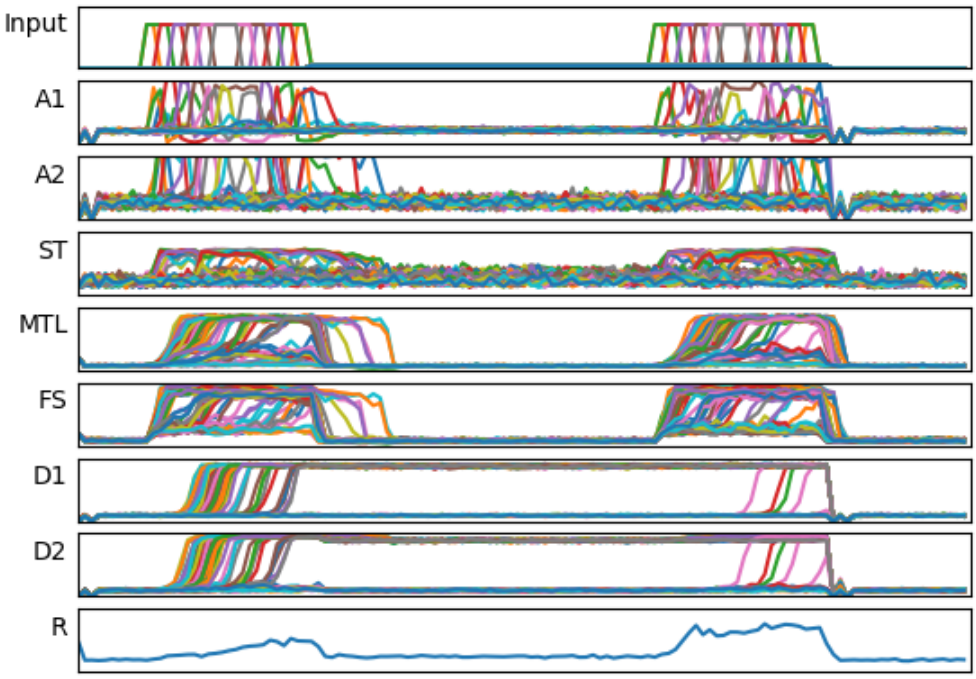

Figure 3.5 Simulated neural activities of the excitatory neurons in selected modules during a single auditory DMS trial. The probe in this trial is a match with the stimulus, the R (response) module successfully fired during the probe presentation.

3. 4 Simulation results

3. 4. 1 Auditory short-term memory experiments

The model successfully performed the auditory DMS task (with and without distractors) and Sternberg's recognition task (see Table 3.1), with accuracy similar to the visual tasks (Liu et al., 2017; Tagamets and Horwitz, 1998). Fig. 3.5 shows the electrical activities of simulated neuronal units of the different modules during a DMS task using the extended auditory model. The input stimuli, represented by MGN activity, are first processed by feature-selective modules in A1 and A2. A2 has longer spectro-temporal windows of integration than A1 and thus is responsive to longer frequency sweeps. The ST module contains the distributed representation of the presenting stimulus and feeds the presentation forward to the gating module MTL and then PFC. A working memory representation is held in the D1 and D2 modules through the delay period. The probe is a match with the presented stimulus so that the R module responds. The model also can handle DMS task with distractors, for which the electrical activities are illustrated in Fig. 3. 6. The first stimulus is the target that the model needs to remember and it is followed by two distractors. The endogenous attention/task-specification unit is set to a high level, but if the probe stimuli don't match the first stimulus, the attention value is reduced to a low value following each probe stimulus. The distractors also evoke some activity in the working memory

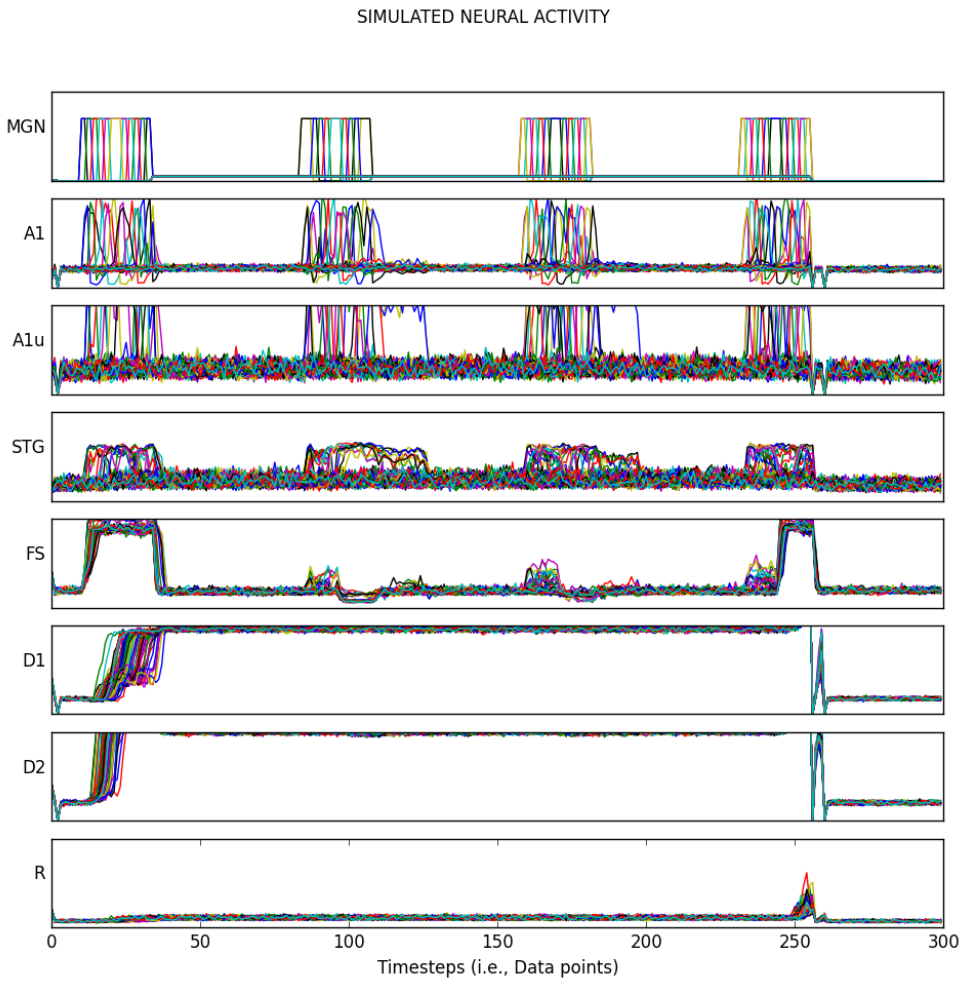

Figure 3.6 Simulated neural activities of the excitatory neurons in selected modules during a single auditory DMS trial with two intervening distractors. The model properly avoided the distractors and responded when the probe was a match of the first stimulus.

Table 3.1 Mean performances of 10 simulated subjects doing three cognitve tasks. Performances are measured by counting the number of neuronal units in the decision-making module (R) firing above a certain threshold during the response period.

Tasks	DMS	DMS w/ distractors	Sternberg's task
Accuracy	83.9%	81.8%	78.7%
Standard deviation	5.71%	6.73%	6.05%

modules (D1, D2), but not strong enough to overwrite the representation of the first stimulus as the model successfully holds its response until the matched probe appears.

Fig. 3.7 demonstrates how the model implements the auditory version of Sternberg's recognition task and handles multiple auditory objects in short-term memory. The first three items are held in short-term memory (D1, D2), which is shown in Fig. 3.7B, and when the probe matches any of the remembered three items the R module is activated (Fig. 3.7A). Different groups of neurons in the gating module MTL responded to each of the stimuli and prevented the representations in working memory from overwriting one other.

In the visual model, we reported that we observed enhanced activity in the IT module during the delay period which helped short-term memory retention and was consistent with experimental findings (J. Fuster et al., 1982). In the current study, we also modeled this type of neuronal activity in ST, as can be seen in Figs. 4 and 6, and this enhanced activity has been reported in auditory experiments (Colombo et al., 1996; Scott, Mishkin, & Yin, 2014).

A

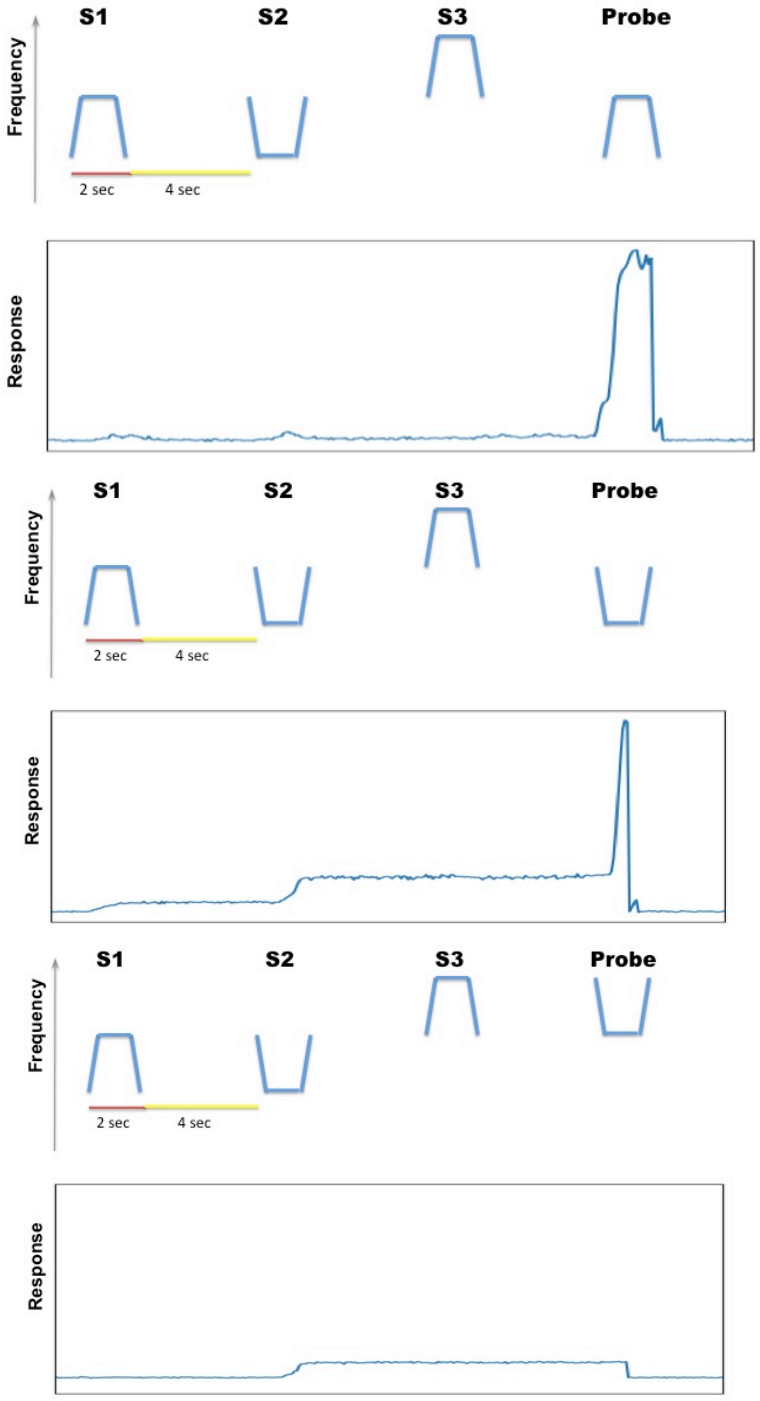
S1
S2
S3
Probe
Frequency
2 sec
4 sec
Response
S1
S2
S3
Probe
Frequency
2 sec
4 sec
Response
S1
S2
S3
Probe
Frequency
2 sec
4 sec
Response

B

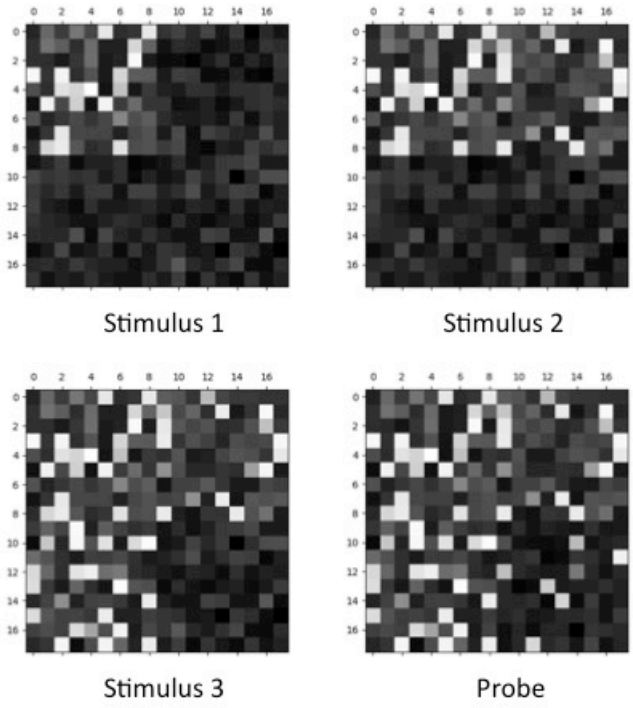

Figure 3.7 Neural activity during Sternberg's task. **A**. The responses of the model in three trials of the Sternberg's task. In the first and second trials shown, the response module made proper responses as the probes were matches with one of the three remembered items. **B.** Snapshots of working memory module D2 during the presentations of three stimuli and the probe.

A

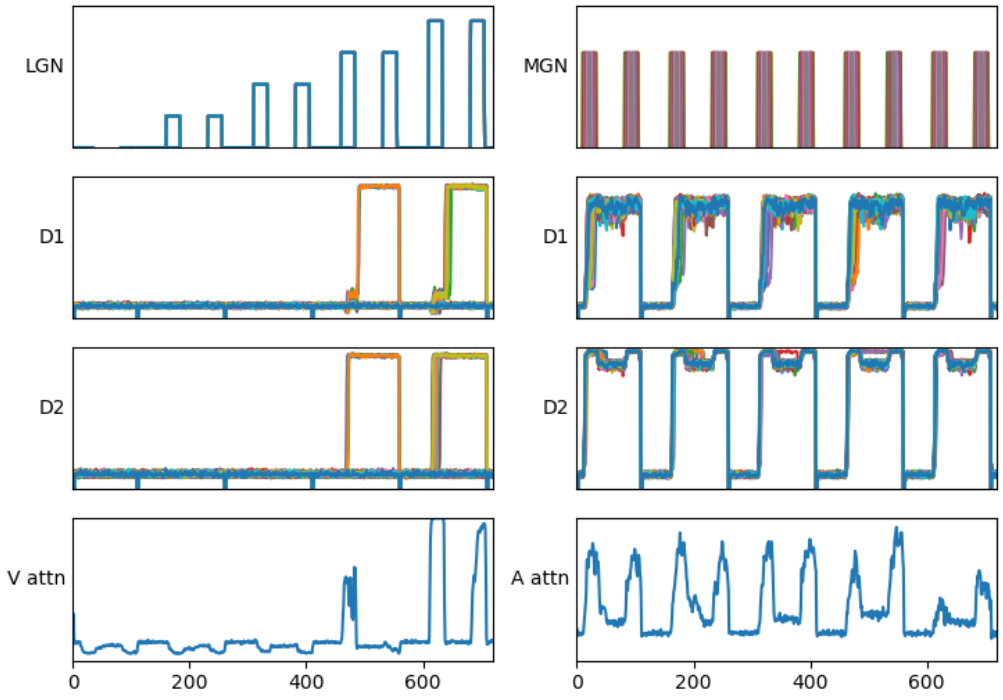

Figure 3.8 A. Bimodality DMS task trials with endogenous + exogenous attention. The endogenous/top-down task signal is set to attend auditory stimuli and regard visual stimuli as distractors. The auditory stimuli are stored in working memory modules (D1/D2) successfully. As the saliency level of visual stimuli increases, the exogenous attention for visual stimuli increases and the auditory attention decreases. Some working memory neurons are fired for visual distractors if they are salient compared to auditory stimuli.

B

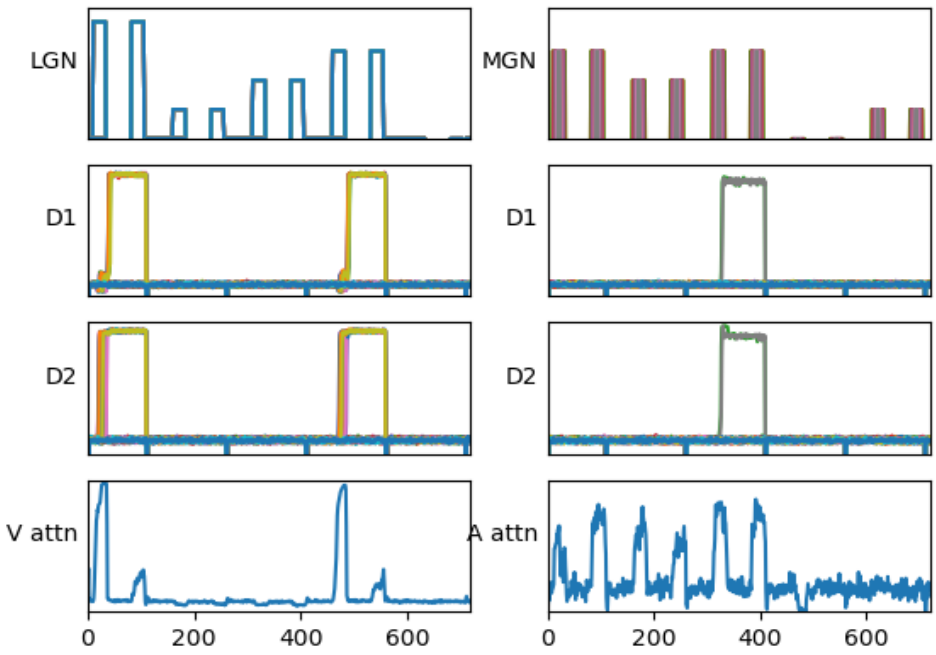

Figure 3.8 B. Bimodality DMS task trials with exogenous attention only. The model decides itself to attend visual or auditory stimuli based on the saliency. Working memory can be formed for salient stimuli as shown in the figure.

3. 4. 2 Visual-auditory bimodality experiments

Fig. 3.8A and 3.8B show the simulated crossmodal attention switch caused by input saliency changes. During the experiment, the attentional inputs into working memory module D2 were both the endogenous attention and the exogenous attention (outputs of multisensory integration module ACC). In the experiment shown in Fig. 3.8A, 5 DMS trials were implemented. The model's endogenous attention was set to attend to auditory stimuli (the auditory attention/task parameter is set to 'high') and not to attend to visual stimuli. The model attended auditory stimuli and treated visual stimuli as distractors in the first three DMS trials during which the saliency of auditory stimuli is higher than the visual stimuli, but started to attend to the visual stimuli because the saliency of visual stimuli was enhanced significantly but the model still could encode auditory stimuli into working memory. In the experiment shown in Fig.3.8B, the endogenous attention was set to 'low' for both visual and auditory stimuli (i.e., no task/goal is specified to the model) and the attentional input to D2 was only the exogenous attention generated in ACC. The model encoded salient visual or auditory stimuli successfully into working memory.

3. 4. 3 Working memory load reduces crossmodal distractions

During simulations we noticed that it is easier to distract one modality with distractors in the other modality during the working memory encoding phase than in the maintenance phase, as shown in Table 3.2. When implementing a visual DMS task (there is one item held in the working memory during the delay period) with an auditory distractor in the delay period, 32% auditory working memory neurons fired

for the distractor. However, when we increased the working memory load to 2 and 3 items, 23.7% and 19.26% of auditory working memory neurons fired for the distractor, respectively. This phenomenon shows that the working memory formed in

Table 3.2 Neurons fired for crossmodal distractors under different WM load.

Memory load	1 item	2 items	3 items
Neurons fired for the distractor	32%	23.7%	19.26%
Standard deviation	2.94%	1.64%	2%

the model is stable and this is also consistent with experimental findings that higher working memory load in one modality reduces distraction from another modality (SanMiguel et al., 2008).

However, little is known about the underlying neural mechanism mediating these phenomena. In our model, two pathways can conduct the working memory load changes to exogenous attention: working memory – V4 – ST/IT – ACC – exogenous attention, and working memory – ST/IT – ACC – exogenous attention. When the feedback connections from PFC to V4 and IT/ST are removed, we no longer observe this working memory load effect.

3. 4. 3 Simulated fMRI experiments

As discussed previously, fMRI BOLD time series are generated for select regions of interests (ROIs) using integrated synaptic activity, and for each task we implement the experiment using either a block design or an event-related design. The event-related scheme has longer duration of delay periods than experiments using

block design. Thus, the event-related experiment can show a more complete response curve in the BOLD signal for each incoming stimulus.

Fig. 3.9 shows the simulated BOLD signal for a block-design auditory DMS task, which successfully replicates the results from Husain, et al. (Husain et al., 2004). In the experiment one block of DMS trials is follow by a block of control trials in which random noises are used. Modules representing early auditory areas A1 and A2 responded equally to DMS stimuli and noises. Higher order modules such as MTL and PFC showed much larger signal changes, which indicate the distinction between meaningful stimuli and irrelevant stimuli are processed in higher order regions.

Fig. 3.10 shows one event-related fMRI BOLD time-series of three visual DMS trials. During the second and the third trials, auditory distractors were played in the delay periods. Early auditory area A1 responded to the auditory distractors, but did not cause much signal changes in auditory PFC regions compared with visual regions. The model finished all three trials correctly, but the presence of auditory stimuli lowered the BOLD activity in visual PFC modules.

One fMRI experiment of visual-auditory crossmodal attention allocation (salient stimuli capture) was also implemented. The BOLD signals of ROIs are displayed in Fig. 3.11. No task instructions were given prior to the simulation, i.e., the endogenous attention was excluded. The model reacted to visual and auditory stimuli purely based on exogenous attention capture. The model first attended to visual stimuli as the BOLD signal for visual PFC spiked (see Fig. 3.11A) and then switched to attend to salient auditory stimuli as the BOLD signal for auditory PFC module increased (see Fig. 3.11B). The ACC module controls the switch by playing the role

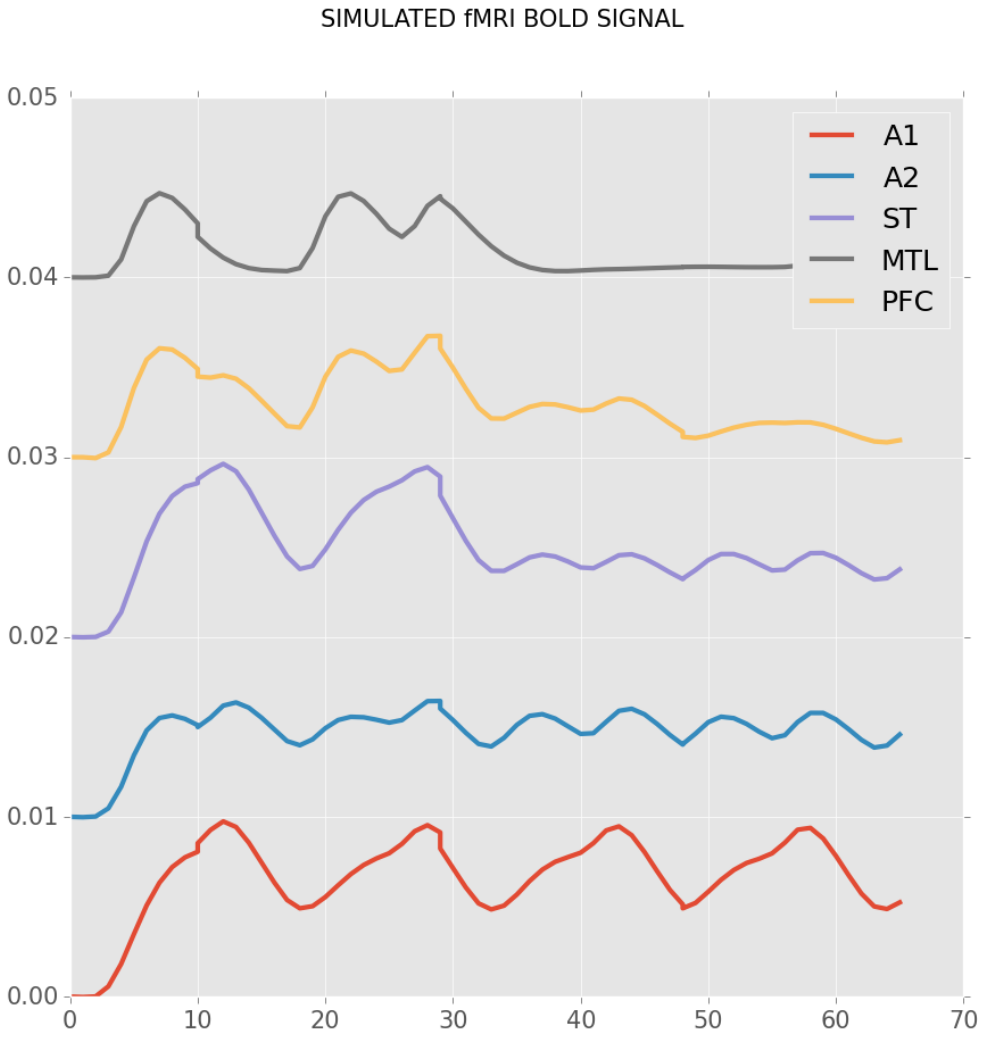

Figure 3.9 Simulated BOLD signal for a block-design auditory delayed match-to-sample (DMS) task. The experiment consists of one block of 3 DMS trials using tonal contours, and one block of 3 control trials using random noise. Modules representing early auditory areas A1 and A2 responded equally to DMS stimuli and noises. Higher order modules such as MTL and PFC showed much larger signal changes.

A

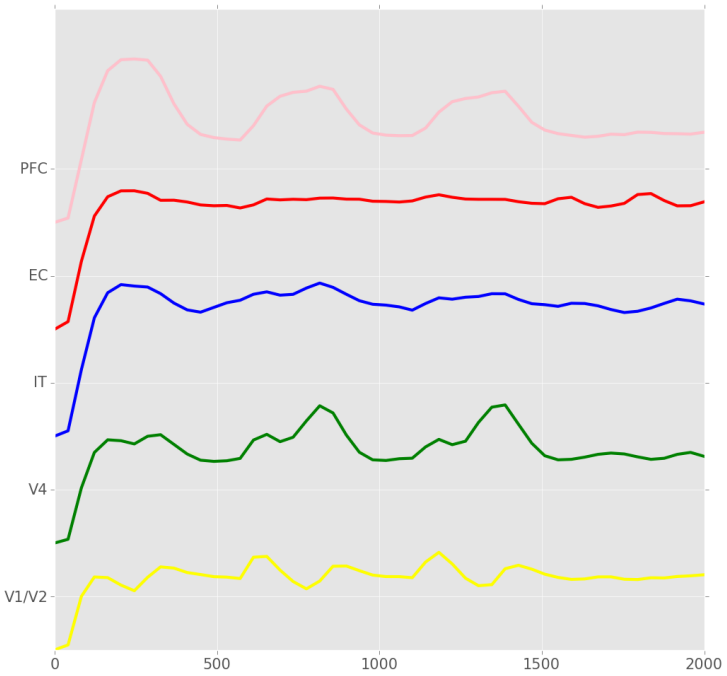

B

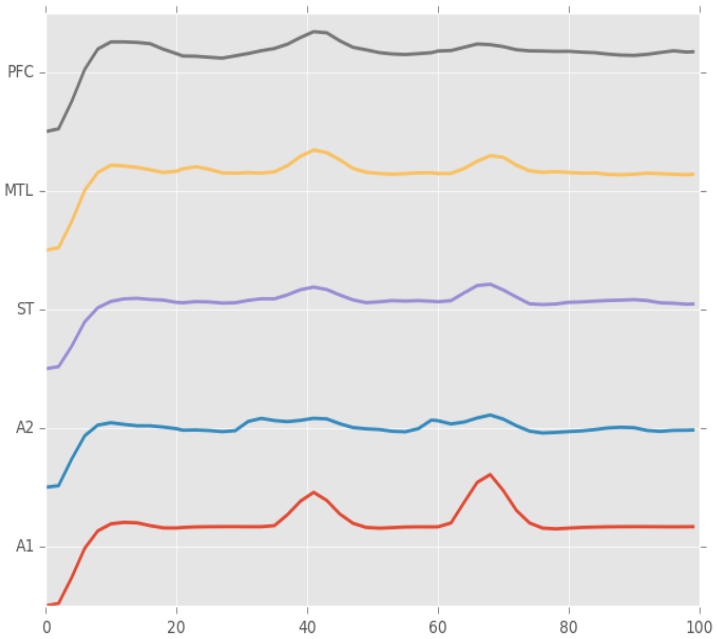

Figure 3.10 Simulated BOLD signal for visual DMS task with auditory distractors. The experiment consists of three visual DMS trials. During the second and the third trials, auditory distractors were played in the delay periods. **A.** BOLD signal for ROIs in the visual model. **B.** BOLD signal for ROIs in the auditory model. Early auditory area A1 responded to auditory distractors, but did not cause much signal changes in auditory PFC regions compared with visual regions. However, the presence of auditory stimuli lowered the BOLD activity in visual PFC modules.

A

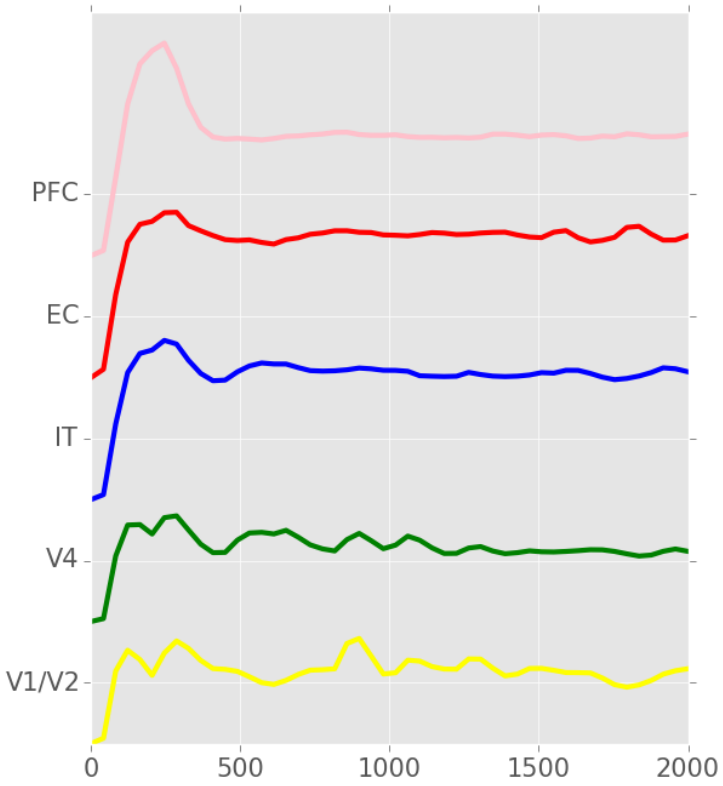

B

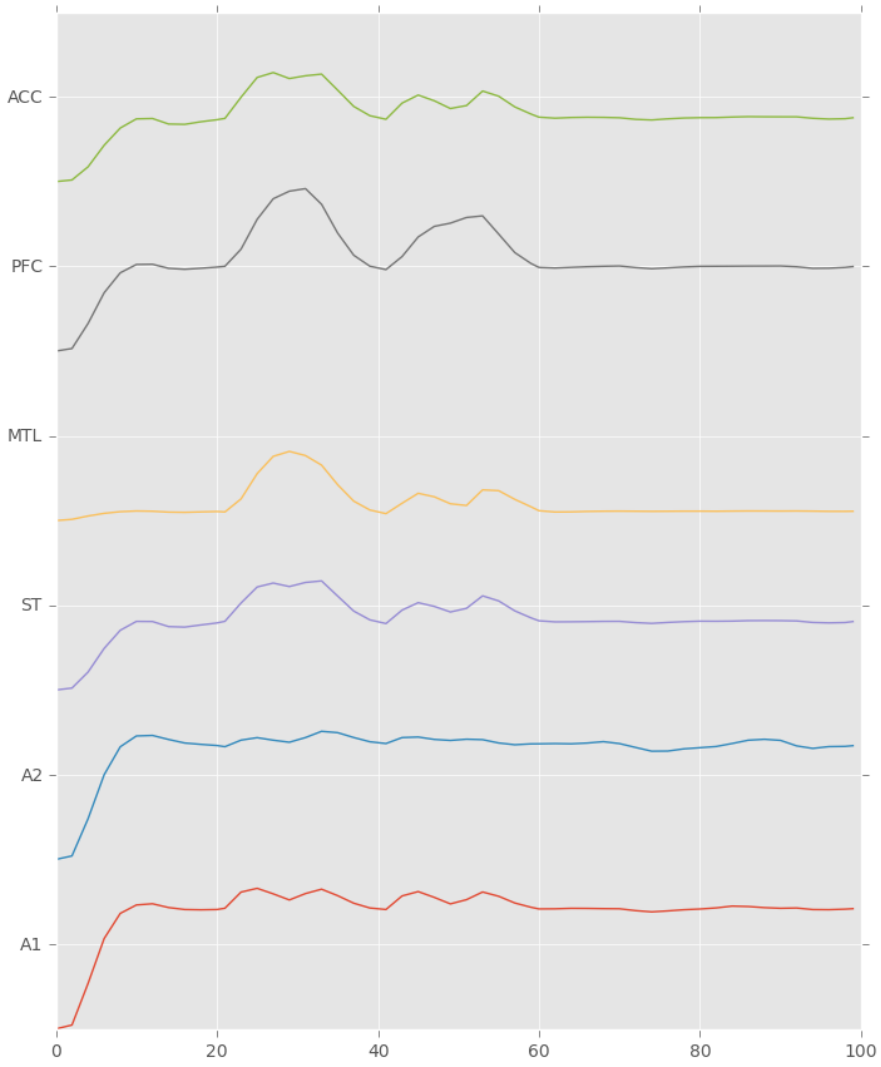

Figure 3.11 Simulated BOLD signal for visual-auditory crossmodal attention allocation experiment. No task instructions were given prior to the simulation, i.e., the model reacted to visual and auditory stimuli purely based on exogenous attention captures. **A.** BOLD signal for ROIs in the visual model. The model attended to visual stimuli in the beginning of the test and the BOLD signal for visual PFC spiked. **B.** BOLD signal for ROIs in the auditory model. The model, after attending visual stimuli in the beginning, switched to attend to salient auditory stimuli as the BOLD signal for auditory PFC module increased. The ACC module controls the switch by playing the role of exogenous attention.

of exogenous attention.

3. 5 Discussion

In this chapter, we first presented a simulation study using a large-scale auditory neural network model. Several cognitive tasks of short-term memory were successfully implemented with auditory stimuli. These short-term memory tasks can include auditory or visual distractor stimuli, or can require that multiple items be retained in mind during a delay period. Second, we added an exogenous module that connected the auditory model and the visual large-scale neural model, and embedded the combined model into a whole brain connectome. We simulated the crossmodal attention capture by presenting salient auditory distractors in a visual DMS task or salient visual distractors in an auditory task. We also simulated involuntary attention switch by presenting visual and auditory stimuli simultaneously with different saliency levels. At last, we investigated how working memory load in one modality could reduce the exogenous attention capture from the other modality

The salience level of one stimulus is typically detected based on the contrast between the stimulus and its surrounding environment. However, the "contrast" can be defined on different metrics, for example, the luminance of visual objects and the loudness of auditory objects which are used in our modeling. There are other metrics based on sensory features to define a salient object, such as bright colors, fast moving stimuli in a static background, etc. An object can also be conceptually salient. A theory has been proposed that schizophrenia may arise out of the aberrant assignment of salience to external or internal objects (Kapur, 2003). In our simulation, stimuli that resulted in high working memory load may also be considered as conceptually

salient, as the effect of high working memory load is similar with high endogenous attention.(Posner & Cohen, 1984)

Several brain regions are thought to be involved in the multisensory integration process. The perirhinal cortex is proposed based on monkey anatomical studies (E. A. Murray & Richmond, 2001; Simmons & Barsalou, 2003; Suzuki & Amaral, 1994), whereas the left posterior superior temporal sulcus/middle temporal gyrus is suggested to be where the multisensory integration takes place based on some human functional imaging findings (Amedi, von Kriegstein, van Atteveldt, Beauchamp, & Naumer, 2005; Beauchamp, 2005; Calvert, 2001). In our study, we mainly focused on the crossmodal attention competition based on bottom-up salience, as opposed to crossmodal integration, so we assigned the anterior cingulate cortex as the module responsible for the exogenous attention computation and visual-auditory competition; as discussed in the methods section, the anterior cingulate cortex is thought to play a major role in salience computation.

In our visual model, we assigned the entorhinal cortex to be the gating module between inferior temporal area and PFC based on a series of experimental results. However, experimental evidence for the corresponding brain region that implements the auditory gating function is less specific. We based our MTL choice for the auditory gating module on a study of Munoz et al. (Munoz, Mishkin, & Saunders, 2009) that shows that ablation of MTL can result in disconnections between the rostral superior temporal gyrus and its downstream targets in thalamus and frontal lobe.

In summary, we investigated the neural mechanisms underlying endogenous (top-down) and exogenous (bottom-up) attention, and how salient stimuli draw more attention, using a large-scale neural network model of visual-auditory object processing with short-term memory. We modeled and incorporated into our visual-auditory object-processing model the neuronal mechanisms for the control of endogenous and exogenous attention. The model successfully performed various bimodal working memory tasks, and produced behavioral, electrophysiological and fMRI results that matched experimental findings. Furthermore, in our visual-auditory bimodality simulations, we found that working memory load in one modality would reduce the distraction from the other modality, and a possible network mediating this effect is proposed based on our model.

Chapter 4: Quantifying the functional network changes with task conditions using complex network measures

In the past two decades, the theory of networks has been applied in a number of fields, such as social networks, the Internet, biology and many social sciences fields (M. E. Newman, 2003). A network is a set of items, which are called vertices or sometimes nodes, with connections between them, called edges or simply connections (in the mathematical literatures this is often defined as "graph"). Thus, using the theory of complex networks to study neural networks is a natural choice.

As discussed in section 1.4, the application of network theories has some unique advantages over traditional analytic techniques in cognitive neuroscience. First, complex network theory provides a reductionistic perspective to the study of human brains by giving a topological abstraction of neural networks. A number of parcellation schemes exist that divide the brain into nodes/vertices. Thus many microscopic features and details, which are not required on the scale of whole brain organization and dynamics, can be neglected. Second, by using the network abstraction we can quantify some of the variability between subjects. Furthermore, the parcellation scheme can be of different scales, from neurons to brain regions, which facilitates the comparison of structural connectivity and functional connectivity.

.

4. 1 Functional connectivity networks

As we have seen in previous chapters, the human brain is a complex network consisting of many nodes (vertices). Depending on the scale we are discussing, one node can be a neuron, a cortical column or a region/subregion. In the large-scale network constructed using empirical data, nodes are usually brain regions/subregions, and edges between nodes can represent one of three types connections: structural, functional or effective connections.

The choice of how to parcellate the brain into nodes in the network should be done carefully, as the nature of nodes can strongly influence the biophysical interpretation of the neural network topology (Butts, 2009). A good parcellation needs to represent brain regions with coherent patterns of functional connections. Studies using different node parcellation schemes usually result in significantly different network properties and cannot be quantitatively compared. In our study, we used the 998-node Hagmann's connectome as a high-resolution parcellation scheme.

Structural connectivity refers to physical attachment or anatomical tracts that link two nodes (neurons, brain regions). Structural connections are undirected and usually binary in analysis due to experimental limitations (weighted in real brains). Functional connectivity is defined as the temporal correlation between the activity of different neurons/regions, and is measured by cross-relating the time-series of their activity (Horwitz, 2003). Effective connectivity represents direct or indirect causal influences of one region on another so that the corresponding network is weighted and directed (Friston, Harrison, & Penny, 2003). The networks of interest in this chapter are functional connectivity networks which are weighted, undirected.

A connection/edge in functional connectivity networks is defined by the correlation of the nodes it connects. The connections are weighted signed upon construction, but weak connections and negative connections can obscure the network properties of interest, thus thresholding of the connectivity matrix is necessary. In general, a negative edge weight implies segregation or antagonism (Fornito, 2016). If we do not want to quantify this feature, negative connections should all be removed before further analysis. Thresholds are often decided arbitrarily, but the network properties should hold across a range of thresholds. Sometimes functional networks are simplified to binary networks. In this chapter, we are going to construct functional networks for a 998-node connectome under different conditions: resting state, passive viewing, DMS task, and auditory-visual bimodal attention switching.

One common caveat in traditional functional connectivity analysis is that the functional networks are assumed to be static. However, some recent studies have shown that human functional network architecture can change in a short time and these changes are closely related to human cognitive functions such as memory, attention, sleep and learning (Bassett et al., 2011; Horovitz et al., 2008), and may even be related to consciousness (Hutchison et al., 2013).

A number of powerful tools adopted from engineering fields have been used to perform dynamic functional connectivity analysis, including the wavelet transform, time-frequency analysis, independent component analysis, etc. For example, independent component analysis has been applied to divide fMRI data into different spatial and temporal components with similar patterns (Weissman-Fogel, Moayedi, Taylor, Pope, & Davis, 2010). Another set of methods is contributed by applied

mathematics such as dynamic graph theory (Sizemore & Bassett, 2017). In our modeling, we have dynamic changes in the functional networks. Thus, we will assess how the graph theoretical measures change as a task proceeds. In this chapter, we are going to apply sliding window analysis to explore the temporal dynamics of the graph theory measures of interest.

4. 2 Basic measures of functional networks

A series of measures can be calculated once we construct a functional network (Rubinov & Sporns, 2010). These measures assess the network's properties from three scales: local, global and regional. Local measures characterize the properties of individual nodes and can also refer to its relation with the neighborhood of one node. Global scale measures depict the aggregate properties of the given network, i.e., consider the network as a whole. Cognitive functions mediated by local or regional networks can cause changes in other parts of the functional network, though they are not directly involved in performing the functions. Global scale measures are useful to quantify such types of phenomena. Global measures are also important for comparing artificial neural networks with empirical "benchmark" networks to test the validity of models. Regional measures are mesoscale, which are used when group segregation exists, usually when we choose the high-resolution node parcellation scheme.

4. 2. 1 Degree

Given one node, the number of nodes connected to it (the sum of incoming and outgoing for directed networks) is called the "degree" of this node. In weighted networks, degree is termed connection strength, which is the sum of all incoming and

outgoing weights. Some nodes in a complex network are considered as "hubs" of the network, i.e., these nodes have much higher degrees than most other nodes. The degree distribution will possess a long tail if a network has many hub nodes.

One important class of networks characterized by the presence of large hubs is scale-free networks, whose degree distribution follows a power law. The fraction $P(k)$ of nodes in the network (the frequency of occurrence in real-world networks) having k degrees is expressed as

$$P(k) = Ck^{-\gamma} \tag{4.1}$$

where the exponent γ is a parameter and C is a constant. The scale-free property is related to another famous network property "small-worldness" which states that most nodes can be reached from any given node within a small number of steps (Latora & Marchiori, 2001).

4. 2. 2 Efficiency

The efficiency of a network measures how efficiently it exchanges information (Latora & Marchiori, 2001). Path is a key concept for efficiency related measures. Paths are potential routes of connecting pairs of nodes, and lengths of paths count the number of distinct nodes and links on the routes. Shorter lengths indicate stronger ability to integrate information or higher efficiency. The average path length, also termed as characteristic path length, is commonly used as a key metric of complex networks.

Global efficiency is a measure of the functional integration, the ability to integrate specific information that is distributed in the brain. To mathematically

define global efficiency for a network G, one needs to examine the average efficiency, which is define as:

$$E_{ave}(G) = \frac{1}{n(n-1)} \sum_{i<j \in G} \frac{1}{d(i,j)} \tag{4.2}$$

where n is the total number of nodes and $d(i,j)$ denotes the length of the shortest path for the pair i and j. The global efficiency then can be defined as:

$$E_{global}(G) = \frac{E_{ave}(G)}{E(G^{ideal})} \tag{4.3}$$

where G^{ideal} is a network with the same number of nodes as G and all possible edges exist. The "ideal" network with all nodes connected to each other has a global efficiency of 1, the largest value possible. The network with no edges at all has a global efficiency of 0, which means no information exchange can occur in the network.

The local efficiency of one node i is defined on the local subgraph G_i which consists of all the immediate neighbors of i, but i itself is not included. The mean local efficiency for a network thus can be expressed as:

$$E_{loc}(G) = \frac{1}{n} \sum_{i \in G} E(G_i) \tag{4.4}$$

The global efficiency is comparable to the inverse characteristic (average) path length $1/L$, which measures the efficiency of moving information through the given network. As the definitions imply, the characteristic path length is more influenced by long paths while the global efficiency is more influenced by short paths.

4. 2. 3 Segregation measures

Besides the integration measures discussed above, another set of import metrics is segregation measures. The human brain is able to implement complex cognitive functions by segregating brain regions into functionally specialized groups, known as modules/clusters/communities in different contexts. In functional networks, such groups suggest nodes have higher statistical dependencies within one group than with nodes in other groups.

Clustering in a network is defined on the density of triplets of nodes. One triplet consists of three connected nodes. If the three nodes are connected to each other, then the triplet is closed; otherwise, the triplet is open. The global clustering coefficient is thus the number of closed triplets over the total number of triplets (both open and closed). The local clustering coefficient of one node in a network is defined the fraction of the node's neighbors that are also neighbors of each other (Watts & Strogatz, 1998). Mathematically, let's define $N(i)$ as the set of directly connected neighbor nodes of node *i*; E as the set of edges of the network; k_i as the number of neighbors. Then the clustering coefficient for node *i* is:

$$C_i = \frac{\sigma\left|\{e_{jk}: v_j, v_i \in N(i), e_{jk} \in E\}\right|}{k_i(k_i - 1)} \tag{4.5}$$

where σ is 1 for directed networks, and 2 for undirected networks. The average clustering coefficient of a network is an alternative measure to the global clustering coefficient.

The clustering coefficient metric is simple yet flawed in networks with few triplet connections and unable to depict the structure and size of these segregated groups. A more superior metric is modularity index whose calculation is based on

knowledge of the community structure of the given network. Mathematically, modularity is defined as the fraction of the connections (edges) that fall inside communities minus the expected fraction if connections were generated randomly but the degree (connection strength) distribution remained the same. The value of the modularity index lies in the range $[-1, 1]$. A higher value of modularity means a higher concentration of connections within communities compared with the expected concentration of an ensemble of randomized networks with the same degree distribution.

The calculation of modularity index depends on the knowledge of given community parcellation. The optimal community structure corresponds to the highest value of modularity, thus is given by certain optimization algorithms rather than exact computations. Girvan and Newman in 2002 provided the first algorithm (Girvan & Newman, 2002), which is known to be accurate but slow for large networks. Blondel et al. gave a more recent and faster algorithm (Blondel, Guillaume, Lambiotte, & Lefebvre, 2008). These algorithms were originally designed for binary networks but later were generalized to weighted networks (M. E. J. Newman, 2004).

Some other complex network metrics are also of great importance in analyzing certain aspects of brain functional networks, such as small-worldness, network motifs, eigenvector centrality, etc. We will restrict our discussion to the aforementioned metrics in the rest part of this chapter.

4. 3 The intrinsic functional connectivity networks under different task conditions

4. 3. 1 Constructing the intrinsic functional connectivity network

Intrinsic brain activity refers to the neural states that are produced spontaneously by the brain and not as responses to stimulation or immediate reactions to the environment (Havlík, 2017). Some authors use the term as an equivalent of resting state activity that occurs when a subject is not performing an explicit task. In our study, we define intrinsic activity as both the resting state activity and the activity of non-task related brain regions when performing cognitive tasks. Unlike the case of real empirical data, in our computational modeling study we know explicitly which neural populations are participating in the task and which aren't. Thus, the intrinsic functional connectivity network is generated by calculating the correlations between connectome nodes excluding the nodes directly mediating the cognitive task.

We embedded a biophysically realistic large-scale neural model into the Hagmann's connectome of 998 nodes (for details, see Chapter 2). A series of cognitive tasks have been successfully implemented, including passive fixation, passive viewing, delayed match-to-sample (DMS) task and Sternberg's list memorization task using visual/auditory/visual-auditory bimodal stimuli. The large- scale model is directly performing the cognitive tasks, and the 998-node connectome provides brain-like neural noise to task nodes (our model) during simulations, and in return receive inputs back from the task nodes.

A

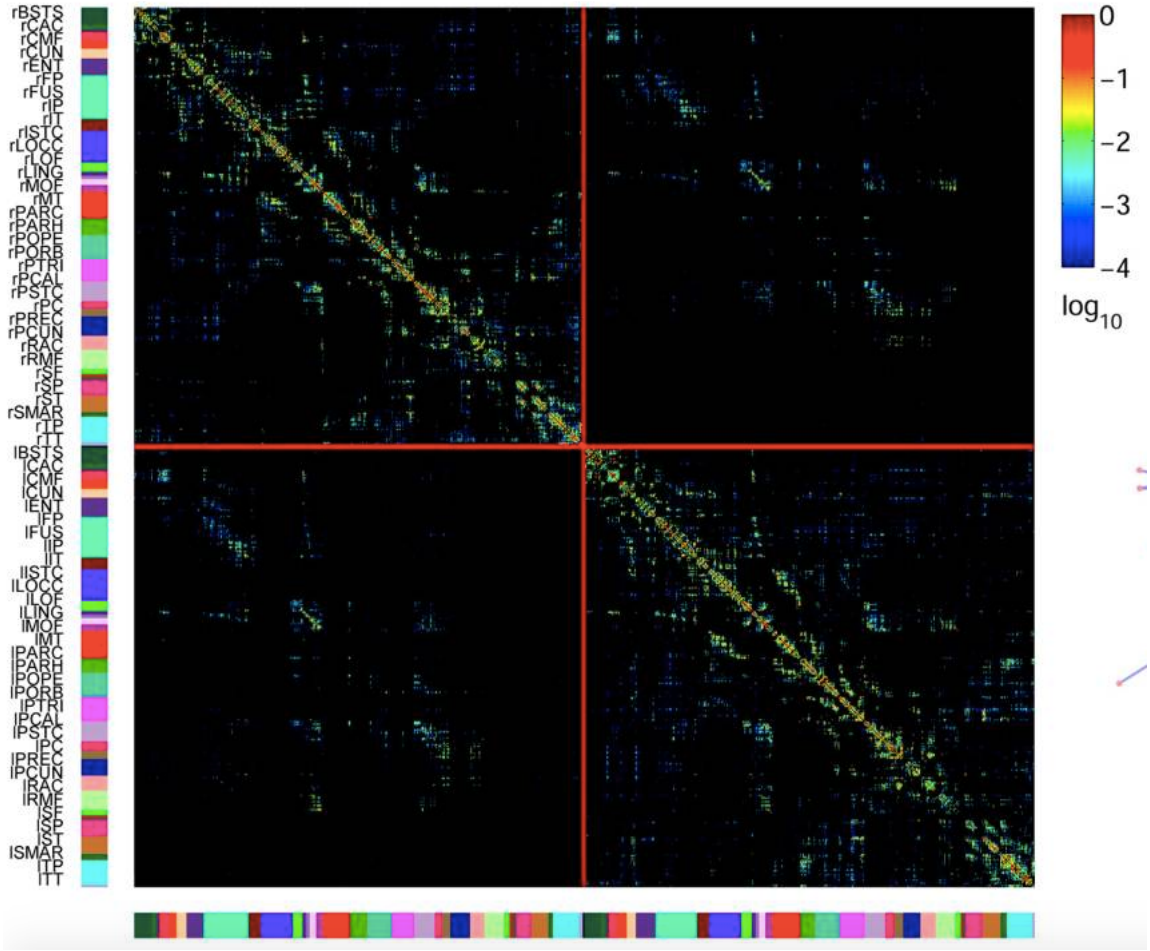

Figure 4.1A The adjacency matrix of structural connectivity in 998-node Hagmann's connectome. The y-axis texts and colors show brain regions that the 998 nodes are from. The red lines separate right hemisphere and left hemisphere. The upper left quarter shows the structural connectivity within right hemisphere.

B

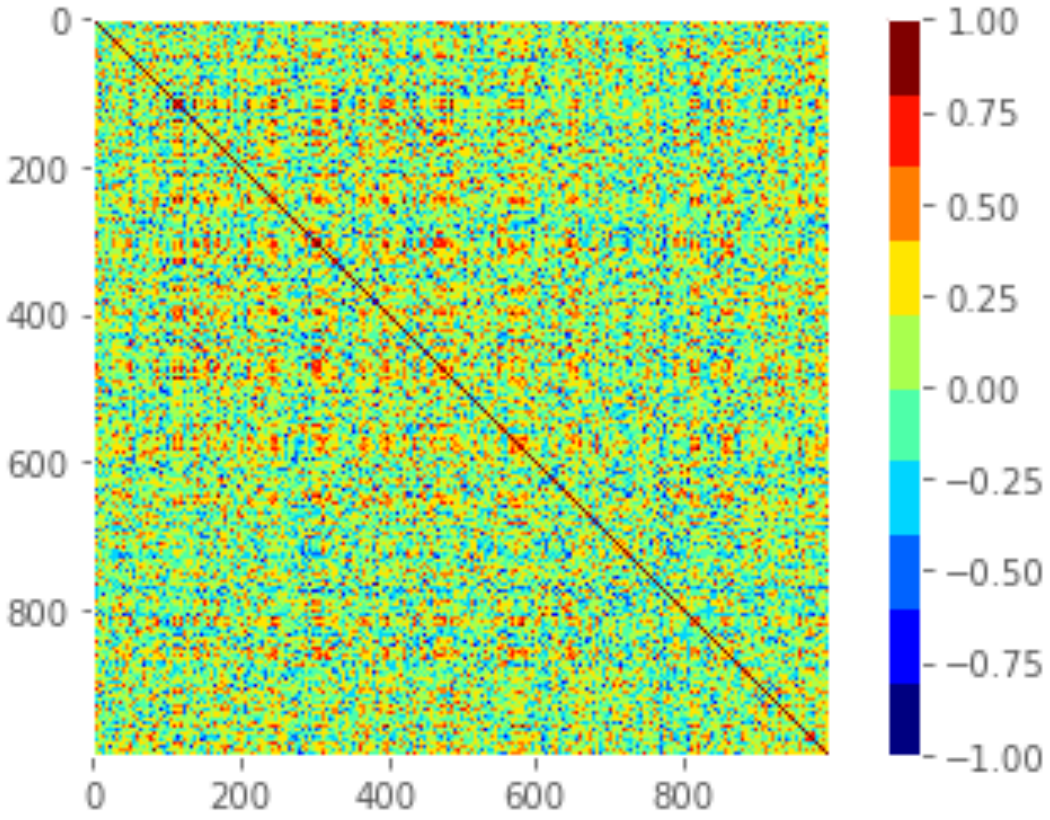

Figure 4.1 B The correlation matrix of the 998 intrinsic brain nodes for the synaptic neural activity in a block of auditory DMS trials. It serves as the adjacency matrix in constructing the intrinsic functional connectivity network. The 998 nodes are the same with Figure 4.1A.

Two types of outputs are generated from the simulation: simulated fMRI BOLD signals and synaptic activity. As discussed in Chapter 2, we use the absolute value of the synaptic activity as the neural substrate that gets convolved with a hemodynamic model to generate the simulated fMRI BOLD activity. We can create the functional connectivity networks for the tasks of interest based on either synaptic activity or fMRI BOLD time series. Simulated fMRI BOLD signals have worse temporal resolution than simulated synaptic activity but can be compared with empirical data since current techniques are unable to collect synaptic activity with comparable spatial resolution as our model. Ulloa and Horwitz (2018) have analyzed how the intrinsic functional connectivity network changes under different visual task conditions using simulated fMRI BOLD signals. In the present work, we are going to extend the analysis to synaptic activity with an updated bimodal model.

Fig. 4.1A shows the adjacency matrix of structural connectivity using the 998-node Hagmann's connectome, and Fig. 4.1B shows the adjacency matrix of the functional connectivity network for a block of auditory DMS trials. Connections in the network are calculated based on simulated synaptic activity.

4. 3. 2 Power scaling

Human brain functional connectivity networks have been shown to be scale-free networks in a number of studies (Barabasi & Albert, 1999; Bonifazi et al., 2009). The scaling parameter γ was found to be 2.0 in human fMRI with voxels as the nodes in the functional network (Eguiluz, Chialvo, Cecchi, Baliki, & Apkarian, 2005). However, the value of γ varies depending on a number of factors including the scale of interest, parcellations of brain regions, etc.

We generated functional connectivity networks for both synaptic and fMRI BOLD time series using our model implementing different cognitive tasks (see section 4. 3. 1). The values of γ were found by first evaluating the connection strength distribution (namely the degree distribution in a binary network) $P(k)$ and then fitting $\log(P(k))$ against $\log(k)$, as for a power law distribution these data points should lie on a straight line with slope γ.

Fig. 4.2A shows the connection strength distribution for the functional connectivity network generated from integrated synaptic activity. The data were collected from the simulation of a block of the auditory DMS task (consisting of three DMS trials and three passive listening trials). The fitting of $\log(P(k))$ versus $\log(k)$ is shown in Fig. 4.2B and the value of γ was found to be 3.6 using a least squares algorithm. The value of γ varies with different thresholds we applied on the functional network, and the simulated tasks from which the simulated data were collected. The relationship between γ and threshold value is plotted in Fig. 4.2C, which shows the scale-free property holds for a wide range of threshold values. The threshold value is the percentage of weakest connections removed. A threshold of 0.4 means the bottom 40% connections are ignored in further analysis.

We also fitted the functional networks generated from simulated fMRI BOLD time series into a power law distribution. The degree distribution of a BOLD functional network (data collected from a block of DMS task) is shown in Fig. 4.3A and the attempt to fit the distribution to a power law is shown in Fig. 4.3B. The value of power exponent γ corresponding to different thresholds is shown in Fig. 4.3C. The

A

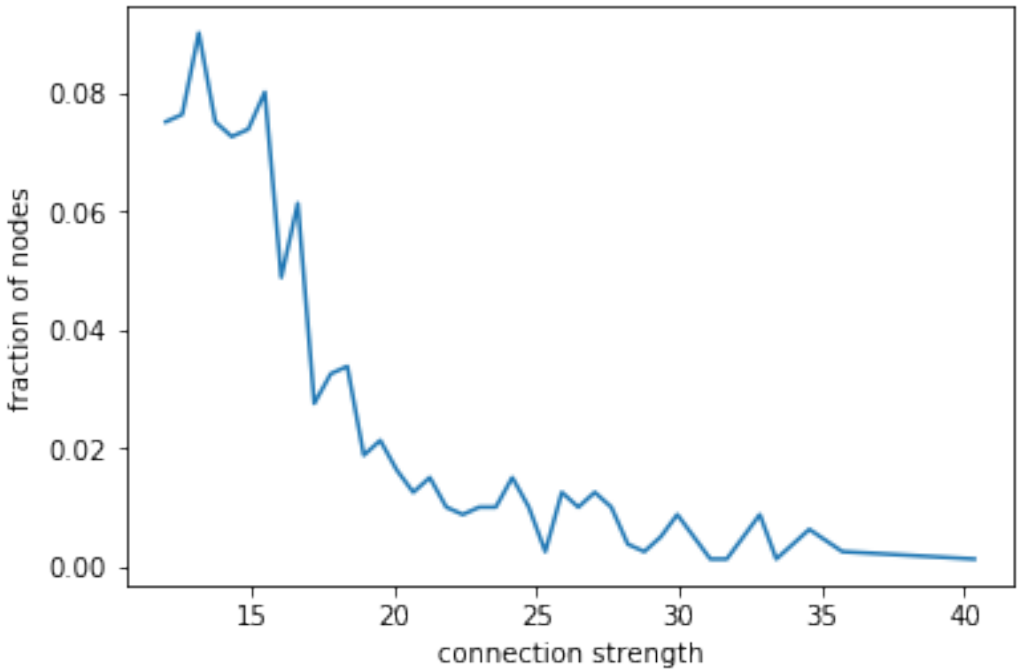
0.08
0.06
0.04
0.02
0.00
fraction of nodes
15
20
25
30
35
40
connection strength

B

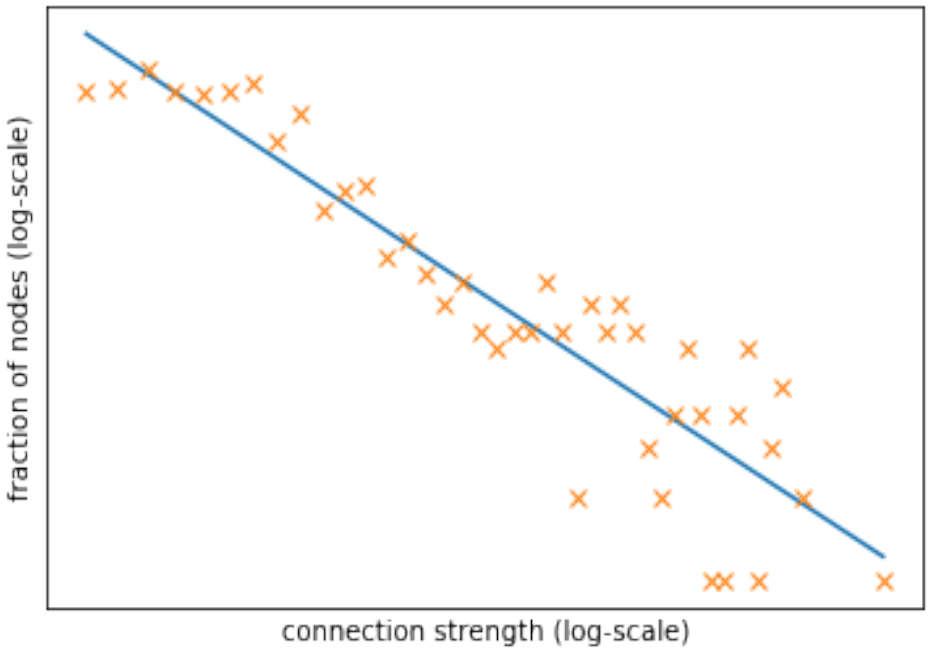
fraction of nodes (log-scale)
connection strength (log-scale)

C

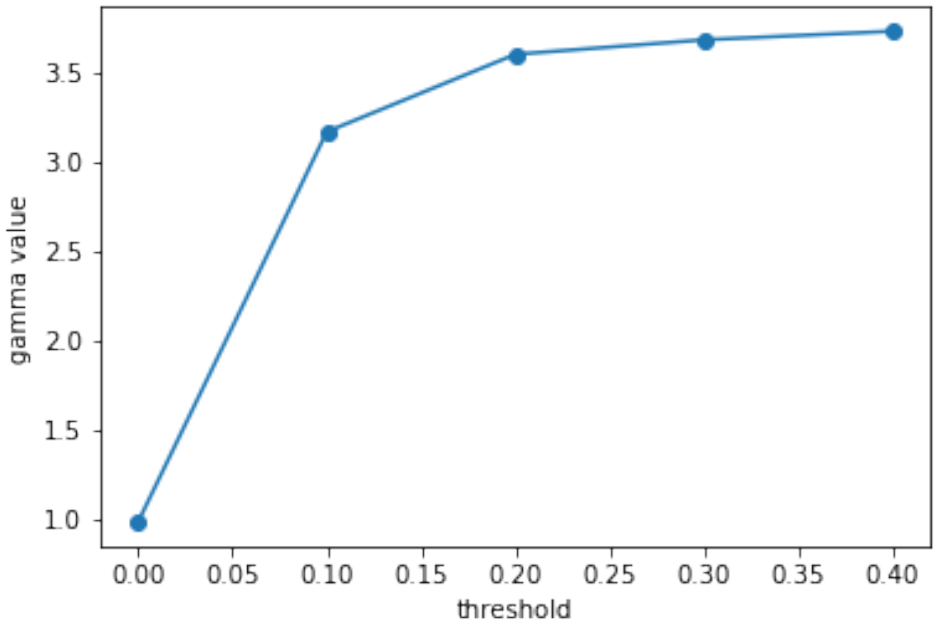

Figure 4.2 Power scaling of synaptic FC networks **A.** The connection strength distribution of the intrinsic functional connectivity network generated from simulated synaptic activity. The connection strength of one node is the sum of its incoming and outgoing weights. **B.** The power law fitting of connection strength distribution. **C.** The value of power-law exponent dependency on threshold of the functional matrix.

A

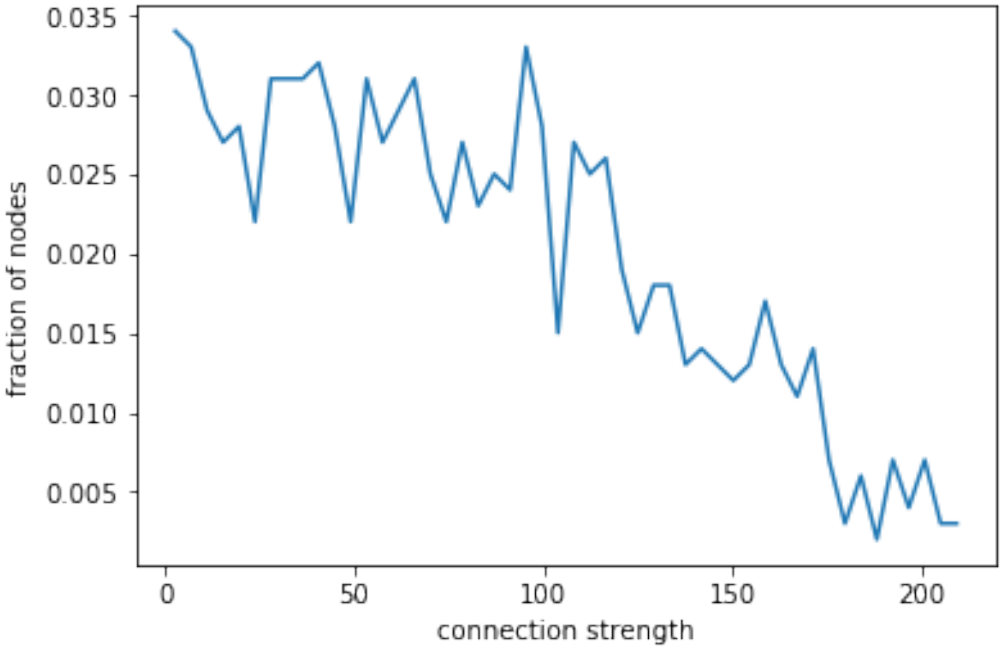
0.035
0.030
0.025
0.020
0.015
0.010
0.005
fraction of nodes
0
50
100
150
200
connection strength

B

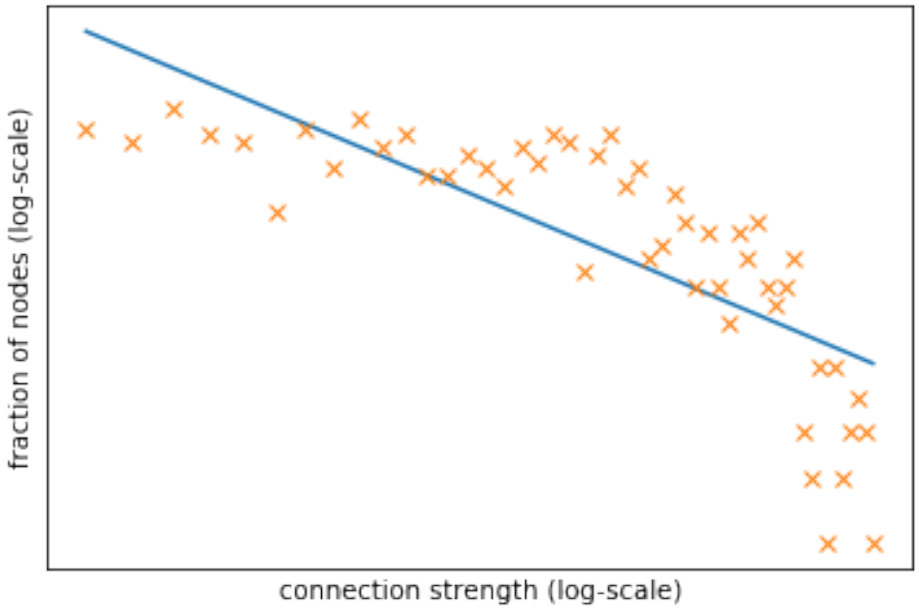
fraction of nodes (log-scale)
connection strength (log-scale)

C

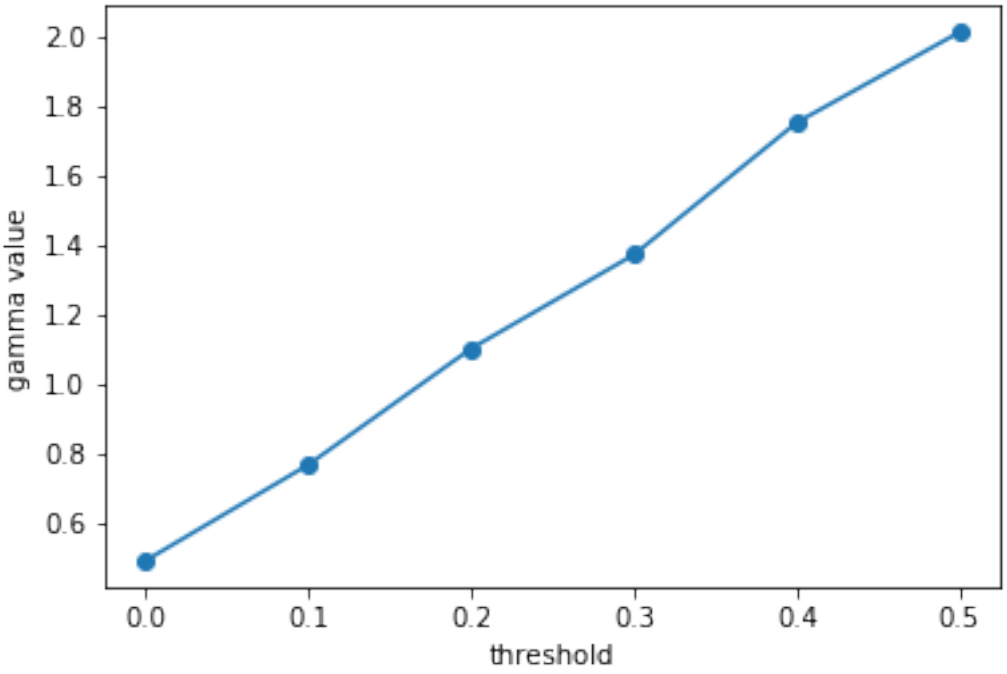

Figure 4.3 Power scaling of fMRI BOLD FC networks. **A.** The connection strength distribution of the intrinsic functional connectivity network generated from simulated fMRI BOLD activity. The connection strength of one node is the sum of its incoming and outgoing weights. **B.** The power law fitting of connection strength distribution (BOLD). **C.** The value of power-law exponent dependency on threshold of the functional matrix (BOLD).

γ value matches empirical results (Eguiluz et al., 2005) when the threshold is 0.5, i.e., half of the connections in the network were ignored, but the value does not converge with the increase of threshold as in the synaptic network (Fig. 2C). Given the fact that synaptic time-series have better temporal resolution than the BOLD signals (5 ms vs. 2 secs), in the following discussion we will use synaptic networks.

4. 3. 3 Quantify the changes between the passive and task-evoked intrinsic functional networks

We used four experimental conditions: passive viewing, visual DMS, visual Sternberg's task and visual-auditory DMS task. During passive viewing the model/subjects watch degraded visual shapes but take no action; thus it can be used to generate the passive intrinsic functional network. Visual DMS is the simplest task condition while the visual Sternberg's task and visual-auditory DMS task are more complex tasks. increasing either the working memory load or the number of brain regions directly involved in the task. To quantify the intrinsic network activity differences between the passive and task evoked conditions, and the changes between different task complexities, we calculated network metrics of synaptic functional connectivity (FC) matrices under different conditions. We choose global efficiency as an example of functional integration metrics, and clustering coefficient as an example of functional segregation metrics.

a. Global efficiency

Ulloa and Horwitz (Ulloa & Horwitz, 2018) have shown, using the visual model, that the global efficiency of task-evoked FC networks is higher than passive

FC networks. Specifically, the value of global efficiency is higher for DMS than for passive viewing, and for passive viewing than for passive fixation. The FC networks in their study were generated from simulated fMRI BOLD time series. As we have seen from the power scaling section, because the functional networks generated from integrated synaptic activity have a more realistic degree distribution, we analyze the changes of network metrics on synaptic functional networks. Furthermore, we investigate the metrics' dependencies on task complexity (Sternberg's task, visual-auditory bimodal tasks, etc.) using the auditory-visual bimodal model.

Fig. 4.4A shows the global efficiency of task-evoked functional networks is higher than passive intrinsic functional networks, which is consistent with Ulloa and Horwitz (2018). The figure also shows that the global efficiency increases with the complexity of cognitive tasks. The visual-auditory bimodal DMS task has higher values of global efficiency than other single modal working memory tasks. The dependency on task complexity has been reported experimentally (Cohen & D'Esposito, 2016). This is expected in our simulation because the increase in complexity may arise from: either higher working memory load (Sternberg's task) which causes higher neural activity in prefrontal cortex, of which the nodes are connected to a wide range of nodes in the intrinsic network; or more task-involved nodes (bimodal DMS task) that have connection strengths much higher than the average.

A

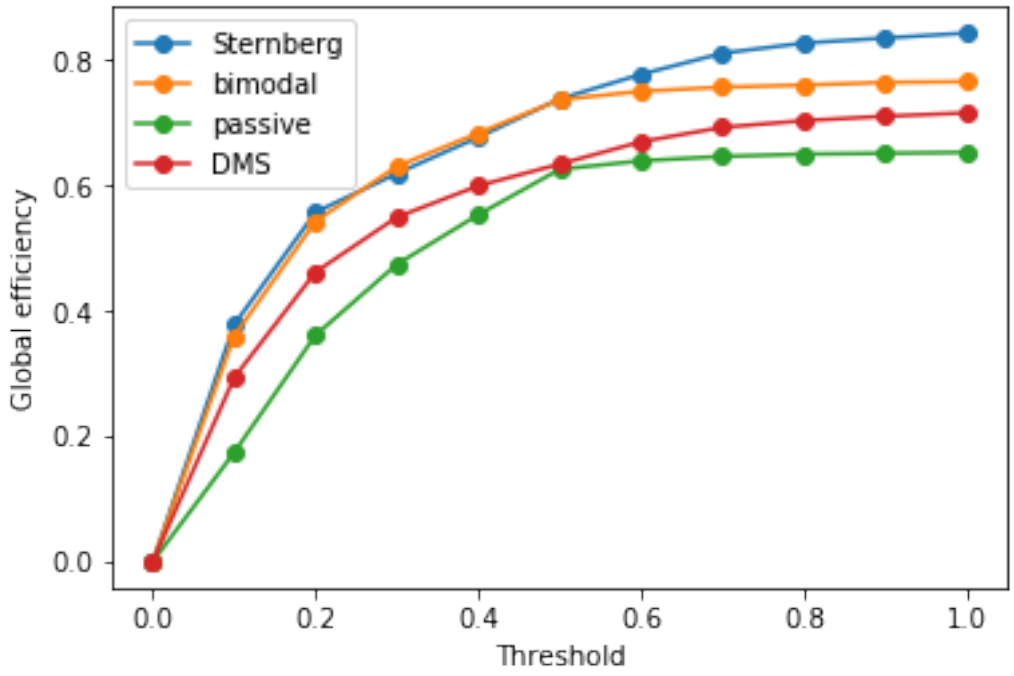

B

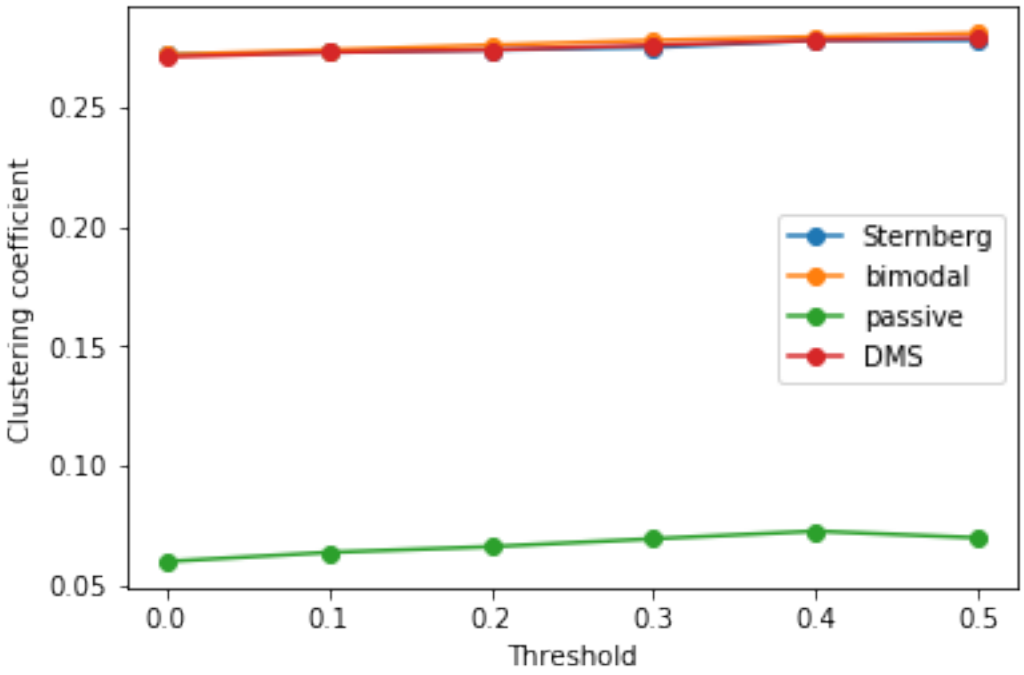

Figure 4.4 Complex network metrics for each experimental condition and for different threshold values. The threshold value represents the percentage of connections we ignored. **A.** The global efficiency for synaptic FC networks in 4 different task conditions with different threshold values. **B.** The clustering coefficient for synaptic FC networks in 4 different task conditions with different threshold values.

b. Increases in modularity and clustering coefficient

Our simulation showed a higher modularity index and clustering coefficient for task-evoked networks than for passive networks. However, modularity and clustering coefficient did not show task complexity dependencies as did the efficiency related network metrics (See Fig. 4.4B). Corresponding to the modularity index, the number of modules of task-evoked networks is smaller than the passive FC network, i.e., the networks are highly modular with less modules in non-passive tasks. The modular structures for passive FC network and task-evoked network are shown in Fig. 4.5.

4. 4 The whole-brain functional networks

In the previous discussion, all nodes directly executing the tasks were excluded in order to study the intrinsic brain activity. What if we include these tasks nodes and thus have a whole-brain functional network? The functional networks discussed in this section are all defined by the synaptic activity.

Since most of the task nodes are highly active during the task, which is characterized by long-range functional connections (e.g., V1 is correlated with visual working memory nodes), they possess high connection strengths and act as functional hubs. Therefore, these nodes extend the long tail in the connection strength distribution.

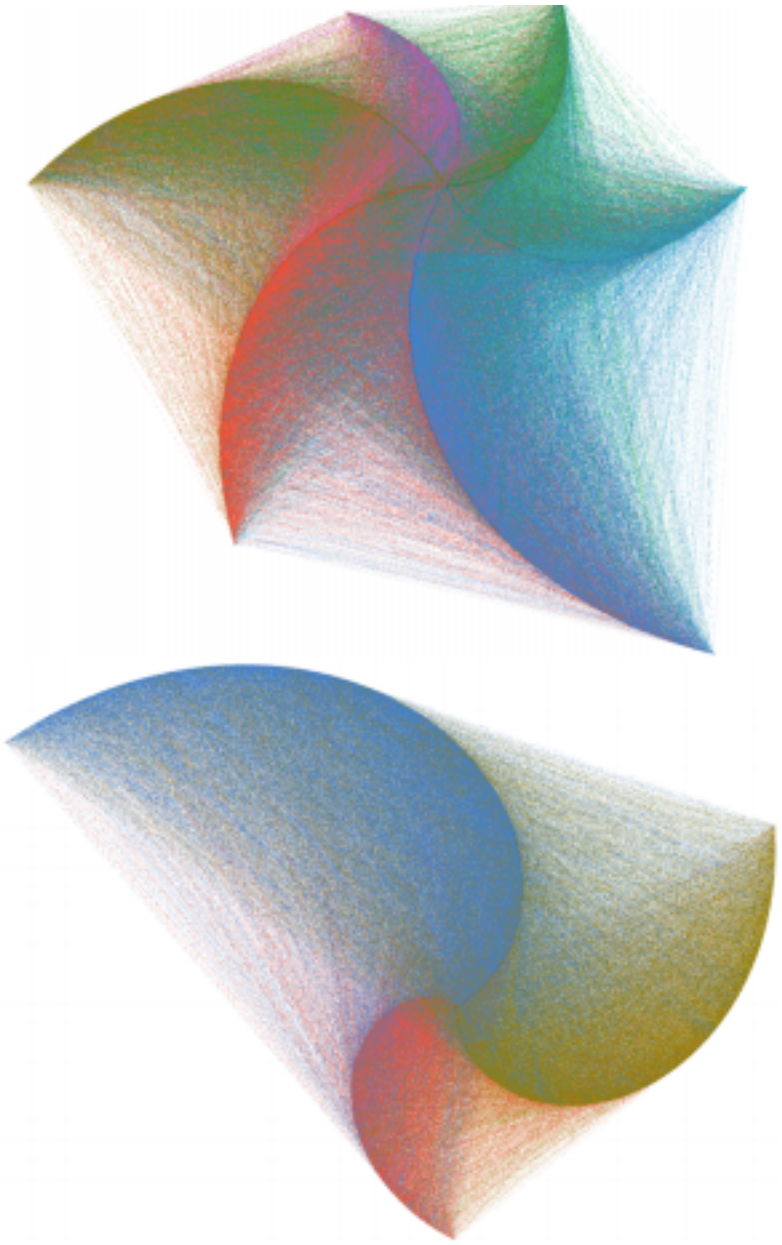

Figure 4.5 The modular structure of two example synaptic FC networks under different task conditions. The upper plot represents the modular structure of FC network in passive viewing task and contains 6 modules. The lower plot is for a DMS task, which has 3 modules in the FC network. The nodes are arranged using radial axis layout. Modules are represented by arcs and the radiuses of the arcs are proportional to the size of modules. The plot is generated using software Gephi.

Similarly, the whole-brain functional network shows a greater local efficiency, a lower characteristic path length, a greater clustering coefficient and modularity than the intrinsic functional network under same experimental conditions.

4. 5 The temporal dynamics of network measures

4. 5. 1 Global efficiency

We performed a sliding window analysis on global efficiency of the functional network generated from a block of the visual DMS task. The simulation corresponds to a 70 second simulated experimental session. Each time window is chosen to be 2 seconds so there are 35 windows in total. In calculating the global efficiency, we used the weighted functional connectivity network and only top 50 percent of the connections were kept.

The experiment is designed to have four visual DMS trials with stimuli of different saliency levels and different noise settings: in the first trial two salient visual stimuli and in the second trial two less salient stimuli were used; in the third and fourth trials, the stimuli and paradigm were the same as the first and second, but auditory distractors were presented. We ran the experiment using 10 simulated subjects, and Fig. 4.6 shows results from one of the ten.

Interestingly, we found that the maintenance of working memory decreases the global efficiency. This phenomenon is consistent with the notion that working memory needs to be encapsulated and protected which can be achieved by decreasing the network efficiency. We also noted that salient stimuli onsets could increase the

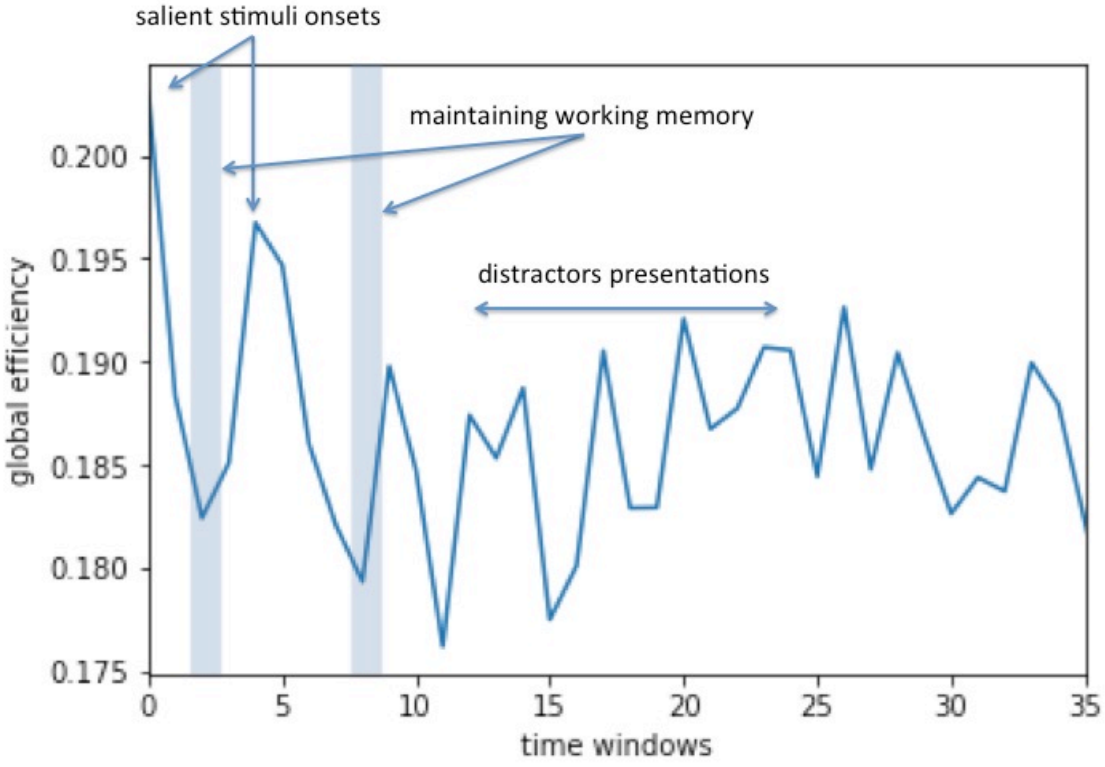

Figure 4.6 The sliding window analysis of global efficiency. Two visual DMS trials and two visual DMS trials with auditory distractors were implemented. The stimuli used were of different saliency levels. The global efficiency decreases for working memory maintenance and increases for salient stimuli onsets.

global efficiency. The input of distractors from the other modality will blur these effects (see Fig. 4.6).

4. 5. 2 Temporal community structure and spontaneous task switching

We simulated spontaneous task switching in which a stream of visual DMS tasks and a stream of auditory DMS tasks were presented simultaneously. The model spontaneously chooses to perform either the visual or the auditory DMS task. The decisions are "spontaneous" in the sense that the model receives no task instruction and the decision as to which task to perform is purely base on bottom-up saliency/exogenous attentional capture.

The whole simulated experiment consists of 5 stages: three trials and two inter-trial intervals. We found the community structures of the functional network (based on synaptic activity) for each stage, using an optimization algorithm to maximize the modularity index (Blondel et al., 2008). During task execution stages, the modularity index is generally higher than during intertrial intervals (see section 4. 2) and the number of communities is in the range 8~11, while during intertrial intervals the number of communities can be as high as 16.

Fig. 4.7 shows the temporal community structures of some of the important task nodes. Non-task related nodes (intrinsic nodes) are not shown. If the model chose to do the visual task during a trial (shown as 'visual' in the figure), the visual task nodes would appear in the same community which indicated they are functionally specialized in this stage; in auditory trials, auditory task node would also be in the same community. During intertrial intervals the previous task specialized community

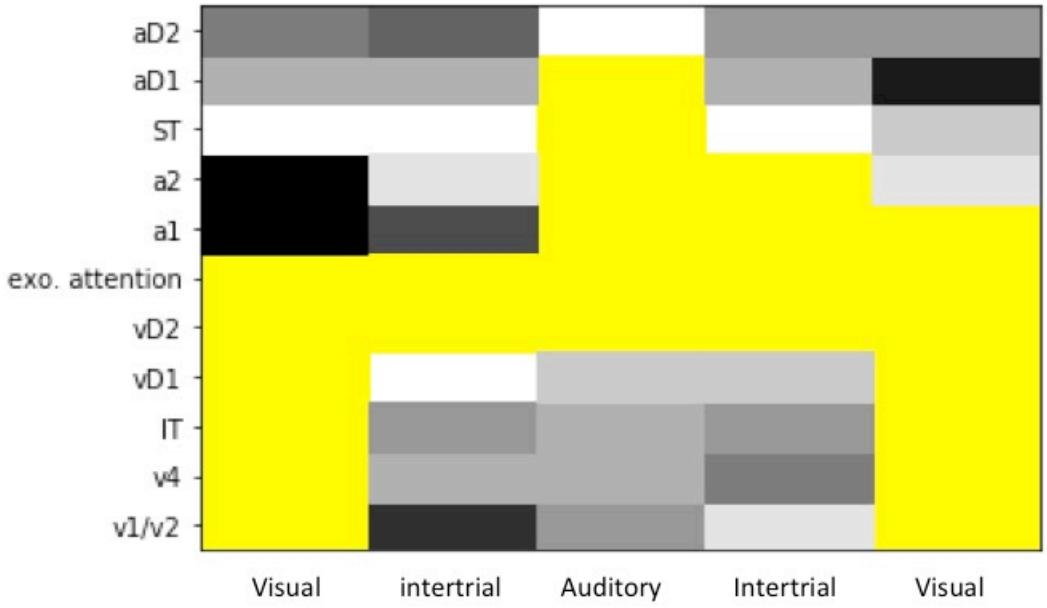

Figure 4.7 The temporal community structure for task execution nodes in a visual-auditory attention-switching task. The experiment session is divided into five stages and the community structure for each stage is shown. The exogenous attention is in the same community with visual (auditory) nodes while performing visual (auditory) tasks, which is highlighted in yellow color. Different gray scales represent other communities.

Table 4.1 The flexibility of task execution nodes in the network during a visual-auditory attention-switching task.

	Nodes/Regions	Flexibility	Mean
Attention	Exo. attention	0.100	0.100
Early-stage processing nodes	A1	0.350	0.369
	A2	0.400	
	V1/V2	0.350	
	V4	0.375	
Integration	ST	0.750	0.688
	IT	0.625	
Working memory	aD1	0.750	0.794
	aD2	0.800	
	vD1	0.750	
	vD2	0.875	

collapsed, and both visual and auditory task nodes showed little modular behavior as most of them appeared in different communities with other non-task related nodes.

However, the exogenous attention node stayed in the same community throughout the entire experiments. Some of the early stage processing nodes would be in the same community with the exogenous attention which indicated they were still functionally correlated during the intertrial intervals. For example, in the simulated experiment shown in Fig. 4.7, V4 in the first intertrial interval and A1 and A2 in the

second intertrial interval stayed in the same community with the exogenous attention node. If we define the flexibility of one node as:

$$f_i = \frac{m}{T-1} \tag{4.6}$$

where m is the number of times the node changes community and T is the total stages/time windows. The exogenous attention node thus has very low flexibility (0 in this case). Higher order task nodes (IT, ST and prefrontal task nodes) have higher flexibility than early processing task nodes (see Table 4.1).

The neural explanation for this phenomenon is related to the wirings of the exogenous attention in our model, which is directly connected with V4, A2 and D2. In the intertrial intervals intervening task executions, early stage processing nodes V1/V2, V2, A1, A2 and the exogenous attention node are the only nodes that stay responsive to simulated environmental noise. Therefore even in the intertrial intervals the early visual or auditory nodes tend to be in the same community with exogenous attention node.

In summary, we have simulated neural activity in both intrinsic and task-execution nodes under different task conditions. We calculated several important graph theoretical measures for simulated functional connectivity networks. We quantitatively compared the changes of these graph measures with task complexity and analyzed their temporal dynamics within one task. We were able to relate the changes to the underlying model mechanism, which shows our work is useful in the design of empirical studies and the test of large-scale hypothesis of brain functions.

Chapter 5: Summary

We have presented a simulation study of human brain visual/auditory processing and how this process interacts with memory and attention. Although many experiments have been done to understand different aspects of these issues, some of the results are controversial and the detailed neural substrates remained unclear. In the previous chapters, we have demonstrated how our modeling and simulation studies can try to relate behavioral and neuroimaging results, and can provide a unique resolution that cannot be achieved by experiments so far. The model can perform a number of cognitive tasks utilizing different cognitive functions with the same structural network and only changing task-specification parameter. Based on the performance and simulated imaging results of these tasks, we proposed a hypothesis for the neural mechanism underlying several important phenomena, which may be tested experimentally in the future.

The present model contains 26 modules representing different brain regions. Each module contains 81 Wilson-Cowan units, namely 162 simulated neurons (except attention modules which contain 4 neurons in each). The model is embedded in Hagmann's connectome, which consists of 998 nodes (1996 neurons) to represent non-task brain regions. The model has 10752 simulate neurons in total. Table 5.1 shows the counts of modules and neurons in our model. The model can perform 16 different cognitive tasks by only changing a task parameter. Table 5.2 gives a list of cognitive tasks that have been successfully implemented so far.

Table 5.1 Modules and neurons in the model

Models	Modules	Neurons *
Auditory processing	MGN A1 (up-sweep selective) A1 (down-sweep selective) A2 (up-sweep selective) A2 (down-sweep selective) A2 (corner selective) ST	1134
Visual processing	LGN V1 (horizontal selective) V1 (vertical selective) V4 (horizontal selective) V4 (vertical selective) V4 (corner selective) IT	1134
Auditory working memory and decision**	EC FS D1 D2 R	3240
Visual working memory and decision**	EC FS D1 D2 R	3240
Attention	Endogenous attention Exogenous attention	8
Non-task nodes	Hagmann's connectome	1996
Total number	54	10752

*One Wilson-Cowan unit is counted as two neurons.
**Modules in this category can have multiple duplicates in order to deal with multiple items. Typically we have 4 duplicates of each module for visual and 4 for auditory objects.

We first proposed a network implementation of storing multiple items in working memory and a potential explanation for primacy and recency effects, which states that human remember the beginning and ending items best in memorizing a list of items. We modeled working memory with local microcircuits (D1, D2) and a

large-scale recurrent network (PFC, IT). We studied various neuronal behaviors in the inferior temporal cortex and prefrontal cortex, which matched experimental findings, and discussed the possible functions related to these behaviors. For generating a brain-like environment, we embedded the model into The Virtual Brain framework. This part of research has been detailed in Chapter 2.

The effect has been studied experimentally that people involuntarily switch attention to salient distractors and are difficult to distract when attending to salient stimuli. We realized the effect by incorporating a pair of exogenous attention modules (one for visual and one for auditory objects) and one endogenous attention module. We then integrated our visual model and auditory model, and simulated spontaneous attention switching between visual and auditory stimuli with different salience. We also proposed a neural network explanation for the "working memory load effect", which suggests higher working memory load in one modality can decrease distractions from another modality. This work can be found in Chapter 3.

Complex network (graph) theory has been applied in the analysis of neuroimaging data, as it provides a topological abstraction of the human brain. We constructed a functional connectivity networks for various simulated experimental conditions using a high spatial-resolution model. We studied a number of important network properties, including the scale-free property, the global efficiency, modular structure, and explored their relations with task complexity. We showed that these network properties and their dynamics of our simulated networks matched empirical studies, which verifies the validity and importance of our modeling work. Please refer to Chapter 4 for more information.

Table 5.2 Cognitive tasks that the model can perform

Task Name
Visual fixation
Auditory fixation
Passive viewing
Passive listening
Visual delayed match-to-sample (DMS)
Auditory delayed match-to-sample (DMS)
Visual DMS with distractors
Visual DMS abba task
Auditory DMS with distractor
Auditory DMS abba task
Visual Sternberg's task
Auditory Sternberg's task
Auditory-visual DMS task
Auditory-visual DMS task with bimodal distractors
Auditory-visual Sternberg's task
Auditory-visual involuntary attention switching task

In summary, our results indicate that computational modeling can be a powerful tool for interpreting human and nonhuman primate neuroimaging data.

Some caveats still remain unsolved. First, although the structural network is modeled biologically realistically, the endogenous attention level and the top-down task control we used in the model are parameters set prior to each simulation and therefore are not realistically modeled. Second, we assigned the modules to represent different brain regions based on experimental literature; however some of them are still controversial or may be corresponding to more than one region. For example, we

hypothesized that the entorhinal cortex is responsible for a gating process in multiple item memorization, but some authors argue this process is governed by basil ganglia (Ashby et al., 2005). Finally, the working memory model that involved 4 prefrontal cortex regions is based on monkey electrophysiological experiments (Funahashi et al., 1989). The locations we chose for prefrontal nodes (D1, D2, FS, R) in the Virtual Brain are somewhat arbitrary.

A major extension of the model we are still working on is to incorporate a long-term memory component. In the model, working memory can be consolidated into long-term storages using an unsupervised Hebbian algorithm (Garagnani et al., 2008). The same mechanism can be used to train the model to remember the associations between different objects, thus the model can implement related cognitive tasks, such as a paired associate task, categorization and naming.

Bibliography

Amedi, A., von Kriegstein, K., van Atteveldt, N. M., Beauchamp, M. S., & Naumer, M. J. (2005). Functional imaging of human crossmodal identification and object recognition. *Exp Brain Res, 166*(3-4), 559-571.

Amit, D. J., Fusi, S., & Yakovlev, V. (1997). Paradigmatic working memory (attractor) cell in IT cortex. *Neural Comput, 9*(5), 1071-1092.

Amit, Y., Yakovlev, V., & Hochstein, S. (2013). Modeling behavior in different delay match to sample tasks in one simple network. *Front Hum Neurosci, 7*, 408.

Ashby, F. G., Ell, S. W., Valentin, V. V., & Casale, M. B. (2005). FROST: a distributed neurocomputational model of working memory maintenance. *J Cogn Neurosci, 17*(11), 1728-1743.

Ashby, F. G., & Valentin, V. V. (2007). Computational Cognitive Neuroscience: Building and Testing Biologically Plausible Computational Models of Neuroscience, Neuroimaging, and Behavioral Data. In M. J. S. Wenger, C. (Ed.), *Statistical and Process Models for Cognitive Neuroscience and Aging* (pp. 15-58). Mahwah, NJ: Erlbaum.

Atkinson, R. C., & Shiffrin, R. M. (1968). Human Memory: A Proposed System and its Control Processes11This research was supported by the National Aeronautics and Space Administration, Grant No. NGR-05-020-036. In K. W. Spence & J. T. Spence (Eds.), *Psychology of Learning and Motivation* (Vol. 2, pp. 89-195): Academic Press.

Baddeley, A. (1986). Modularity, mass-action and memory. *Q J Exp Psychol A, 38*(4), 527-533.

Baddeley, A. (1992). Working Memory: The Interface between Memory and Cognition. *J Cogn Neurosci, 4*(3), 281-288.

Baddeley, A. (1996). The fractionation of working memory. *Proc Natl Acad Sci U S A, 93*(24), 13468-13472.

Baddeley, A. D., & Hitch, G. (1974). Working Memory. In G. H. Bower (Ed.), *Psychology of Learning and Motivation* (Vol. 8, pp. 47-89): Academic Press.

Baddeley, A. D., & Hitch, G. (1993). The recency effect: implicit learning with explicit retrieval? *Mem Cognit, 21*(2), 146-155.

Barabasi, A. L., & Albert, R. (1999). Emergence of scaling in random networks. *Science, 286*(5439), 509-512.

Barak, O., & Tsodyks, M. (2014). Working models of working memory. *Curr Opin Neurobiol, 25*, 20-24.

Barak, O., Tsodyks, M., & Romo, R. (2010). Neuronal population coding of parametric working memory. *J Neurosci, 30*(28), 9424-9430.

Bassett, D. S., Wymbs, N. F., Porter, M. A., Mucha, P. J., Carlson, J. M., & Grafton, S. T. (2011). Dynamic reconfiguration of human brain networks during learning. *Proc Natl Acad Sci U S A, 108*(18), 7641-7646.

Bays, P. M., & Husain, M. (2008). Dynamic shifts of limited working memory resources in human vision. *Science, 321*(5890), 851-854.

Beauchamp, M. S. (2005). Statistical criteria in FMRI studies of multisensory integration. *Neuroinformatics, 3*(2), 93-113.

Berti, S., & Schroger, E. (2003). Working memory controls involuntary attention switching: evidence from an auditory distraction paradigm. *Eur J Neurosci, 17*(5), 1119-1122.

Bieser, A. (1998). Processing of twitter-call fundamental frequencies in insula and auditory cortex of squirrel monkeys. *Exp Brain Res, 122*(2), 139-148.

Blondel, V., Guillaume, J.L., Lambiotte,R., & Lefebvre, E. (2008). Fast unfolding of communities in large networks. *Journal of Statistical Mechanics: Theory and Experiment, 2008*(10), P10008.

Bonifazi, P., Goldin, M., Picardo, M. A., Jorquera, I., Cattani, A., Bianconi, G., et al. (2009). GABAergic hub neurons orchestrate synchrony in developing hippocampal networks. *Science, 326*(5958), 1419-1424.

Braver, T. S., & Cohen, J. D. (2000). On the control of control: The role of dopamine in regulating prefrontal function and working memory. In S. Monsell & J. Driver (Eds.), *Control of cognitive processes: Attention and performance* (Vol. XVIII, pp. 713-737). Cambridge, MA: MIT Press.

Butts, C. T. (2009). Revisiting the foundations of network analysis. *Science, 325*(5939), 414-416.

Cairo, T. A., Liddle, P. F., Woodward, T. S., & Ngan, E. T. (2004). The influence of working memory load on phase specific patterns of cortical activity. *Brain Res Cogn Brain Res, 21*(3), 377-387.

Calvert, G. A. (2001). Crossmodal processing in the human brain: insights from functional neuroimaging studies. *Cereb Cortex, 11*(12), 1110-1123.

Chaudhuri, R., Knoblauch, K., Gariel, M. A., Kennedy, H., & Wang, X. J. (2015). A Large-Scale Circuit Mechanism for Hierarchical Dynamical Processing in the Primate Cortex. *Neuron, 88*(2), 419-431.

Cohen, J. D., Braver, T. S., & O'Reilly, R. C. (1996). A computational approach to prefrontal cortex, cognitive control and schizophrenia: recent developments and current challenges. *Philos Trans R Soc Lond B Biol Sci, 351*(1346), 1515-1527.

Cohen, J. R., & D'Esposito, M. (2016). The Segregation and Integration of Distinct Brain Networks and Their Relationship to Cognition. *J Neurosci, 36*(48), 12083-12094.

Colombo, M., Rodman, H. R., & Gross, C. G. (1996). The effects of superior temporal cortex lesions on the processing and retention of auditory information in monkeys (Cebus apella). *J Neurosci, 16*(14), 4501-4517.

Corchs, S., & Deco, G. (2002). Large-scale neural model for visual attention: integration of experimental single-cell and fMRI data. *Cereb Cortex, 12*(4), 339-348.

Courtney, S. M., Petit, L., Maisog, J. M., Ungerleider, L. G., & Haxby, J. V. (1998). An area specialized for spatial working memory in human frontal cortex. *Science, 279*(5355), 1347-1351.

Cowan, N. (2001). The magical number 4 in short-term memory: a reconsideration of mental storage capacity. *Behav Brain Sci, 24*(1), 87-114; discussion 114-185.

D'Esposito, M., Detre, J. A., Alsop, D. C., Shin, R. K., Atlas, S., & Grossman, M. (1995). The neural basis of the central executive system of working memory. *Nature, 378*(6554), 279-281.

Dehaene, S., & Changeux, J. P. (1989). A simple model of prefrontal cortex function in delayed-response tasks. *J Cogn Neurosci, 1*(3), 244-261.

Desimone, R., & Schein, S. J. (1987). Visual properties of neurons in area V4 of the macaque: sensitivity to stimulus form. *J Neurophysiol, 57*(3), 835-868.

DeWitt, I., & Rauschecker, J. P. (2012). Phoneme and word recognition in the auditory ventral stream. *Proc Natl Acad Sci U S A, 109*(8), E505-514.

Druzgal, T. J., & D'Esposito, M. (2003). Dissecting contributions of prefrontal cortex and fusiform face area to face working memory. *J Cogn Neurosci, 15*(6), 771-784.

Durstewitz, D., Seamans, J. K., & Sejnowski, T. J. (2000). Neurocomputational models of working memory. *Nat Neurosci, 3 Suppl*, 1184-1191.

Eguiluz, V. M., Chialvo, D. R., Cecchi, G. A., Baliki, M., & Apkarian, A. V. (2005). Scale-free brain functional networks. *Phys Rev Lett, 94*(1), 018102.

Eliasmith, C., Stewart, T. C., Choo, X., Bekolay, T., DeWolf, T., Tang, Y., et al. (2012). A Large-Scale Model of the Functioning Brain. *Science, 338*(6111), 1202-1205.

Erickson, C. A., & Desimone, R. (1999). Responses of macaque perirhinal neurons during and after visual stimulus association learning. *J Neurosci, 19*(23), 10404-10416.

Etkin, A., Egner, T., & Kalisch, R. (2011). Emotional processing in anterior cingulate and medial prefrontal cortex. *Trends Cogn Sci, 15*(2), 85-93.

Fornito, A. (2016). Chapter 11 - Statistical Connectomics A2 - Fornito, Alex. In A. Zalesky & E. T. Bullmore (Eds.), *Fundamentals of Brain Network Analysis* (pp. 383-419). San Diego: Academic Press.

Fougnie, D., Suchow, J. W., & Alvarez, G. A. (2012). Variability in the quality of visual working memory. *Nat Commun, 3*, 1229.

Friston, K. (1994). Functional and effective connectivity in neuroimaging: A synthesis. *Hum Brain Mapp, 2*(1-2), 56-78.

Friston, K. J., Harrison, L., & Penny, W. (2003). Dynamic causal modelling. *Neuroimage, 19*(4), 1273-1302.

Fritz, J., Mishkin, M., & Saunders, R. C. (2005). In search of an auditory engram. *Proc Natl Acad Sci U S A, 102*(26), 9359-9364.

Funahashi, S., Bruce, C. J., & Goldman-Rakic, P. S. (1989). Mnemonic coding of visual space in the monkey's dorsolateral prefrontal cortex. *J Neurophysiol, 61*(2), 331-349.

Funahashi, S., Bruce, C. J., & Goldman-Rakic, P. S. (1990). Visuospatial coding in primate prefrontal neurons revealed by oculomotor paradigms. *J Neurophysiol, 63*(4), 814-831.

Funahashi, S., Inoue, M., & Kubota, K. (1993). Delay-related activity in the primate prefrontal cortex during sequential reaching tasks with delay. *Neurosci Res, 18*(2), 171-175.

Fuster, J., Bauer, R., & Jervey, J. (1982). Cellular Discharge in the Dorsolateral Prefrontal Cortex of the Monkey in Cognitive Tasks. *Experimental Neurology, 77*, 679-694.

Fuster, J. M., & Alexander, G. E. (1971). Neuron activity related to short-term memory. *Science, 173*(3997), 652-654.

Fuster, J. M., & Alexander, G. E. (1973). Firing changes in cells of the nucleus medialis dorsalis associated with delayed response behavior. *Brain Res, 61*, 79-91.

Fuster, J. M., & Jervey, J. P. (1982). Neuronal firing in the inferotemporal cortex of the monkey in a visual memory task. *J Neurosci, 2*(3), 361-375.

Gallant, J. L., Braun, J., & Van Essen, D. C. (1993). Selectivity for polar, hyperbolic, and Cartesian gratings in macaque visual cortex. *Science, 259*(5091), 100-103.

Garagnani, M., Wennekers, T., & Pulvermuller, F. (2008). A neuroanatomically grounded Hebbian-learning model of attention-language interactions in the human brain. *Eur J Neurosci, 27*(2), 492-513.

Girvan, M., & Newman, M. E. (2002). Community structure in social and biological networks. *Proc Natl Acad Sci U S A, 99*(12), 7821-7826.

Gisiger, T., & Kerszberg, M. (2006). A model for integrating elementary neural functions into delayed-response behavior. *PLoS Comput Biol, 2*(4), e25.

Goolsby, B. A., Shapiro, K. L., & Raymond, J. E. (2009). Distractor devaluation requires visual working memory. *Psychon Bull Rev, 16*(1), 133-138.

Hackett, T. A. (2011). Information flow in the auditory cortical network. *Hear Res, 271*(1-2), 133-146.

Hagmann, P., Cammoun, L., Gigandet, X., Meuli, R., Honey, C. J., Wedeen, V. J., et al. (2008). Mapping the structural core of human cerebral cortex. *PLoS Biol, 6*(7), e159.

Havlík, M. (2017). From Anomalies to Essential Scientific Revolution? Intrinsic Brain Activity in the Light of Kuhn's Philosophy of Science. *Frontiers in Systems Neuroscience, 11*(7).

Haxby, J., Ungerleider, L., Horwitz, B., Rapoport, S., & Grady, C. (1995). Hemispheric differences in neural systems for face working memory: a PET-rCBF study. *Hum Brain Mapp, 3*, 68-82.

Hopfinger, J. B., & West, V. M. (2006). Interactions between endogenous and exogenous attention on cortical visual processing. *Neuroimage, 31*(2), 774-789.

Horel, J. A., Pytko-Joiner, D. E., Voytko, M. L., & Salsbury, K. (1987). The performance of visual tasks while segments of the inferotemporal cortex are suppressed by cold. *Behav Brain Res, 23*(1), 29-42.

Horovitz, S. G., Fukunaga, M., de Zwart, J. A., van Gelderen, P., Fulton, S. C., Balkin, T. J., et al. (2008). Low frequency BOLD fluctuations during resting wakefulness and light sleep: a simultaneous EEG-fMRI study. *Hum Brain Mapp, 29*(6), 671-682.

Horwitz, B. (2003). The elusive concept of brain connectivity. *Neuroimage, 19*(2 Pt 1), 466-470.
Horwitz, B., & Banerjee, A. (2012). A role for neural modeling in the study of brain disorders. *Front Syst Neurosci, 6*, 57.
Horwitz, B., Duara, R., & Rapoport, S. I. (1984). Intercorrelations of glucose metabolic rates between brain regions: application to healthy males in a state of reduced sensory input. *J Cereb Blood Flow Metab, 4*(4), 484-499.
Horwitz, B., Grady, C. L., Haxby, J. V., Schapiro, M. B., Rapoport, S. I., Ungerleider, L. G., et al. (1992). Functional Associations among Human Posterior Extrastriate Brain Regions during Object and Spatial Vision. *J Cogn Neurosci, 4*(4), 311-322.
Horwitz, B., & Tagamets, M. A. (1999). Predicting human functional maps with neural net modeling. *Hum Brain Mapp, 8*(2-3), 137-142.
Hubel, D. H., Wiesel, T. N., & Stryker, M. P. (1977). Orientation columns in macaque monkey visual cortex demonstrated by the 2-deoxyglucose autoradiographic technique. *Nature, 269*(5626), 328-330.
Husain, F. T., Nandipati, G., Braun, A. R., Cohen, L. G., Tagamets, M. A., & Horwitz, B. (2002). Simulating transcranial magnetic stimulation during PET with a large-scale neural network model of the prefrontal cortex and the visual system. *Neuroimage, 15*(1), 58-73.
Husain, F. T., Tagamets, M. A., Fromm, S. J., Braun, A. R., & Horwitz, B. (2004). Relating neuronal dynamics for auditory object processing to neuroimaging activity: a computational modeling and an fMRI study. *Neuroimage, 21*(4), 1701-1720.
Hutchison, R. M., Womelsdorf, T., Allen, E. A., Bandettini, P. A., Calhoun, V. D., Corbetta, M., et al. (2013). Dynamic functional connectivity: promise, issues, and interpretations. *Neuroimage, 80*, 360-378.
Izhikevich, E. M., & Edelman, G. M. (2008). Large-scale model of mammalian thalamocortical systems. *Proc Natl Acad Sci U S A, 105*(9), 3593-3598.
Kaas, J. H., & Hackett, T. A. (1999). 'What' and 'where' processing in auditory cortex. *Nat Neurosci, 2*(12), 1045-1047.
Kapur, S. (2003). Psychosis as a state of aberrant salience: a framework linking biology, phenomenology, and pharmacology in schizophrenia. *Am J Psychiatry, 160*(1), 13-23.
Keshvari, S., van den Berg, R., & Ma, W. J. (2013). No evidence for an item limit in change detection. *PLoS Comput Biol, 9*(2), e1002927.
Kikuchi, Y., Horwitz, B., & Mishkin, M. (2010). Hierarchical auditory processing directed rostrally along the monkey's supratemporal plane. *J Neurosci, 30*(39), 13021-13030.
Kim, J., & Horwitz, B. (2009). How well does structural equation modeling reveal abnormal brain anatomical connections? An fMRI simulation study. *Neuroimage, 45*(4), 1190-1198.
Kim, S. G., Richter, W., & Ugurbil, K. (1997). Limitations of temporal resolution in functional MRI. *Magn Reson Med, 37*(4), 631-636.

Kubat-Silman, A. K., Dagenbach, D., & Absher, J. R. (2002). Patterns of impaired verbal, spatial, and object working memory after thalamic lesions. *Brain Cogn, 50*(2), 178-193.
Kubota, K., & Niki, H. (1971). Prefrontal cortical unit activity and delayed alternation performance in monkeys. *J Neurophysiol, 34*(3), 337-347.
Latora, V., & Marchiori, M. (2001). Efficient Behavior of Small-World Networks. *Physical Review Letters, 87*(19), 198701.
Lech, R. K., & Suchan, B. (2014). Involvement of the human medial temporal lobe in a visual discrimination task. *Behav Brain Res, 268*, 22-30.
Levy, R., & Goldman-Rakic, P. S. (1999). Association of storage and processing functions in the dorsolateral prefrontal cortex of the nonhuman primate. *J Neurosci, 19*(12), 5149-5158.
Liu, Q., Ulloa, A., & Horwitz, B. (2017). Using a Large-scale Neural Model of Cortical Object Processing to Investigate the Neural Substrate for Managing Multiple Items in Short-term Memory. *J Cogn Neurosci*, 1-17.
Liu, Q., Ulloa, A., & Horwitz, B. Modeling visual-auditory bimodal processing and crossmodal attention capture of salient stimuli. In preparation.
Logothetis, N. K., Pauls, J., Augath, M., Trinath, T., & Oeltermann, A. (2001). Neurophysiological investigation of the basis of the fMRI signal. Natur*e, 412*(6843), 150-157.
Ma, W. J., Husain, M., & Bays, P. M. (2014). Changing concepts of working memory. *Nat Neurosci, 17*(3), 347-356.
Maex, R., & Steuber, V. (2009). The first second: models of short-term memory traces in the brain. *Neural Netw, 22*(8), 1105-1112.
Markram, H. (2006). The Blue Brain Project. *Nature Reviews Neuroscience, 7*, 153.
McIntosh, A. R., Grady, C. L., Ungerleider, L. G., Haxby, J. V., Rapoport, S. I., & Horwitz, B. (1994). Network analysis of cortical visual pathways mapped with PET. *J Neurosci, 14*(2), 655-666.
McIntosh, A. R., Nyberg, L., Bookstein, F. L., & Tulving, E. (1997). Differential functional connectivity of prefrontal and medial temporal cortices during episodic memory retrieval. *Hum Brain Mapp, 5*(4), 323-327.
Mendelson, J. R., & Cynader, M. S. (1985). Sensitivity of cat primary auditory cortex (AI) neurons to the direction and rate of frequency modulation. *Brain Res, 327*(1-2), 331-335.
Menon, V., & Uddin, L. Q. (2010). Saliency, switching, attention and control: a network model of insula function. *Brain Struct Funct, 214*(5-6), 655-667.
Miller, E. K., Erickson, C. A., & Desimone, R. (1996). Neural mechanisms of visual working memory in prefrontal cortex of the macaque. *J Neurosci, 16*(16), 5154-5167.
Miller, E. K., Gochin, P. M., & Gross, C. G. (1993). Suppression of visual responses of neurons in inferior temporal cortex of the awake macaque by addition of a second stimulus. *Brain Res, 616*(1-2), 25-29.
Miller, G. A. (1956). The magical number seven plus or minus two: some limits on our capacity for processing information. *Psychol Rev, 63*(2), 81-97.
Miyashita, Y. (1988). Neuronal correlate of visual associative long-term memory in the primate temporal cortex. *Nature, 335*(6193), 817-820.

Monchi, O., & Taylor, J. G. (1999). A hard wired model of coupled frontal working memories for various tasks. *Information Sciences, 113*(1999), 221-243.
Munoz, M., Mishkin, M., & Saunders, R. C. (2009). Resection of the medial temporal lobe disconnects the rostral superior temporal gyrus from some of its projection targets in the frontal lobe and thalamus. *Cereb Cortex, 19*(9), 2114-2130.
Murray, E. A., & Richmond, B. J. (2001). Role of perirhinal cortex in object perception, memory, and associations. *Curr Opin Neurobiol, 11*(2), 188-193.
Murray, J. D., Jaramillo, J., & Wang, X.-J. (2017). Working Memory and Decision-Making in a Frontoparietal Circuit Model. *The Journal of Neuroscience, 37*(50), 12167-12186.
Newman, M. E. (2003). The structure and function of complex networks. *SIAM review, 45*(2), 167-256.
Newman, M. E. J. (2004). Analysis of weighted networks. *Physical Review E, 70*(5), 056131.
O'Reilly, R. C., & Frank, M. J. (2006). Making working memory work: a computational model of learning in the prefrontal cortex and basal ganglia. *Neural Comput, 18*(2), 283-328.
Ogawa, S., Lee, T. M., Kay, A. R., & Tank, D. W. (1990). Brain magnetic resonance imaging with contrast dependent on blood oxygenation. *Proc Natl Acad Sci U S A, 87*(24), 9868-9872.
Peterhans, E., & von der Heydt, R. (1993). Functional organization of area V2 in the alert macaque. *Eur J Neurosci, 5*(5), 509-524.
Peters, J. C., Goebel, R., & Roelfsema, P. R. (2009). Remembered but unused: the accessory items in working memory that do not guide attention. *J Cogn Neurosci, 21*(6), 1081-1091.
Petrides, M. (2000). Dissociable roles of mid-dorsolateral prefrontal and anterior inferotemporal cortex in visual working memory. *J Neurosci, 20*(19), 7496-7503.
Posner, M. I., & Cohen, Y. (1984). Components of visual orienting. *Attention and Performance X, 32*, 531-556.
Preissl, R., Wong, T. M., Datta, P., Flickner, M., Singh, R., Esser, S. K., et al. (2012, 10-16 Nov. 2012). *Compass: A scalable simulator for an architecture for cognitive computing.* Paper presented at the High Performance Computing, Networking, Storage and Analysis (SC), 2012 International Conference for.
Preston, A. R., & Eichenbaum, H. (2013). Interplay of hippocampus and prefrontal cortex in memory. *Curr Biol, 23*(17), R764-773.
Quintana, J., & Fuster, J. M. (1992). Mnemonic and predictive functions of cortical neurons in a memory task. *Neuroreport, 3*(8), 721-724.
Rainer, G., & Miller, E. K. (2002). Timecourse of object-related neural activity in the primate prefrontal cortex during a short-term memory task. *Eur J Neurosci, 15*(7), 1244-1254.
Ranganath, C., & D'Esposito, M. (2005). Directing the mind's eye: prefrontal, inferior and medial temporal mechanisms for visual working memory. *Curr Opin Neurobiol, 15*(2), 175-182.

Rauschecker, J. P. (1997). Processing of complex sounds in the auditory cortex of cat, monkey, and man. *Acta Otolaryngol Suppl, 532*, 34-38.
Rauschecker, J. P. (1998). Parallel processing in the auditory cortex of primates. *Audiol Neurootol, 3*(2-3), 86-103.
Riley, M. R., & Constantinidis, C. (2015). Role of Prefrontal Persistent Activity in Working Memory. *Front Syst Neurosci, 9*, 181.
Roe, A. W., & Ts'o, D. Y. (1995). Visual topography in primate V2: multiple representation across functional stripes. *J Neurosci, 15*(5 Pt 2), 3689-3715.
Rolls, E. T., Dempere-Marco, L., & Deco, G. (2013). Holding multiple items in short term memory: a neural mechanism. *PLoS One, 8*(4), e61078.
Rubinov, M., & Sporns, O. (2010). Complex network measures of brain connectivity: uses and interpretations. *Neuroimage, 52*(3), 1059-1069.
Rypma, B., Berger, J. S., & D'Esposito, M. (2002). The influence of working-memory demand and subject performance on prefrontal cortical activity. *J Cogn Neurosci, 14*(5), 721-731.
Rypma, B., & D'Esposito, M. (1999). The roles of prefrontal brain regions in components of working memory: effects of memory load and individual differences. *Proc Natl Acad Sci U S A, 96*(11), 6558-6563.
SanMiguel, I., Corral, M. J., & Escera, C. (2008). When loading working memory reduces distraction: behavioral and electrophysiological evidence from an auditory-visual distraction paradigm. *J Cogn Neurosci, 20*(7), 1131-1145.
Sanz Leon, P., Knock, S. A., Woodman, M. M., Domide, L., Mersmann, J., McIntosh, A. R., et al. (2013). The Virtual Brain: a simulator of primate brain network dynamics. *Front Neuroinform, 7*, 10.
Schon, K., Quiroz, Y. T., Hasselmo, M. E., & Stern, C. E. (2009). Greater working memory load results in greater medial temporal activity at retrieval. *Cereb Cortex, 19*(11), 2561-2571.
Schon, K., Ross, R. S., Hasselmo, M. E., & Stern, C. E. (2013). Complementary roles of medial temporal lobes and mid-dorsolateral prefrontal cortex for working memory for novel and familiar trial-unique visual stimuli. *Eur J Neurosci, 37*(4), 668-678.
Schreiner, C. E., Read, H. L., & Sutter, M. L. (2000). Modular organization of frequency integration in primary auditory cortex. *Annu Rev Neurosci, 23*, 501-529.
Scott, B. H., Mishkin, M., & Yin, P. (2014). Neural correlates of auditory short-term memory in rostral superior temporal cortex. *Curr Biol, 24*(23), 2767-2775.
Sejnowski, T. J., Churchland, P. S., & Movshon, J. A. (2014). Putting big data to good use in neuroscience. *Nat Neurosci, 17*(11), 1440-1441.
Shamma, S. (2001). On the role of space and time in auditory processing. *Trends Cogn Sci, 5*(8), 340-348.
Shamma, S. A., Fleshman, J. W., Wiser, P. R., & Versnel, H. (1993). Organization of response areas in ferret primary auditory cortex. *J Neurophysiol, 69*(2), 367-383.
Simmons, W. K., & Barsalou, L. W. (2003). The similarity-in-topography principle: reconciling theories of conceptual deficits. *Cogn Neuropsychol, 20*(3), 451-486.

Sizemore, A. E., & Bassett, D. S. (2017). Dynamic graph metrics: Tutorial, toolbox, and tale. *Neuroimage*.
Sporns, O. (2012). From simple graphs to the connectome: networks in neuroimaging. *Neuroimage, 62*(2), 881-886.
Squire, L., Berg, D., Bloom, F. E., Lac, S. d., Ghosh, A., & Spitzer, N. C. (2012). *Fundamental Neuroscience*: Academic Press.
Stephan, K. E., Weiskopf, N., Drysdale, P. M., Robinson, P. A., & Friston, K. J. (2007). Comparing hemodynamic models with DCM. *Neuroimage, 38*(3), 387-401.
Sternberg, S. (1966). High-speed scanning in human memory. *Science, 153*(3736), 652-654.
Sternberg, S. (1969). Memory-scanning: mental processes revealed by reaction-time experiments. *Am Sci, 57*(4), 421-457.
Suzuki, W. A., & Amaral, D. G. (1994). Perirhinal and parahippocampal cortices of the macaque monkey: cortical afferents. *J Comp Neurol, 350*(4), 497-533.
Tagamets, M. A., & Horwitz, B. (1998). Integrating electrophysiological and anatomical experimental data to create a large-scale model that simulates a delayed match-to-sample human brain imaging study. *Cereb Cortex, 8*(4), 310-320.
Talairach, J., Tournoux, P. (1988). *Co-Planar Stereotaxic Atlas of the Human Brain*. New York: Thieme Medial Publishers, Inc.
Ulloa, A., & Horwitz, B. (2016). Embedding task-based neural models into a connectome-based model of the cerebral cortex. *Frontiers in Neuroinformatics*.
Ulloa, A., & Horwitz, B. (2016). Embedding Task-Based Neural Models into a Connectome-Based Model of the Cerebral Cortex. *Front Neuroinform, 10*, 32.
Ulloa, A., & Horwitz, B. (2018). Quantifying differences between passive and task-evoked intrinsic functional connectivity in a large-scale brain simulation. *bioRxiv*.
Ulloa, A., Husain, F. T., Kemeny, S., Xu, J., Braun, A. R., & Horwitz, B. (2008). Neural mechanisms of auditory discrimination of long-duration tonal patterns: a neural modeling and fMRI study. *Journal of integrative neuroscience, 7*(04), 501-527.
Ungerleider, L. G., & Mishkin, M. (1982). Two cortical visual systems. In *Analysis of Visual Behavior.* (pp. 549-586). Cambridge: MIT Press.
Veltman, D. J., Rombouts, S. A., & Dolan, R. J. (2003). Maintenance versus manipulation in verbal working memory revisited: an fMRI study. *Neuroimage, 18*(2), 247-256.
Wang, S. H., Tse, D., & Morris, R. G. M (2012). Anterior cingulate cortex in schema assimilation and expression. *Learn Mem, 19*(8), 315-318.
Watts, D. J., & Strogatz, S. H. (1998). Collective dynamics of 'small-world' networks. *Nature, 393*(6684), 440-442.
Weissman-Fogel, I., Moayedi, M., Taylor, K. S., Pope, G., & Davis, K. D. (2010). Cognitive and default-mode resting state networks: do male and female brains "rest" differently? *Hum Brain Mapp, 31*(11), 1713-1726.

Williams, C. C., Henderson, J. M., & Zacks, R. T. (2005). Incidental visual memory for targets and distractors in visual search. *Percept Psychophys, 67*(5), 816-827.

Wilson, H. R., & Cowan, J. D. (1972). Excitatory and inhibitory interactions in localized populations of model neurons. *Biophys J, 12*(1), 1-24.

Wright, A. A. (1999). Auditory list memory and interference processes in monkeys. *J Exp Psychol Anim Behav Process, 25*(3), 284-296.

Yantis, S., & Jonides, J. (1990). Abrupt visual onsets and selective attention: voluntary versus automatic allocation. *J Exp Psychol Hum Percept Perform, 16*(1), 121-134.

Qin LIU

Phone：301-693-9705
Email: qinliu.christoph@gmail.com

EDUCATION

Ph.D. Program in Physics, University of Maryland, College Park;
Graduate Partner Program, National Institutes of Health
09/2012 – 05/2018
Research Focus: neural network modeling, computational neuroscience
National Base Class of Fundamental Sciences-Physics, Sichuan University, CHINA
09/2008 – 06/2012 Bachelor of Science in Physics

RESEARCH EXPERIENCE

- **National Institutes of Health Research Fellow**
  09/2014 – present
  Brain Imaging & Modeling Section, NIDCD, National Institutes of Health
  Built a large-scale neural network model for human visual and auditory objects processing, attention, short-term memory and long-term memory;
  Trained the model to do multiple cognitive tasks to test the mechanisms underlying and to integrate empirical data from different techniques;
  Investigated the values and dynamics of graph theory metrics to in simulated networks.
- **Research Assistant: Econo-physics** 09/2012 – 09/2014
  Department of Physics & Department of Finance, University of Maryland

PEER-REVIEWED PUBLICATIONS

- **Using a large-scale neural model of cortical object processing to investigate the neural substrate**
  for holding multiple items in short-term memory, **Qin Liu**, Antonio Ulloa, Barry Horwitz, *Journal of Cognitive Neuroscience*. 29(**11**), 2017
- **Global Inequality in Energy Consumption from 1980 to 2010**, Scott Laurence, **Qin Liu**, Victor Yakovenko, *Entropy*. 12(**15**), 2013.

CONFERENCE PAPERS/PRESENTATIONS

- **Using a large-scale neural model of object processing to build associations between long-term memory representations and to perform a paired associate task**, Qin Liu, Antonio Ulloa, Barry Horwitz, *Society for Neuroscience 2016.*
- **Modifying a large-scale neural model of cortical processing of objects to improve the match between experimental and simulated data**, Qin Liu, Antonio Ulloa, Barry Horwitz, *Society for Neuroscience 2015*.

HONORS & AWARDS

- National Institutes Graduate Student Fellowship 2014 - 2017
- Dean's Fellowship, University of Maryland 2012, 2013
- Honorable Mention, American Interdisciplinary Contest in Modeling 2012
- National Outstanding Students Scholarship (China) 2009, 2010 & 2011
- Silver Medal in National Mathematics Olympiad of China 2008